ABSTRACT

Title of Thesis: RE-OS AND OXYGEN SYSTEMATICS OF
                               VARIABLY ALTERED ULTRAMAFIC
                               ROCKS, NORTH CAROLINA

                               Tracey L. Centorbi, Master of Science, 2020

Thesis directed by: Professor Richard J. Walker
                               Department of Geology

This study focuses on the origin and modification of six ultramafic bodies located in the Blue Ridge Province of North Carolina. The bodies consist mainly of harzburgites and dunites with associated chromites. Some of the bodies are associated spatially and genetically with mafic lithologies while others are fault bounded. All the bodies in the study are characterized by variations in their initial Os isotopic compositions, assuming a formation age of 490 Ma ($^{187}Os/^{188}Os_{initial}$ 0.1114 to 0.1360). Most of the initial $^{187}Os/^{188}Os$ ratios are chondritic to subchondritic and can be explained by Re depletion during a partial melting event prior to ophiolite formation. By contrast, some initial $^{187}Os/^{188}Os$ ratios, particularly for those bodies in the Tallulah Falls formation, are suprachondritic suggesting the addition of radiogenic Os during a melt percolation or melt/rock reaction event, most likely during the event that led to the formation of the bodies. Oxygen isotopic $\delta^{18}O$ values of the bodies range from +4.85 to +7.60 which overlap with and extend above mantle estimates. The cause of

the higher values remains unresolved, but serpentinization and contamination by large amounts of crustal material can be excluded. It is concluded that the six bodies in this study have a common history as the residues of mantle partial melting, with chemical compositions and isotopic systematics similar to Phanerozoic ophiolite peridotites associated with the same collisional event, as well as modern abyssal peridotites. Nevertheless, Os isotopic characteristics indicate different processes acted within the bodies despite their relatively close spatial association.

RE-OS AND OXYGEN SYSTEMATICS OF VARIABLY ALTERED
ULTRAMAFIC ROCKS, NORTH CAROLINA

by

Tracey L. Centorbi

Thesis submitted to the Faculty of the Graduate School of the
University of Maryland, College Park, in partial fulfillment
of the requirements for the degree of
Master of Science
2020

Advisory Committee:
 Professor Richard J. Walker, Chair
 Professor James Farquhar
 Faculty Lecturer William G. Minarik

Acknowledgements

First, I want to thank Richard Walker and Bill Minarik for their patience in helping me to finish this thesis. I'm sure there were plenty of times when they both doubted I would ever finish- as did I. I would also like to thank James Farquhar for serving on my committee and being such a calm and reassuring influence on me. I would like to thank the former members of my committee- Roberta Rudnick and Bill McDonough- for the time and effort they put into this project. I am grateful to the Dean of the Graduate School at UMD, the graduate director Sarah Penniston-Dorland, and the faculty of the geology department who all had a role to play in allowing me to finish this thesis. In particular, I'd like to give a special thank you to Phil Piccoli and Karen Prestegaard for the many talks, answers to my questions, and positive encouragement over the years.

It has been such a long road that many people who I laughed, kvetched, and commiserated with have left the department. To the many, thank you for your support, friendship, and scientific insights. In particular, Ruth Schulte, Carolyn Plank, and Laura Hebert. Don't know what I would have done without my gal pals…

Last but certainly not least, my amazing family. My boys have grown into awesome men over these years and I am very proud of them. I'm glad they can see me finish out this odyssey. To my amazing (and lately rather saintly) husband. You never lost faith in my ability to finish. You are extraordinary! I could not have done this without you by my side every single day.

Table of Contents

List of Tables

List of Figures

Chapter 1: Introduction

A discontinuous chain of more than 1000 ultramafic bodies extends from Alabama to Newfoundland within the Appalachian Mountains. It is well established that the history of the Appalachian orogeny involved complex structural relationships and a multi-metamorphic history for most of the significant formations and lithologies (Hatcher et al., 1989). Based on their ubiquity and distribution, the ultramafic bodies evidently played an integral role in the Taconic (~490 Ma) evolution of the Appalachian Wilson Cycle, yet numerous questions remain about the origin and history of these bodies.

The ultramafic bodies in the Appalachians have been studied for their economic importance since Hunter et al. (1941) conducted the first systematic survey of chromite containing ultramafic bodies in the Eastern United States. In the Blue Ridge Province, more than 300 individual ultramafic bodies have been identified. In western North Carolina, the area of this study, the bodies are generally small and lenticular, approximately 0.2-0.6 km wide and 1.5-8.0 km long, and display relatively low degrees of serpentinization, which is unusual for ultramafic bodies in the crust. Most of the bodies are fault-bounded and do not appear to be associated with adjacent lithologies making their origins difficult to determine. Although the bodies are closely spaced, they are hosted in different formations and may not have been emplaced or subsequently modified by the same processes. Numerous studies have concluded that some of the bodies are heterolithic and record a history of multiple metamorphic events (Raymond and Abbott, 1987; Tenthorey et al., 1996; Berger et al., 2001; Raymond et al., 2003; Peterson et al., 2009; Raymond et al., 2016).
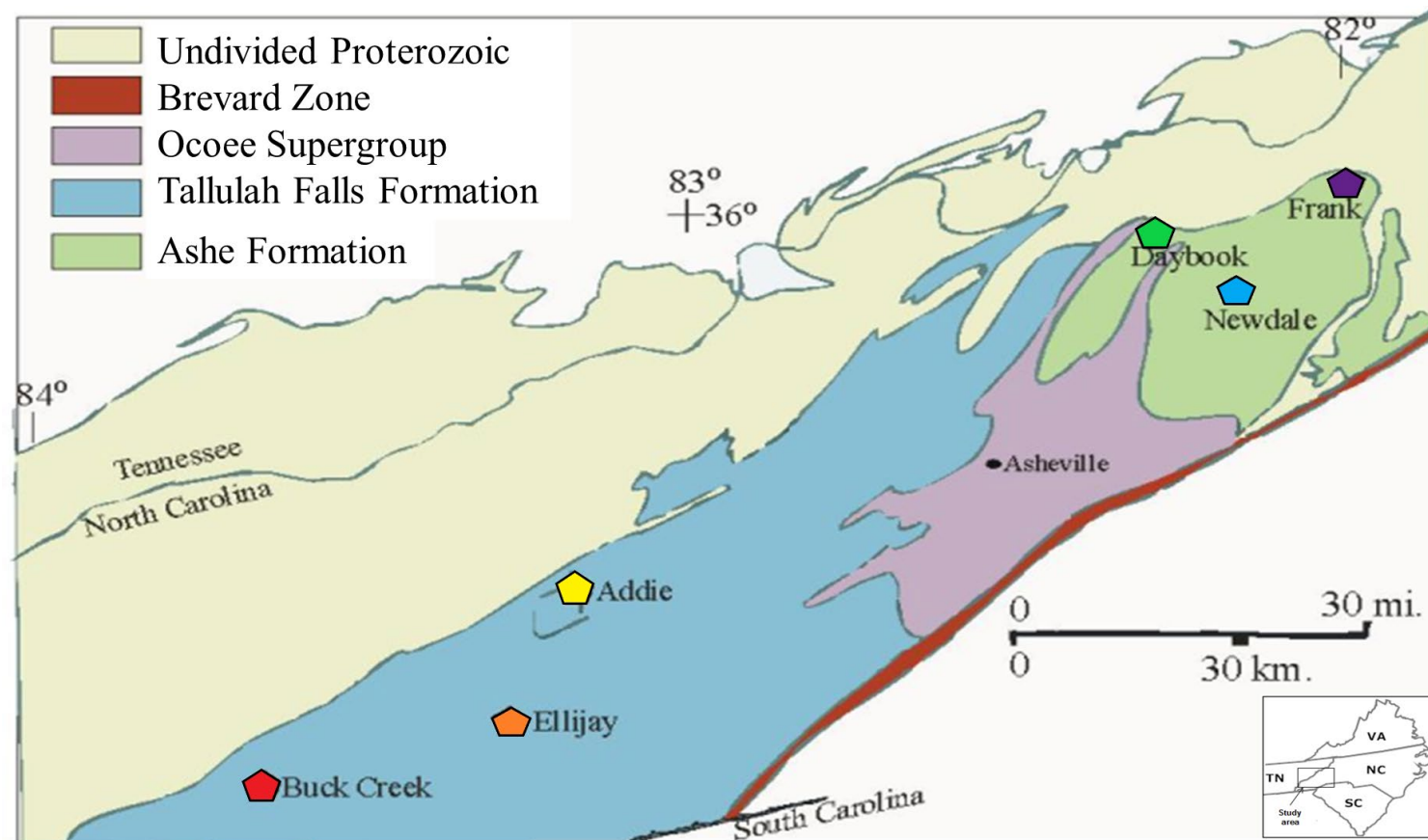
Figure 2-1: Regional overview map showing significant regional structures and the location of each of the ultramafic bodies in this study. The Brevard Zone divides the Blue Ridge Province to the west from the Inner Piedmont Province to the east. All the ultramafic bodies in this study are hosted in Blue Ridge formations. Map adapted from Lipin (1984).

Emplacement ages are difficult to determine as the bodies typically have limited primary phases and, in most cases, do not appear to be related to spatially associated rocks. The age of formation is not know precisely, but it is most likely to have been between the creation of the pre-metamorphic suture Hayesville fault (460-500 Ma) to the west of the bodies and the formation of a back-arc spreading center 460-490 Ma (Massey and Moecher, 2005; Moecher et al., 2011).

A variety of processes have been proposed for the origin of the North Carolina bodies. Options include the possibility that they are residual mantle following the melting events to produce basalt, possibly representing the ultramafic portions of dismembered ophiolites, or crustal cumulates (Carpenter and Chen, 1976; McSween et al., 1989; Peterson et al., 2009; Swanson and Raymond, 2010; Raymond et al., 2016). The bodies may have been emplaced as crystal mush, or as solid pods or lenses. The bodies may have been serpentinized and subsequently dehydrated (Scotford and Williams, 1983).

For this study, six ultramafic bodies in the Western Blue Ridge Province are examined. Within these bodies, variations in composition, percentage of spinel and hydrous minerals, and degrees and type of alteration have been previously noted (Misra and Keller, 1978; McElhaney and McSween, 1983; McSween and Hatcher, 1985; Raymond et al., 2003; Swanson et al., 2005; Peterson et al., 2009; Raymond et al., 2016). Some of the bodies have been genetically linked with associated mafic lithologies, while others are fault bounded. Ultramafic rocks in the six discrete bodies vary from pure dunite to harzburgite compositions with variable alteration of olivine and spinel within each body. In some samples, textures suggest that anhydrous

recrystallization has occurred. Some samples from the same bodies exhibit variable degrees of serpentinization.

When attempting to understand the origin of these ultramafic bodies, three main questions arise. 1) What were the processes involved in the production of the rocks? These processes could include partial melting, crystal accumulation, refertilization, or melt-rock reaction, although these processes are not mutually exclusive. 2) Has there been subsequent processing or modification of the bodies following their emplacement? 3) Why do many of these bodies have such low degrees of serpentinization compared to most other global ultramafic bodies? Were they initially serpentinized and then later dehydrated or were they always relatively dry?

Towards these ends, the major and trace element composition and the Re-Os and O isotopic systematics of whole rock powders, olivine, and chromite of six discrete ultramafic bodies are examined. In particular, the chemical and Re-Os isotopic compositions may reveal information related to melt depletion or post-crystallization effects such as refertilization and melt-rock reactions. For example, a comparison of the ultramafic bodies to the isotopic composition of the modern convecting upper mantle, also referred to as the depleted mid-ocean ridge basalt source mantle (DMM), may help to assess the origin and alteration history of the ultramafic bodies.

Studies of the DMM based on mid-ocean ridge basalt (MORB), abyssal peridotites, and ophiolite peridotites have shown chemical and isotopic heterogeneities at a variety of scales from centimeters to meters (e.g. Dick et al., 1984; Sharma et al., 1995; Workman and Hart, 2005; Schulte et al., 2009; Warren et al., 2009). These heterogeneities can be interpreted to reflect processes such as melt depletion,

refertilization, or melt-rock reactions (Allegre and Turcotte, 1986; Snow et al., 1994; Sharma and Wasserburg, 1996; Liu et al., 2009). For example, a comparison of presumed mantle derived materials to the model for the evolution of DMM may allow for the identification of primary mantle characteristics versus subsequent post-mantle processes. Further, comparing the Os isotopic compositions of whole rock samples to spatially associated, alteration-resistant spinel separates may be particularly useful for documenting the effects of metamorphism on these types of rock. Comparison of whole rock and olivine O isotope compositions are made to provide insight into alteration and assess whether there has been crustal contamination, or alteration via seawater or meteoric waters. Assessing the protoliths and later alteration histories may help place these bodies in a more robust tectonic framework that could help to improve understanding of the Appalachian Orogeny.

Chapter 2: Regional Geology

The ultramafic bodies that are the focus of this study (Figure 2-1) are found in the Blue Ridge Province of the southern Appalachians and are hosted in the Tallulah Falls and Ashe Metamorphic Suite (AMS- hereafter called the Ashe) formations. The Blue Ridge Province is separated from the Carolina Piedmont to the east by the Brevard shear zone. The Blue Ridge Province is generally interpreted to be a series of thrust sheets overlying Precambrian basement (Horton and Zullo, 1991; Hatcher and Goldberg, 1991).

Within the Blue Ridge, the Tallulah Falls and Ashe formations are described as volcanic-sedimentary sequences which have been variably metamorphosed from greenschist to granulite and eclogite facies (Hatcher and Goldberg, 1991). The Tallulah Falls formation consists of metgraywackes, muscovite-biotite and aluminous schists, and amphibolites (Hatcher et al., 1984). The Ashe formation consists of amphibolite (possible metabasalt), pelitic schist, and quartzofeldspathic gneiss with isolated ultramafic pods (McSween et al., 1989). The Tallulah Falls and Ashe formations are geographically separated by the Ocoee Supergroup which has been interpreted to be a Precambrian rift valley graben structure. Ultramafic rocks are present in both the Ashe and Tallulah Falls formations primarily as isolated fault bounded bodies.

In the northern sections of the Appalachians, many of the ultramafic rocks are interpreted to be parts of nearly complete ophiolites formed in suprasubduction-zone settings (Elthon, 1991). In North Carolina, the origin of the bodies has been equivocal (Misra and Keller, 1978; Raymond, 1995). Some have been presumed to be portions of dismembered ophiolites based on composition and observed petrogenetic

relationships with other rocks in the area, although most are fault bounded and other genetically related portions of ophiolites are absent (Misra and Keller, 1978; McElhaney and McSween, 1983; McSween and Hatcher, 1985; Raymond et al., 2003; Swanson et al., 2005). Dating of ultramafic bodies is difficult due to limited primary phases. Determining the age of emplacement of these bodies has also remained problematic because metamorphic fabrics in the surrounding and presumed related formations differ from fabrics within some of the ultramafic bodies (Misra and Keller, 1978; Raymond, 1995).

Carpenter and Chen (1978) concluded that some of the ultramafic bodies in the southern Appalachians were emplaced after magmatic differentiation as either crystal mush or as serpentine that then recrystallized after emplacement. More recently, Miller et al. (1998) concluded that associated plutons and dikes in the area were emplaced at approximately 400 Ma and suggested that the magmas were generated syntectonically in a convergent setting. McElhaney and McSween (1983) reported a Rb-Sr age constraint of 650-900Ma for one of the bodies examined in this study, the dunite body at Buck Creek in the Tallulah Falls formation.

Several of the presumably genetically related rocks in the region show evidence for complex metamorphic histories within the regional framework (Tenthorey et al., 1996; Berger et al., 2001; Peterson et al., 2009). Peak metamorphic conditions for interfingering mafic lithologies in Buck Creek are calculated to be approximately 9-10kbar and *ca.* 850°C (Tenthorey et al., 1996). Rare earth element (REE) systematics have been used to constrain tectonic settings and relate suites of rocks in metamorphosed settings, given that most REE are not appreciably mobilized by

metasomatic fluids (Brookins et al., 1989). McDonough and Frey (1989) determined that pyroxenites from one of the bodies in this study, the Webster-Addie complex, have REE patterns consistent with a residual mantle-derived origin for the ultramafic portions of the body. Warner and Swanson (2010) concluded that the composition and mineral chemistry of the meta-ultramafic rock were originally the ultramafic cumulate portions of an ophiolite sequence that has since been dismembered.

Most studies have concentrated on the Buck Creek mafic/ultramafic complex, the largest and most lithologically diverse body in the southern Blue Ridge Province. Observations of metamorphic fabrics suggest that Buck Creek is an anticline with a core of ultramafic rocks, although limited data do not permit an interpretation of the original intrusive structural or stratigraphic relationships. McElhaney and McSween (1983) concluded that the Buck Creek ultramafic bodies and spatially associated Chunky Gal amphibolites were in contact prior to metamorphism and deformation. The current proximity of amphibolites to the ultramafic rocks is consistent with a petrogenetic relationship, however, the mafic/ultramafic contact was not observed for Buck Creek due to lack of outcrop. Kuntz and Hedge (1981) suggested that the entire Buck Creek ultramafic complex is fault bounded. Tenthorey (1996) concluded that the ultramafic rocks at Buck Creek are basal oceanic crustal cumulates that have moderately high Sr contents consistent with formation in a continental rift or back-arc setting. Berger et al. (2001) concluded that the overall REE systematics of Buck Creek indicate a likely origin as an oceanic crustal cumulate. Peterson et al. (2009) integrated a variety of observations and suggested that Buck Creek originated as a mid-ocean-ridge cumulate massif that was emplaced in a deep subduction-zone setting as a portion

of a lherzolite ophiolite type (LOT) ophiolite as described by Ishiwatari et al. (2003). Lherzolite ophiolite type (LOT), lherzolite-harzburgite ophiolite (LHOT) type, and harzburgite ophiolite type (HOT) ophiolites may correspond with ultraslow-, slow- to intermediate-, and fast-spreading centers, respectively. The geochemical affinities between the mafic and ultramafic rocks suggest that they were associated as a unit through much of the history of the complex.

The possible petrogenetic relationship between the ultramafic rocks and surrounding rocks can be used to infer the metamorphic history of the bodies. At Buck Creek in particular, several studies have interpreted the peak metamorphic pressure of portions of the complex based on chromite veins in the host metamorphic rocks. In some places, these veins have sub-solidus reaction coronas between the plagioclase and olivine that suggest minimum pressures of 5 – 7 kbar (Trommsdorf and Evans, 1974). Based on meta-troctolites within Buck Creek, Tenthorey et al. (1996) proposed a multistage process of metamorphism for the complex with initial burial under dry conditions with temperatures up to 800°C and pressures of 5-7 kbar. A second metamorphic episode is proposed to have occurred at approximately 850°C and 9-10 kbar, and that may have involved partial hydration of the rocks based on sapphirine-bearing assemblages.

The variations in metamorphic conditions and diverse compositions of the ultramafic bodies make interpretation of their origins difficult. Raymond et al. (2016) attempted to put the range of variation among the ultramafic bodies into the context of ophiolite petrologic types as described by Ishiwatari et al. (2003). The Buck Creek and Webster-Addie complexes represent LHOT or LOT type while bodies to the northeast

along strike represent HOT-type and LOT-type fragments. This may suggest that the back-arc basin in which these bodies formed was rotating, causing faster spreading to the south than to the north, or the bodies may represent different levels of crustal extraction.

Detailed descriptions of specific samples and images of thin sections in both plane-polarized (PPL) and cross-polarized light (XPL) are provided in Appendix 2.

Chapter 3: Analytical Methods

Thin section billets were cut from each sample to assess textures, mineral composition, and alteration. For bulk sample powder preparation, rocks were examined for weathered surfaces and veins, which were excluded from the processed fractions. Chromium spinel grains were separated from the silicate portion of some samples using a *Franz* isodynamic magnetic separator. Whole rock samples were ground in an agate *Shatterbox* until finely powdered. Chromium spinel separates were hand-picked using tweezers and a binocular microscope and then ground to a fine powder using an agate mortar and pestle under ethanol.

3-1: X-ray Fluorescence

Whole rock powders were analyzed via X-ray fluorescence (XRF) at Franklin & Marshall College in Lancaster, PA. The methods used for XRF analysis have been described in detail in Boyd and Mertzman (1987). The major elements Si, Ti, Al, Fe, Mn, Mg, Ca, Na, K, and P trace elements Sr, Zr, Cr, and V were analyzed from material cast in the lid of a crucible. The trace elements Rb, Sr, Y, Zr, Nb, Ni, Ga, Cu, Zn, U, Th, Co, Pb, Sc, Cr, and V were analyzed from sample powder pressed into a briquette. An X-ray line and mass absorption correction were calibrated using La, Ce, and Ba. The data were acquired and reduced by a Philips 2404 X-ray fluorescence vacuum spectrometer equipped with a 102-position sample changer and a 4 kW Rh X-ray tube. Loss on ignition (LOI) was determined by heating an aliquot of sample at 950°C for one hour. Ferrous Fe was titrated using a method modified from Richen and Fahey (1962). Total Fe content was determined as Fe_2O_{3T}. Internal reproducibility (2σ) based

on repeated analyses of sample 98-54 was 0.12% for Al_2O_3, 0.09% for Fe_2O_{3T}, 0.93% for MgO, 0.04% for CaO, 16% for V, 3% for Ni, and 1% for Co. The percent deviation of the standard BVHO-1 from accepted values is 0.94% for Al_2O_3, 2.29% for Fe_2O_{3T}, 1.94% for MgO, 0.18% for CaO, 2% for V, 5% for Ni, and 9% for Co. A table of XRF analytic standards is included in Appendix 1 (Table A-1).

3-2: Electron Microprobe Analysis

Olivine and chromium-rich spinel compositions were analyzed by standard wavelength dispersive spectroscopy (WDS) using a JEOL JXA-8900 electron probe microanalyzer (EPMA) at the *Center for Microscopy and Microanalysis* at the University of Maryland. Thin sections were coated with ~300Å carbon, and were analyzed with an accelerating voltage of 15 kV, a sample current of 50 nA (chromium spinel) or 20 nA (olivine), and a beam diameter of 3 mm. The instrumentation was calibrated before each session using a variety of standards to ensure operation within accepted parameters. Olivine grains were analyzed for Mg, Co, Al, Ca, Si, Mn, Cr, Fe and Ni, while chromium spinel grains were analyzed for Mg, Co, Al, Si, Mn, Cr, Fe, Zn, Ni, and Ti. Raw X-ray intensities were corrected using a CIT-ZAF algorithm. Spinel samples were initially assumed to be pure Fe^{2+} and later reevaluated based on the cation chemistry after Droop (1987). Precision was based on the analysis of sample measurements to determine minimum detection limits and uncertainty for each element. For olivine analyses, the minimum detection limits were 0.01 wt% for Mg, Co, and Mn, 0.02 wt % for Al, Ca, Si, Cr, and Fe, and 0.03 wt % for Ni. For chromite analyses, the minimum detection limits were 0.01 wt% for Mg, Co, Al, and Si, 0.02

wt% for Mn, Ce, Ni, Fe, and Ti, 0.04 wt% for Zn. Precision as 2σ error of the mean was determined as weight %: Mg- 0.16, Co- 0.01, Al- 0.05, Ca- 0.02, Si- 0.40, Mn-0.04, Cr- 0.01, Fe- 0.22, Ni- 0.03. A table of analyses of the Forsterite Fo90 standard is included in Appendix I (Table A-2).

3-3: Rhenium-Osmium Isotopic Analysis

Rhenium and Os were analyzed at the *Isotope Geochemistry Laboratory* at the University of Maryland. For Re and Os analysis, powdered samples were digested in Pyrex Carius tubes using approximately 3 g of concentrated HCl and approximately 6 g of concentrated HNO_3 and equilibrated with Re-Os spikes after the methods of Shirey and Walker (1996). Typically, seven samples were processed with one total analytical blank (TAB) analysis per batch. The amount of sample powder added to Carius tubes varied from approximately 0.01-1.0 gram of chromite to ~2.0 grams of whole rock powder. Spike solutions of known concentration were added to the sample with the intention of attaining a ~1:1 Os ratio of spike to sample. Each tube was sealed using an oxygen-propane torch. Tubes were put in metal jackets and placed in an oven at 220 - 240°C for at least 24 hours.

Osmium was loaded onto platinum filaments and coated with BaOH. Isotopic compositions were analyzed using negative thermal ionization mass spectrometry (N-TIMS) on a *VG Sector 54* mass spectrometer with 7 faraday cups in a static mode, or on an NBS 12" 68º sector mass spectrometer (Bobcat I) with an electron multiplier at the University of Maryland. All total analytical blanks (TAB) were analyzed on the Bobcat I. Sample concentrations were blank corrected using the Os TAB which ranged

from 2.0 to 4.5 pg during this study. External precision was monitored by analyzing a UMD Os standard (^{187}Os/^{188}Os = 0.11385) during each session. On the *VG Sector 54*, 35 ng Os standards were measured while on the Bobcat I, 150 pg standards were measured. For the Bobcat I, the average ^{187}Os/^{188}Os was 0.1143 ± 0.0003 ($2\sigma_m$) determined from 6 analyses yielding an external uncertainty of $\pm0.26\%$ ($2\sigma_m$). For the VG Sector 54, the ^{187}Os/^{188}Os of the standard was 0.1138 ± 0.0001 ($2\sigma_m$) determined from 15 analyses yielding an external uncertainty of $\pm0.05\%$ ($2\sigma_m$). Blank corrections were negligible (<<1%) for most Os analyses. Tables of Os standard analyses for the Bobcat-1 (Table A-5) and *VG Sector-54* (Table A-6) are included in Appendix 1.

The Re isotopic composition of samples and total analytical blank (TAB) were analyzed using a *Nu-Plasma* multi-collector inductively coupled plasma mass spectrometer (MCICPMS) at the University of Maryland (Table A-4). The Re was dissolved in a 2% nitric solution for introduction through an *Aridus I* membrane desolvation system. A 200 ppt UMD ^{185}Re/^{187}Re standard was analyzed during each session for sample to standard bracketing and isotopic ratios of the samples were normalized to 0.5975. Rhenium concentrations were blank corrected for the TAB which ranged from 1.6 to 12.4 pg for the seven TAB measured during this study. Blank corrections were minor (0.8%) or better for most Re analyses. Analytical uncertainties for Re were typically $\pm 2\%$ ($2\sigma_m$).

3-4: Whole Rock Oxygen Isotopic Analysis

Whole rock oxygen isotopic determinations from bulk rock powders were made at the *Mineralogical Laboratories* at Indiana University using the method of Clayton

14

and Mayeda (1963). Powdered whole rock samples were loaded into pure nickel reaction tubes in quantities allowing for a five-fold addition of reagent. The reaction tubes were heated to 250°C for two hours in a box with air dried with P_2O_5 in order to remove adsorbed gases and water. The reaction tubes were then treated with a cold BrF_5 treatment for 20 minutes several times to remove any oxygen-bearing compounds that may have formed on the walls of the reaction tubes. The reaction vessels were then evacuated, charged with BrF_5, closed, and heated to 600-700°C for 12-14 hours. Oxygen was collected and purified as it passed through a series of cold traps. The quantity of oxygen generated was measured and reacted with a heated graphite disk to convert it to CO_2. The CO_2 was transferred to a sample tube in order to be measured via mass spectrometer using a *Finnigan MAT 252* stable isotope ratio mass spectrometer with results reported in standard delta notation. Results were corrected relative to repeated analyses of the standard San Carlos olivine (5.4 ± 0.3‰). Analytical uncertainty was less than 0.46‰ and blanks were less than 1 μmol.

3-5: Oxygen Isotopic Analysis of Olivine

Individual olivine grains weighing 1.3 – 1.6 mg were analyzed using established procedures. A metallic stage with sample wells was loaded with the olivine samples and standards. The stage was then placed into a lasing chamber and the air was evacuated. The chamber was pre-fluorinated for at least 24 hours to remove any water molecules adhering to the surfaces. Oxygen analyses are particularly susceptible to perturbation by water in the chamber and vacuum lines, so this step is of critical importance and has proven successful.

Olivine oxygen isotopic determinations were made via laser fluorination at the *Stable Isotope Laboratory* at the University of Maryland. Measurements were made with a 25-W *Synrad* CO_2 laser and BrF_5 after Sharp (1990) and Farquhar and Rumble (1998) on a *Finnigan Delta Plus* mass spectrometer. Data are reported using the delta notation relative to standard mean ocean water (SMOW) by assuming a mass-dependent $\delta^{18}O$ value of 5.8 ‰ for the University of Wisconsin (UWG-2) garnet standard (Valley et al., 1995), analyzed concurrently with the olivine samples. The UWG-2 garnet standard is used to correct analyses based on the accepted $\delta^{18}O$ value. Stability of the vacuum line and internal reproducibility the were monitored using the University of Maryland Gore Mountain Garnet (UMDGMG) standard (Farquhar and Rumble, 1998) and individual olivine grains from the Simcoe xenolith (Sim9) suite after Widom and Farquhar (2003). The UWG-2 standards were averaged and a correction factor relative to the accepted value was applied to the samples. Valley et al. (1995) found that analyses were susceptible to slight variations in the vacuum within the line. During this study, it was also noted that variability of was seen in individual stages when analyses were performed on different days. Standard analyses average $\delta^{17}O$ of 3.04±0.03‰ and $\delta^{18}O$ of 5.80±0.08‰. A table of oxygen standard analyses is included in Appendix 1 (Table A-7).

Chapter 4: Results

4-1: Major Elements

Whole rock major element oxide compositions are compared to the primitive mantle (PM) estimates of McDonough and Sun (1995) in Table 4-1 and Figure 4-1. All samples are depleted in Ti, Al, Ca, and P relative to PM. None of the samples have K above the detection limit of 100 ppm K_2O. The normalized abundance diagram reveals that Fe ranges from slightly enriched to slightly depleted relative to the primitive undepleted mantle (PM) estimate (Figure 4-2). Although all the ultramafic rocks in the study are peridotites, they can be further subdivided into dunite and harzburgite via IUGS classification scheme (Figure 4-3). Given their variable states of modification resulting from metamorphism, all the rocks are classified here based on their chemical composition. Data from the ~6 Ma Taitao Ophiolite in Chile are included in the figure for comparison.

The ultramafic rocks in this study are depleted in most incompatible major elements when compared to the primitive mantle composition. In particular, Al_2O_3 ranges from 0.03-1.36 wt. %, compared to a PM estimate of 4.4 wt. %. The correlation of Al_2O_3 with MgO appears to follow the melting trend proposed by Niu (1997) and suggests relatively high degrees of partial melt extraction (Figure 4-4). Other melt depletion trends, as can be seen in plots of MgO versus Al_2O_3 (Figure 4-3), Al_2O_3 versus CaO (Figure 4-4), and MgO versus CaO (Figure 4-5) are broadly consistent with variable extents of melting and coincident with melting trends recorded by abyssal peridotite data (Brandon et al., 2000) and ophiolite peridotite data (Büchl et al., 2002 and 2004; Godard et al., 2000; Schulte et al., 2009). The Mg# $(Mg^{2+}/(Mg^{2+} + Fe^{2+}))$

was calculated from Fe_2O_{3T} and MgO. The Fe^{2+} content was calculated as 0.85 of Fe_2O_{3T} based on the studies of MORB glass iron ratios of Cottrell and Kelley (2011) and Bezos et al. (2005). The Mg #'s range from 0.886 to 0.944.

Table 4-1: Major element oxide compositions of whole rock powders determined by XRF analysis. Major oxides are given in weight %. All samples were below detection in K_2O so it has been excluded from the table. Not all samples were analyzed for FeO.

Sample	SiO_2	TiO_2	Al_2O_3	Fe_2O_3	FeO	MnO	MgO	CaO	Na_2O	P_2O_5	LOI	Total	Fe_2O_3T	Mg #
Buck Creek:														
Buck 03-1	39.30	0.02	0.53	1.29	8.69	0.17	47.23	0.13	0.02	0.01	1.78	99.17	10.95	0.910
Buck 04-1	39.29	0.01	0.74	13.59		0.18	45.15	0.15	0.05	0.01	0.91	99.17	13.59	0.886
Pow 04-1	38.73	0.02	0.65	1.59	10.56	0.20	45.35	0.09	0.03	0.01	1.84	99.07	13.33	0.888
Ellijay:														
Ell 03-1	39.45	0.01	0.61	10.20		0.16	45.56	0.08	0.05	b.d.	1.30	96.12	10.2	0.912
Ell 03-2	40.55	0.10	0.62	9.95		0.16	46.07	0.08	0.06	b.d.	0.16	97.50	9.95	0.915
Ell 04-T	38.86	0.01	0.05	1.97	6.40	0.15	48.54	0.05	0.02	0.01	2.75	98.81	9.08	0.926
Webster-Addie:														
Add 03-1	40.74	0.01	0.37	10.20		0.15	47.70	0.19	0.06	b.d.	2.49	99.41	10.2	0.916
Add 03-2	36.09	0.03	0.85	3.70	5.58	0.16	44.48	0.18	0.05	0.01	4.61	95.74	9.9	0.913
Add 03-3	39.85	b.d.	0.35	9.72		0.14	48.34	0.07	0.06	b.d.	1.86	98.54	9.72	0.921
Add 03-4	37.07	0.02	1.36	11.25		0.20	44.92	0.09	0.06	0.01	1.11	94.98	11.25	0.903
Newdale:														
New 03-1	41.85	b.d.	0.15	8.83		0.12	47.98	0.08	0.06	b.d.	3.62	99.08	8.83	0.927
New 04-1	42.22	b.d.	0.34	8.05		0.11	48.07	0.24	0.06	b.d.	1.73	99.09	8.05	0.933
New 04-2	45.05	b.d.	0.33	7.43		0.10	46.27	0.09	0.04	b.d.	4.67	99.31	7.43	0.936
New 04-3	39.42	0.01	0.03	2.20	4.83	0.12	48.17	0.11	0.01	0.01	4.33	99.24	7.57	0.937
Daybook:														
Day 03-1	39.73	0.01	0.03	1.13	6.10	0.12	50.17	0.13	0.01	0.01	2.14	99.58	7.91	0.937
Day 03-2	39.98	0.01	0.21	1.23	5.71	0.11	49.06	0.40	0.02	0.01	2.70	99.44	7.58	0.938

Frank:

Frk 04-1	45.36	b.d.	0.60	6.40		0.15	45.92	0.75	0.05	b.d.	12.08	99.23	6.4	0.944
Frk 04-2	38.87	0.01	0.74	2.48	5.10	0.15	44.08	0.16	0.02	0.01	7.98	99.60	8.15	0.927
Frk 04-3	39.49	0.01	0.07	1.16	5.38	0.12	50.86	0.08	b.d.	0.01	2.48	99.66	7.14	0.943

20
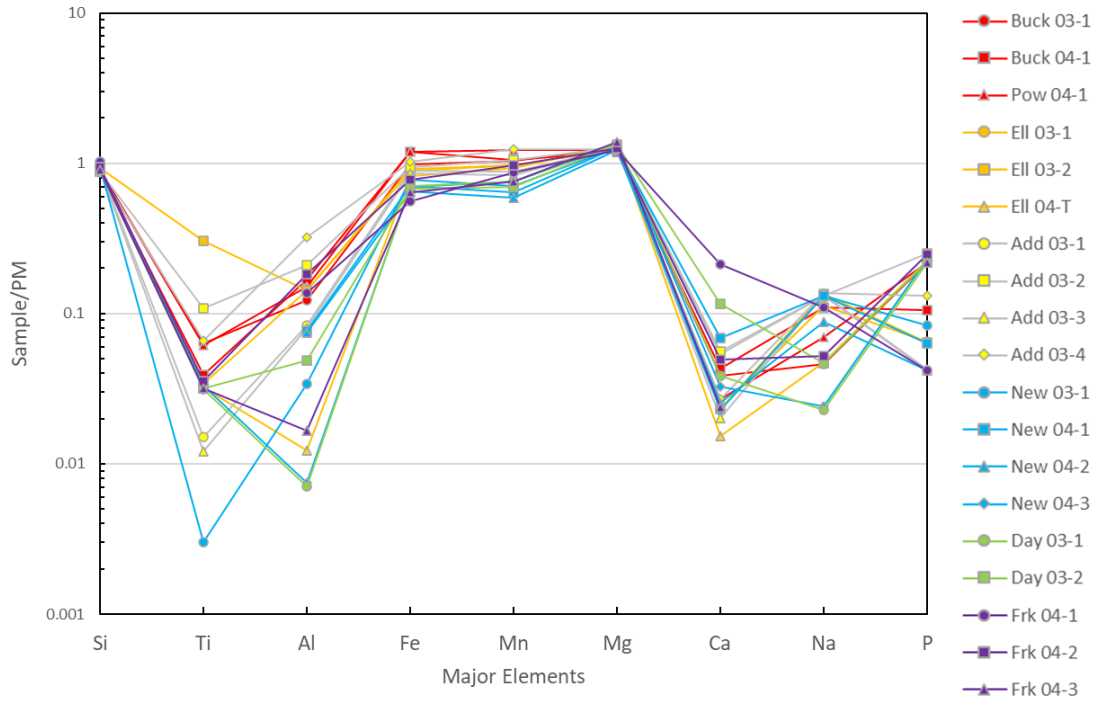
Figure 4-1. Abundance diagram of cation data for ultramafic whole rock (recalculated to anhydrous) and normalized to primitive mantle estimates (McDonough and Sun, 1995; Workman and Hart, 2005).
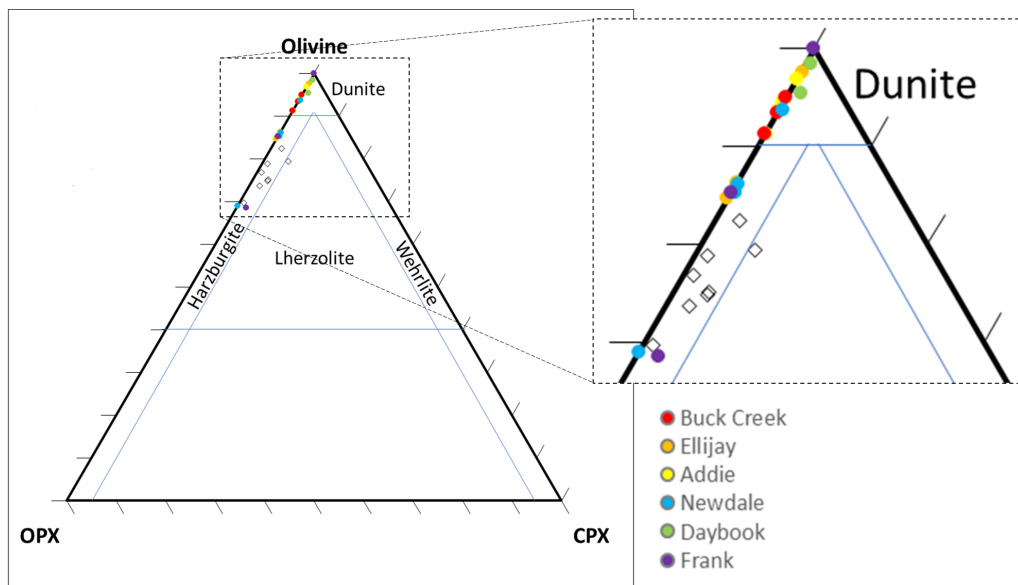
Figure 4-2. Calculated CIPW norms for whole rock peridotites. Peridotite data (open diamonds) from Taitao Ophiolite provided for comparison (Schulte et al., 2009).
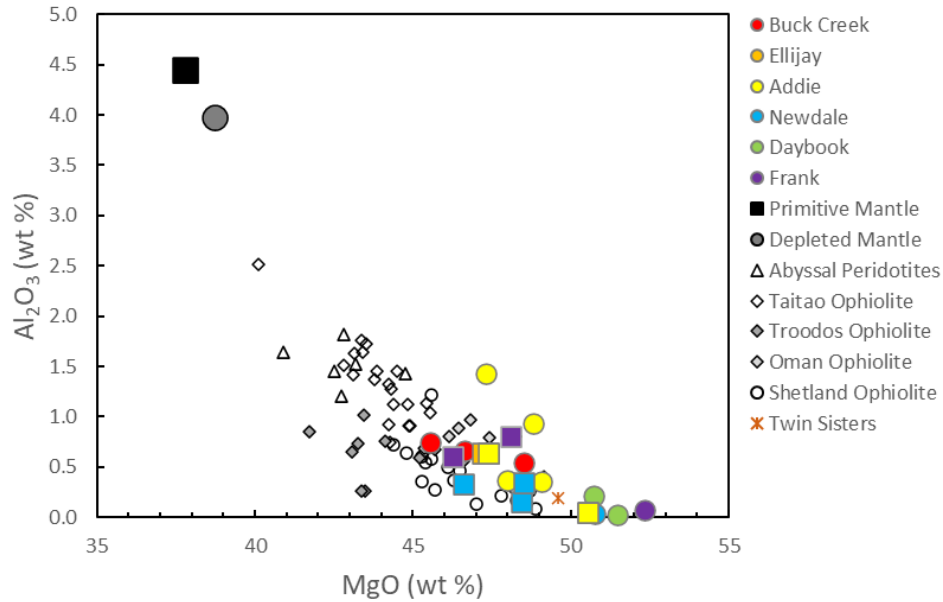
Figure 4-3. Plot of MgO versus Al_2O_3 of North Carolina whole rock peridotites recalculated to anhydrous. Dunite samples are represented by circles, harzburgite samples by squares. For this graph and following graphs, primitive mantle (PM) estimate for MgO and Al_2O_3 is from McDonough and Sun (1995), the depleted mantle (DMM) estimate is from Workman and Hart (2005), abyssal peridotite data are from Brandon et al. (2000), Taitao Ophiolite data are from Schulte et al. (2009), Troodos ophiolite data are from Büchl et al. (2002, 2004), Shetland ophiolite peridotites are from O'Driscoll et al. (2012, 2018), Oman ophiolite peridotites are from Godard et al. (2000), and Twin Sisters Dunite is from Govindaraju (1994).
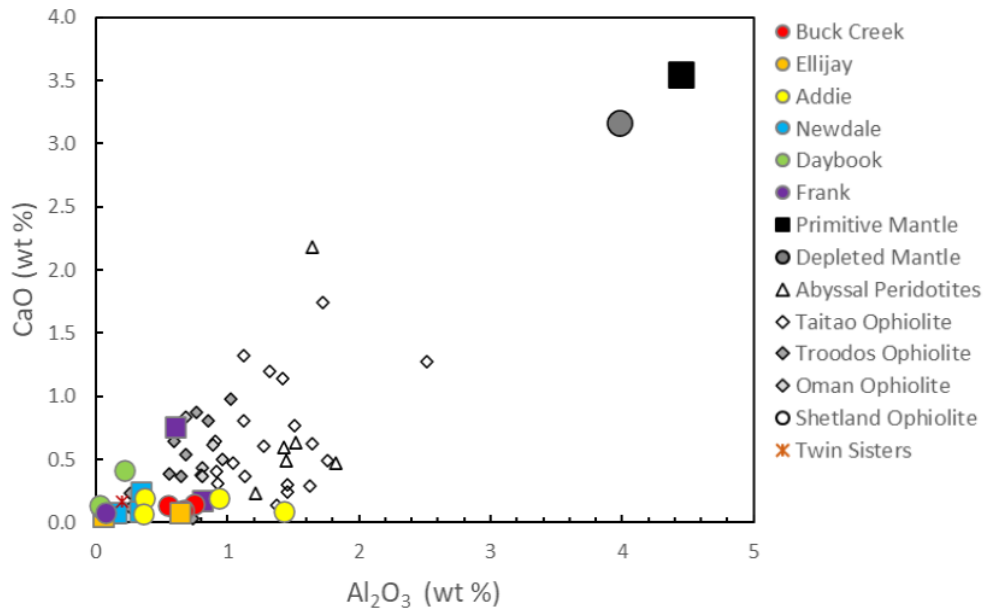
Figure 4-4. Plot of Al$_2$O$_3$ versus CaO (recalculated to anhydrous) of North Carolina whole rock peridotites. PM estimate for Al$_2$O$_3$ (McDonough and Sun, 1995) and CaO and DMM are from (Workman and Hart, 2005). See Figure 4-3 for other references.
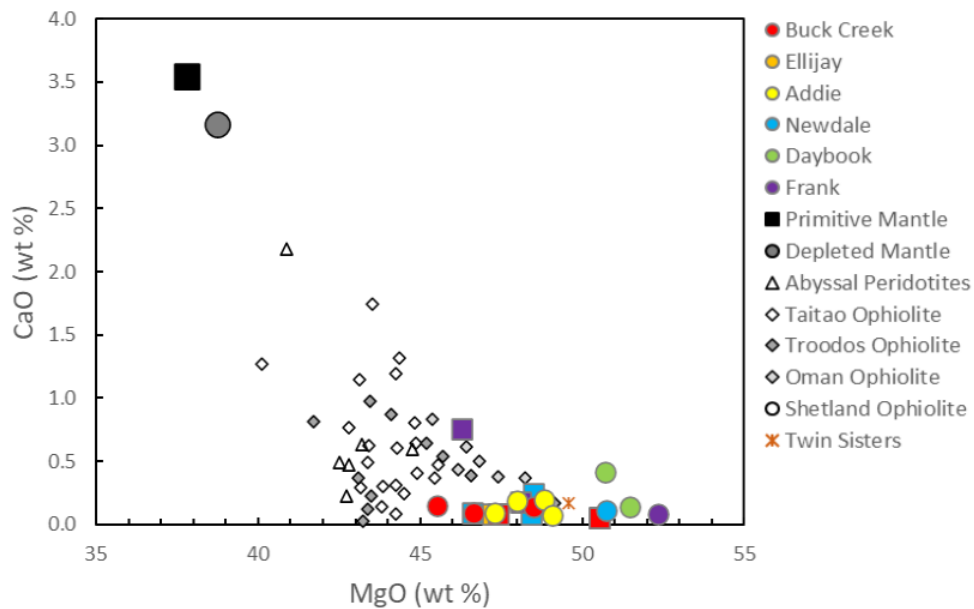
Figure 4-5. Plot of MgO versus CaO (recalculated to anhydrous) of North Carolina whole rock peridotites. PM estimate for MgO (McDonough and Sun, 1995) and CaO and DMM are from (Workman and Hart, 2005). See Figure 4-3 for other references.

4-2: Trace Elements

Trace element data are provided in Table 4-2. Concentrations of U, Th, and Ba were all below detection limits and therefore excluded from the table. Samples were enriched in Nb, Pd, Co, and Ni relative to primitive mantle (PM) (Figure 4-6). Samples were depleted in Sr, Y, Sc, V, Ga and Cu relative to PM with the exceptions of Add 03-4 which was enriched in V and Pow 04-1 which was enriched in Cu. Most samples ranged from modestly depleted to slightly enriched in Cr content. However, Ell 03-1, Ell 03-2, Add 03-2, and Add 03-4 show significant enrichment relative to PM of approximately 2.5, 1.5, 2.6, and 3.4 wt. % respectively.

Incompatible refractory elements, such as V, show a positive correlation with Al_2O_3 (Figure 4-7). For the samples for which there are analyses, compatible trace elements like Ni and Co scatter in relation to Al_2O_3 and MgO (Figures 4-8, 4-9, 4-10).

Table 4-2: Trace element compositions of whole rock powders determined by XRF analysis. Trace element concentrations given in weight %. U, Th, and Ba analyses were below detection limits and excluded from the table. Some samples were only analyzed for Sr, Zr, V and Cr- noted as nd.

Sample	Rb	Sr	Y	Zr	V	Ni	Cr	Nb	Ga	Cu	Zn	Co	Sc	Pb
Buck Creek:														
Buck 03-1	<0.5	1	1.1	9	13	2520	2162	1.4	0.6	3	39	150	5	4
Buck 04-1		<2	nd	3	16	nd	2674	nd	nd	nd	nd	nd	nd	nd
Pow 04-1	<0.5	2	<0.5	9	20	2105	3325	1.2	1.2	50	72	198	5	4
Ellijay:														
Ell 03-1	nd	<2	nd	6	47	nd	24960	nd	nd	nd	nd	nd	nd	nd
Ell 03-2	nd	<2	nd	4	26	nd	15590	nd	nd	nd	nd	nd	nd	nd
Ell 04-1	<0.5	1	0.8	9	12	1930	5183	1.4	<0.5	1	47	136	3	5
Webster-Addie:														
Add 03-1	nd	<2	nd	6	21	nd	1838	nd	nd	nd	nd	nd	nd	nd
Add 03-2	<0.5	2	0.7	9	34	2381	25890	1.4	1.1	5	49	130	5	5
Add 03-3	Nd	<2	nd	4	18	nd	7553	nd	nd	nd	nd	nd	nd	nd
Add 03-4	nd	<2	nd	7	89	nd	34130	nd	nd	nd	nd	nd	nd	nd
Newdale:														
New 03-1	nd	<2	nd	5	10	nd	2396	nd	nd	nd	nd	nd	nd	nd
New 04-1	nd	<2	nd	6	13	nd	2830	nd	nd	nd	nd	nd	nd	nd
New 04-2	nd	<2	nd	5	10	nd	2989	nd	nd	nd	nd	nd	nd	nd
New 04-3	<0.5	1	0.5	9	7	3040	2451	1.3	<0.5	<1	32	117	1	2
Daybook:														
Day 03-1	<0.5	1	<0.5	10	4	2867	1553	1.5	<0.5	<1	31	120	3	3
Day 03-2	<0.5	2	1	9	13	2860	2440	1.7	<0.5	<1	34	116	5	4
Frank:														
Frk 04-1	nd	4	nd	6	18	nd	3249	nd	nd	nd	nd	nd	nd	nd
Frk 04-2	<0.5	3	0.8	10	5	3155	1982	1.2	<0.5	<1	38	113	3	3
Frk 04-3	<0.5	1	1	9	17	2645	2473	1.4	<0.5	<1	46	108	4	3
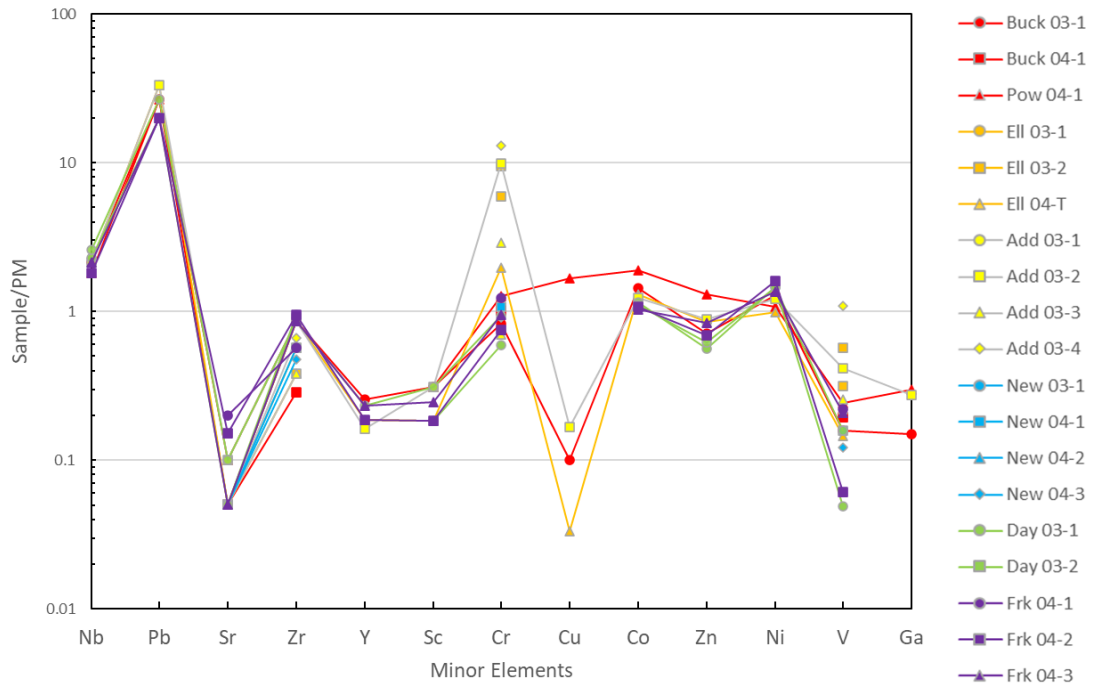
Figure 4-6. Abundance diagram trace element data for ultramafic whole rocks normalized to primitive mantle estimates (McDonough and Sun, 1995; Workman and Hart, 2005). Rb, Ba, U, and Th were below detection limits and have been excluded from the figure.
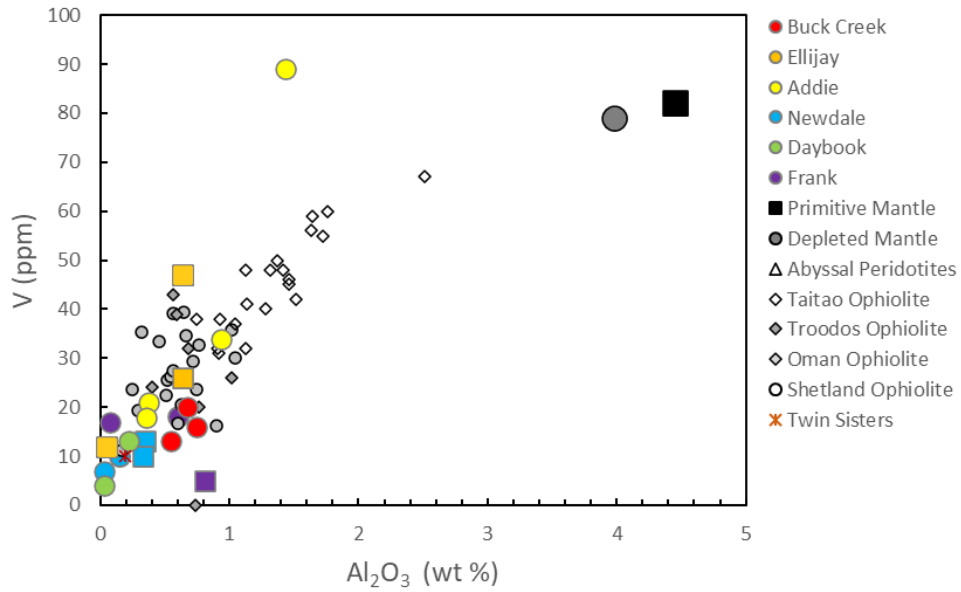
Figure 4-7. Plot of V vs. Al_2O_3 (recalculated to anhydrous) for whole rock samples. The primitive mantle (PM) estimate for MgO and Al_2O_3 is from McDonough and Sun (1995), depleted mantle (DMM) is from Workman and Hart (2005). See Figure 4-3 for other references.
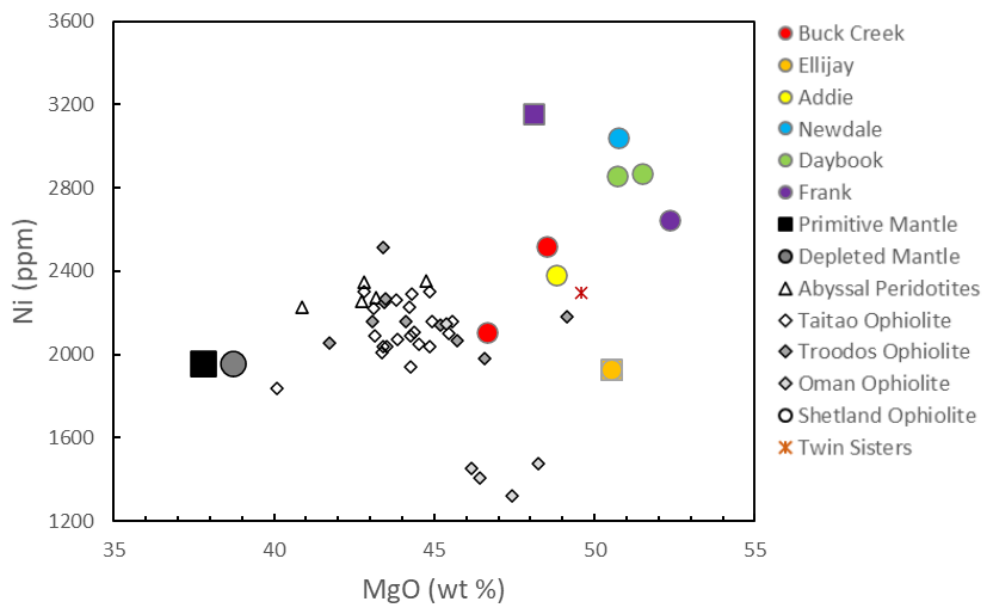
Figure 4-8. Plot of Ni vs. MgO (recalculated to anhydrous) for whole rock samples. See Figure 4-7 for other references.
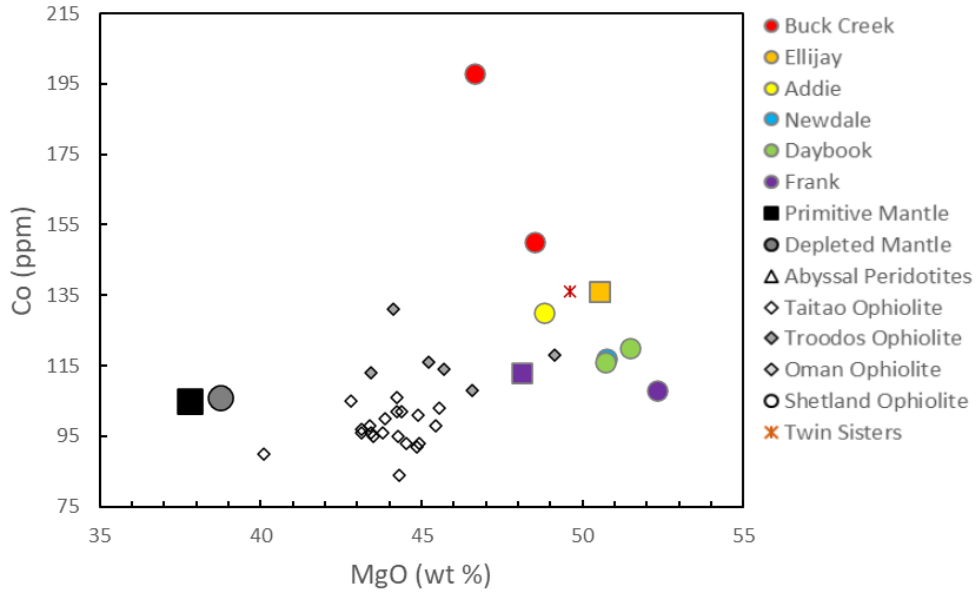
Figure 4-9. Plot of Co vs. MgO (recalculated to anhydrous) for whole rock samples. See Figure 4-7 for other references.
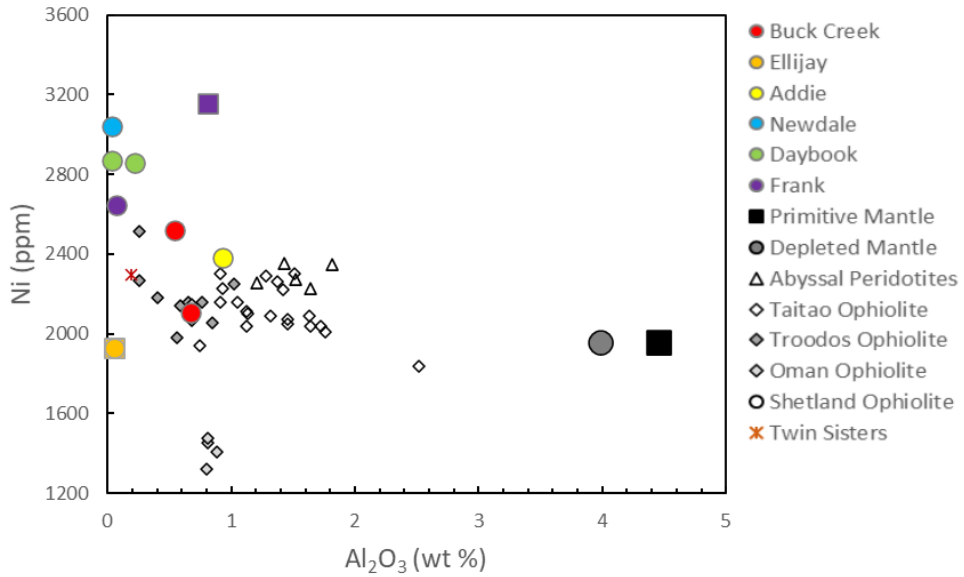
Figure 4-10. Plot of Ni vs. Al$_2$O$_3$ (recalculated to anhydrous) for whole rock samples. See Figure 4-7 for other references.

4-3: Olivine and Chromite Compositions

Averaged major element compositions of olivine and chromite grains analyzed in polished thin sections via electron microprobe are provided in Tables 4-3 and 4-4. Results are provided in oxide weight % along with the analytical uncertainty for each element. The Mg# is calculated as $(Mg^{2+}/(Mg^{2+} + Fe^{2+}))$ and Cr# is calculated as $(Cr^{3+}/(Cr^{3+} + Al^{3+}))$. For chromite, the oxide weight % of FeO and Fe_2O_3 were calculated from the total measured FeO and adjusted stoichiometrically according to Droop (1987). All measurements were taken in eight sessions. Analytical uncertainty and minimum detection limits were calculated as averages. For elements below minimum detection limits, they are reported as b.d. in the table.

For olivine, individual points on the core and rim of grains as well as some grains too small to reliably discriminate between the two regions were measured. The number of individual spot measurements are noted, and core and rim analyses were averaged separately. If differences beyond statistical uncertainty were found, they are represented in the table as core and rim. For samples with no variation between core and rim, an average of both regions is reported. Not all elements varied between core and rim. Multiple grains showed insignificant variation in most elements but significant variation in Mg and Fe. Calculated Mg#'s of olivine range from 0.855 to 0.940 with overlap between different samples and locations.

The chromites did not exhibit zoning between the core and rim for most samples. The number of individual spot measurements are noted, and for samples with zoning, core and rim analyses were averaged separately. The Cr #'s range from 0.745 to 0.961 while Mg #'s range from 0.065 to 0.522.
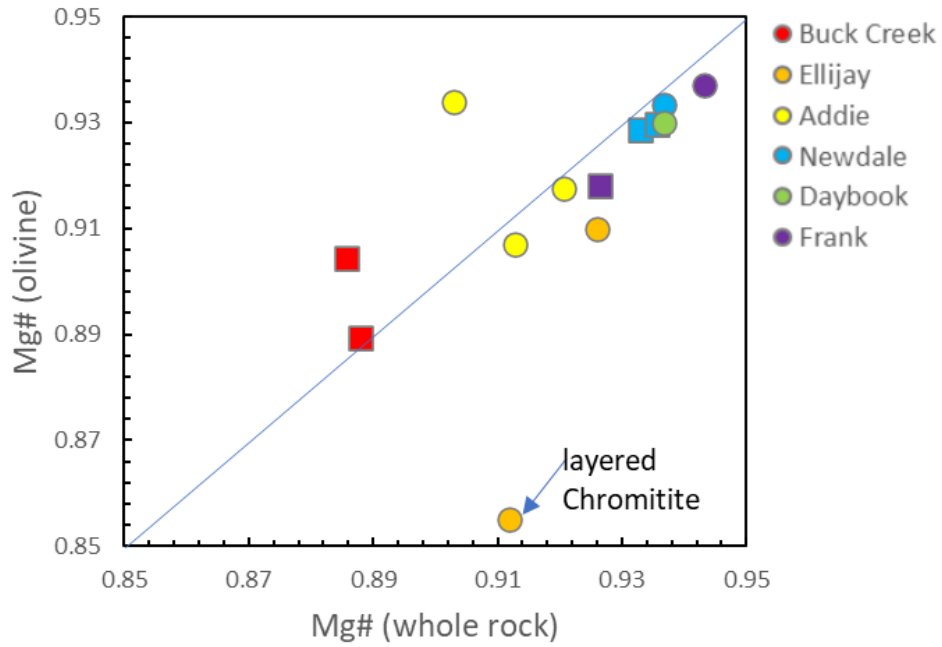
Figure 4-11. Mg# of whole rock determined by XRF analysis versus Mg# of olivine grain cores determined by EPMA. Circles are dunites and squares are harzburgites. The Ellijay sample is strongly banded with centimeter thick layers of olivine alternating with half centimeter layers of chromium spinel. The olivine analyzed were located in the dunitic layers.

Table 4-3. The average major element composition of olivine based on electron microprobe analyses. Values are in oxide weight %. All grains were measure in situ from thin sections.

Sample	# data points		SiO$_2$	Al$_2$O$_3$	Cr$_2$O$_3$	FeO	MnO	MgO	NiO	CoO	CaO	Total	Mg#
Buck Creek:													
Buck 04-1	n = 6	core	40.43	0.02	b.d.	9.29	0.12	49.36	0.42	0.02	0.05	99.71	0.904
	n = 4	rim	40.90	0.02	b.d.	9.29	0.11	50.22	0.36	0.03	b.d.	100.92	0.906
Pow 04-1	n = 6	core	40.30	b.d.	b.d.	10.78	0.15	48.69	0.35	0.03	b.d.	100.32	0.889
	n = 5	rim	40.85	b.d.	b.d.	10.51	0.14	48.38	0.36	0.04	b.d.	100.28	0.891
Ellijay:													
Ell 03-1	n = 8	core	39.71	b.d.	b.d.	13.85	0.25	45.92	0.46	0.04	b.d.	100.23	0.855
	n = 7	rim	40.29	0.07	b.d.	9.45	0.14	48.57	0.43	0.04	0.12	99.10	0.902
Ell 04-1	n = 6	core	40.68	b.d.	b.d.	8.87	0.11	50.32	0.31	0.03	b.d.	100.32	0.910
	n = 8	rim	41.08	b.d.	b.d.	8.68	0.10	50.08	0.25	0.02	b.d.	100.22	0.911
Webster-Addie:													
Add 03-2	n = 11	core	40.80	b.d.	b.d.	9.25	0.10	50.22	0.24	0.03	b.d.	100.65	0.907
	n = 11	rim	40.61	b.d.	b.d.	9.46	0.10	50.27	0.23	0.03	b.d.	100.70	0.905
Add 03-3	n = 14	core	40.75	b.d.	b.d.	8.21	0.08	50.85	0.31	0.02	b.d.	100.24	0.918
	n = 9	rim	40.78	b.d.	b.d.	8.30	0.08	50.61	0.36	0.03	b.d.	100.16	0.916
Add 03-4	n = 5	core	41.54	b.d.	0.02	6.55	0.11	51.89	0.24	0.03	b.d.	100.36	0.934
	n = 3	rim	41.74	b.d.	b.d.	6.55	0.09	51.97	0.26	0.02	b.d.	100.64	0.934
	n = 3	inclusion	41.70	0.02	b.d.	6.36	0.09	52.20	0.29	0.03	b.d.	100.70	0.936
Add 04-1	n = 6	core	41.48	b.d.	b.d.	6.58	0.10	52.25	0.29	0.01	b.d.	100.73	0.934
	n = 4	rim	41.35	b.d.	b.d.	6.77	0.11	52.07	0.28	0.03	b.d.	100.62	0.932

Newdale:												
New 04-1	n = 12	core	41.41	b.d.	b.d.	7.17	0.08	51.98	0.40	0.03	b.d.	101.08	0.929
	n = 12	rim	41.26	b.d.	b.d.	7.23	0.08	51.81	0.35	0.03	b.d.	100.78	0.928
New 04-2	n = 12	core	41.03	b.d.	b.d.	7.10	0.07	52.14	0.46	0.03	b.d.	100.83	0.930
	n = 12	rim	41.05	b.d.	b.d.	7.08	0.06	51.75	0.49	0.03	b.d.	100.46	0.929
New 04-3	n = 12	core	41.31	b.d.	b.d.	6.72	0.07	52.35	0.39	0.03	b.d.	100.88	0.933
	n = 12	rim	41.27	0.02	b.d.	6.72	0.07	52.39	0.42	0.03	b.d.	100.91	0.933
	n = 3	inclusion	41.34	0.06	0.44	6.06	0.06	52.76	0.42	0.02	b.d.	101.16	0.940
Daybook:												
Day 03-1	n = 12	core	41.33	b.d.	b.d.	7.06	0.07	52.10	0.44	0.03	b.d.	101.02	0.930
	n = 12	rim	41.31	b.d.	b.d.	7.14	0.06	52.06	0.43	0.02	b.d.	101.03	0.929
Frank:												
Frk 04-2	n = 6	core	40.94	b.d.	b.d.	8.12	0.08	50.58	0.40	0.04	b.d.	100.17	0.918
	n = 6	rim	41.04	0.03	b.d.	8.14	0.07	50.56	0.39	0.03	b.d.	100.27	0.918
Frk 04-3	n = 6	core	40.98	b.d.	b.d.	6.30	0.06	52.30	0.47	0.02	b.d.	100.15	0.937
	n = 6	rim	41.10	b.d.	b.d.	6.32	0.07	51.85	0.45	0.02	b.d.	99.83	0.937
Frk 04-4	n = 6	core	40.62	b.d.	b.d.	7.83	0.08	50.64	0.30	0.03	b.d.	99.51	0.921
	n = 6	rim	41.45	b.d.	0.03	8.05	0.07	49.85	0.49	0.02	b.d.	99.97	0.918

b.d. indicates measurement was below detection limits.

Table 4-4. The average major element composition of chromite based on electron microprobe analyses. Values are in oxide weight %.

Sample	# data points		SiO$_2$	TiO$_2$	Al$_2$O$_3$	Cr$_2$O$_3$	FeO	Fe$_2$O$_3$	MnO	MgO	NiO	ZnO	CoO	total	Cr#	Mg#
Buck Creek:																
Buck 04-1	n = 7		0.11	1.34	1.89	38.66	29.58	25.49	0.61	1.65	0.11	0.43	0.12	99.99	0.940	0.090
Buck 04-4	n = 4		0.11	1.29	1.25	39.75	30.33	25.01	0.68	1.18	0.06	0.21	0.12	99.99	0.961	0.065
Pow 04-1	n = 6		16.94	0.74	2.94	22.73	22.30	12.54	0.45	20.85	0.15	0.16	0.09	99.88	0.868	0.522
Ellijay:																
Ell 03-1	n = 12		0.03	0.11	4.98	57.46	20.90	8.80	0.50	7.41	0.03	0.16	0.09	100.47	0.886	0.387
Ell 04-1	n = 18		0.50	0.20	1.16	41.23	27.28	25.79	0.60	2.87	0.13	0.24	0.13	100.14	0.960	0.155
Webster-Addie:																
Add 03-2	n = 10	core	0.02	0.16	9.23	53.08	24.08	7.08	0.65	5.60	0.02	0.28	0.12	100.31	0.794	0.293
	n = 8	rim	0.06	0.32	6.86	53.38	25.61	8.36	0.73	4.33	0.02	0.37	0.13	100.15	0.841	0.231
Add 03-3	n = 12	core	0.03	0.17	12.23	53.28	22.16	3.89	0.59	7.16	0.02	0.32	0.12	99.96	0.745	0.365
	n = 12	rim	0.98	0.38	7.09	52.46	24.78	6.45	0.69	5.50	0.04	0.33	0.13	98.83	0.834	0.278
Add 03-4	n = 16		0.08	0.26	9.25	53.2	24.16	6.26	0.66	5.54	0.02	0.34	0.13	99.91	0.803	0.284
Add 04-1	n = 2		0.03	0.17	10.68	53.51	23.97	4.77	0.64	5.73	0.02	0.41	0.13	100.06	0.772	0.299
Newdale:																
New 04-1	n = 12	core	0.01	0.07	7.36	54.75	22.59	8.28	0.57	6.37	0.05	0.29	0.12	100.46	0.834	0.336
	n = 9	rim	0.04	0.08	6.76	53.92	23.02	8.90	0.58	5.86	0.06	0.31	0.12	99.62	0.841	0.315
New 04-2	n = 12	core	b.d.	0.03	6.19	56.35	22.33	8.25	0.58	6.41	0.03	0.31	0.12	100.60	0.860	0.339
	n = 9	rim	0.01	0.04	6.72	55.67	22.32	8.36	0.57	6.51	0.04	0.31	0.12	100.68	0.847	0.342
Daybook:																
Day 03-1	n = 16	core	0.03	0.17	3.05	54.95	24.76	12.26	0.66	4.55	0.08	0.32	0.12	100.96	0.924	0.246
	n = 13	rim	0.06	0.20	3.01	53.26	24.97	13.71	0.66	4.42	0.09	0.29	0.13	100.80	0.923	0.240

Frank:

Frk 04-1	n = 8	0.30	0.03	2.35	48.27	25.33	18.77	0.98	3.84	0.07	0.37	0.11	100.42	0.935	0.210
Frk 04-2	n = 8	0.03	0.11	1.36	48.88	26.45	20.25	0.66	3.20	0.16	0.36	0.13	101.59	0.960	0.177
Frk 04-3	n = 9	0.02	0.06	5.47	57.34	22.66	8.38	0.54	6.25	0.06	0.42	0.12	101.33	0.876	0.330
Frk 04-4	n = 9	0.03	0.06	4.82	47.69	24.54	17.36	0.52	4.65	0.14	0.34	0.12	100.27	0.870	0.252

4-4: Isotopic systematics – Rhenium-Osmium

Results of Re-Os analyses are reported in Table 4-5. In the Table, $\gamma_{(Os)i}$ notation is the percent derivation from a chondritic reference at 490 Ma. The age of 490 Ma for γ_{Os} was chosen to approximate the timing of the formation of protoliths, prior to the peak of the Taconian orogeny and development of the nearby Hayesville thrust (Miller et al., 1998; Massey and Moecher, 2005).

Whole rock Re and Os concentrations range from 0.001 to 0.814 ppb and 0.129 to 16.1 ppb respectively (Figure 4-12). Most samples have Re concentrations that are lower than the average Re concentration of upper oceanic mantle peridotite (~0.3 ppb). Osmium concentrations are generally in the range reported for upper mantle peridotites, although vary considerably (e.g. Meisel et al., 1996; Walker et al., 1996; O'Driscoll et al., 2012). Chromite separate Re and Os concentrations range from 0.002 to 4.71 ppb and 1.65 to 339 ppb respectively. Concentrations of Re and Os in spinels are comparable to other ophiolite derived chromites. Concentrations of Os are in the range seen in other ophiolite complexes apart from the extremely high concentrations (311 and 339 ppb) in distinct 1 cm thick chromitite layers from Ellijay.

Duplicate analyses of some chromite separates were completed by W. Minarik and are included in the table. Concentrations of Re and Os of these analyses vary from 8 to 45% for five duplicates compared to those determined in this study but all isotopic ratios agree within ±1%. No replicates of whole rock samples were performed.

Analytical uncertainty of the $^{187}Os/^{188}Os$ ratio is given immediately following each value. $^{187}Os/^{188}Os$ ratios for chromite separates within each location vary <2% except for Ellijay where there is a 4.8% difference between strongly layered chromite

and disseminate chromite with weakly layered chromite falling between the two extremes (Figure 4-13). The $^{187}Os/^{188}Os$ ratios between locations show variations of up to 10%, significantly beyond analytical uncertainties.

For most samples, there is agreement between initial Os isotopic ratios in the whole rock and chromite separates (Figure 4-14). Since chromite can be resistant to alteration, agreement likely means that the isotopic ratios are representative of primary values. A lack of agreement between whole rock and chromite initial Os isotopic values for the one Ellijay sample is likely a calculation artefact. It most likely had Re added to it after ophiolite formation.
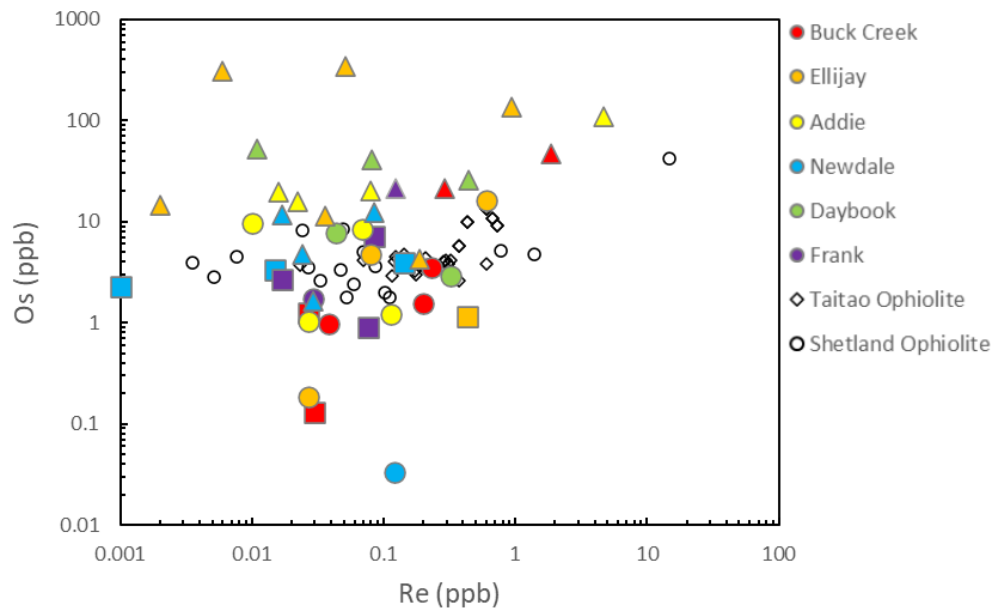

Figure 4-12. Rhenium vs. Os concentrations of dunite (circles), harzburgite (squares) whole rock, and chromite separates (triangles). Data from the Taitao (Schulte et al., 2009) and Shetland (O'Driscoll et al., 2012, 2018) Ophiolites are provided for comparison. Note the log scale for both axes.
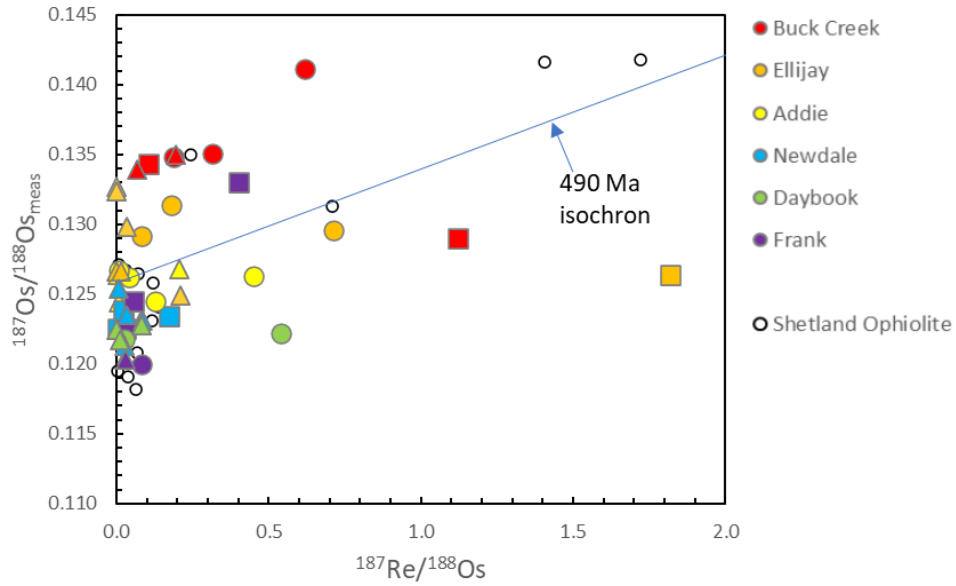
Figure 4-13. $^{187}Re/^{188}Os$ vs. $^{187}Os/^{188}Os$ isotopic compositions of dunite (circles), harzburgite (squares) whole rock, and chromite separates (triangles). Data from the 492 ± 3 Ma Shetland ophiolite (O'Driscoll et al., 2012, 2018) are provided for comparison. A 490 Ma chondritic reference isochron was calculated with an initial $^{187}Os/^{188}Os$ of 0.126.

Figure 4-14. $\gamma Os_{(490Ma)}$ of whole rock vs. $\gamma Os_{(490Ma)}$ of chromite separates for dunite (circles) and harzburgite (squares). $\gamma Os(t)$ notation describes % difference between the initial Os isotopic composition of samples compared to a chondritic reference value at 490 Ma.

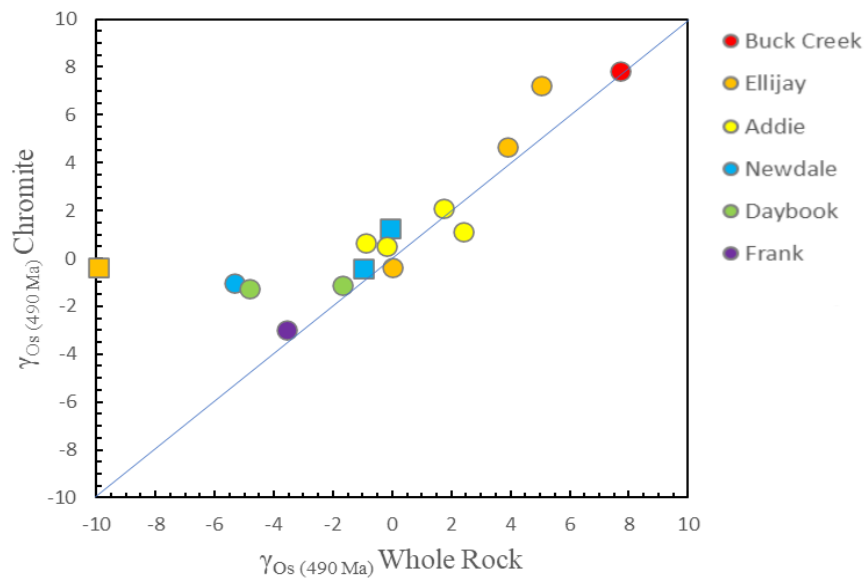Table 4-5: Re-Os and O isotopic data for whole rock and spinel separates. The uncertainties reported are two standard deviations of the mean ($2\sigma_m$) of the mass spectrometry data sets and are shown in parentheses following each value. γOs is calculated for 490 Ma. T_{MA} are and T_{RD} are Re-Os model ages after Shirey and Walker (1998), 'f' indicates a future model age. [a] Spinel separate duplicates analyzed by W. Minarik

Sample	Rock Type	Re (ng/g)	Os (ng/g)	$^{187}Re/^{188}Os$	$^{187}Os/^{188}Os\pm2\sigma$	$^{187}Os/^{188}Os$ (490 Ma)	γ(Os) 490Ma	T_{MA} (Ga)	T_{RD} (Ga)	Ol δ^{18}O (‰)	WR δ^{18}O (‰)
Buck Creek:											
buck 03-1	dunite	0.0377	0.969	0.1876	0.1348±0.0002	0.1332	+7.7	f	f	+5.29	+5.69
buck 03-1	spinel sep	0.2912	21.35	0.0658	0.1339±0.0001	0.1334	+7.8	f	f		
buck 03-1[a]	spinel sep	1.881	46.72	0.1942	0.1350±0.0002	0.1334	+7.8	f	f		
buck 04-1	dunite	0.2322	3.540	0.3164	0.1351±0.0015	0.1325	+7.1	f	f		+7.60
buck 04-4	harzburgite	0.0300	0.129	1.117	0.1290±0.0001	0.1199	-3.1	0.22	f		+6.19
buck-str	harzburgite	0.0269	1.241	0.1044	0.1343±0.0003	0.1334	+7.8	f	f		
pow 04-1	dunite	0.1994	1.560	0.6171	0.1411±0.0002	0.1360	+10.0	3.79	f	+5.17	+5.58
Ellijay:											
ell 03-1	chromitite	0.6000	16.06	0.1801	0.1314±0.0001	0.1299	+5.0	f	f	+6.34	+6.98
ell 03-1T	spinel sep	0.0514	339.4	0.0007	0.1327±0.0001	0.1327	+7.2	f	f		
ell 03-1[a]	spinel sep	0.0064	311.1	0.0001	0.1323±0.0002	0.1323	+7.0	f	f		
ell 03-2	harzburgite	0.4316	1.141	1.822	0.1264±0.0002	0.1114	-9.9	f	0.11	+5.19	+6.01
ell 03-2	spinel sep	0.0022	14.37	0.0008	0.1266±0.0001	0.1266	+2.3	0.07	0.08		
ell 03-2[a]	spinel sep	0.0361	11.47	0.0152	0.1266±0.0002	0.1265	+2.3	0.07	0.07		
ell 04-T	dunite	0.0272	0.184	0.7126	0.1296±0.0004	0.1237	+0.01	0.58	f		
ell 04-T	spinel sep	0.1872	4.322	0.2087	0.1249±0.0001	0.1232	-0.4	0.30	0.32		
ell 04-1	dunite	0.0801	4.719	0.0818	0.1292±0.0001	0.1285	+3.9	f	f		+6.39
ell 04-1	spinel sep	0.9341	135.5	0.0332	0.1298±0.0001	0.1295	+4.7	f	f		
Addie:											
add 03-1	dunite	0.1146	1.228	0.4495	0.1263±0.0001	0.1226	-0.9	f	0.13	+5.41	+5.67
add 03-1	spinel sep	0.0794	19.99	0.0191	0.1246±0.0016	0.1245	+0.6	0.38	0.37		

38

add 03-2	dunite	0.0690	8.350	0.0398	0.1262±0.0001	0.1258	+1.7	0.15	0.14	+5.35	+6.06
add 03-2	spinel sep	0.0160	19.77	0.0039	0.1264±0.0002	0.1263	+2.1	0.11	0.11		
add 03-3	dunite	0.0271	1.028	0.1268	0.1245±0.0001	0.1235	-0.2	0.53	0.39		+5.52
add 03-3	spinel sep	0.0216	15.93	0.0065	0.1244±0.0003	0.1243	+0.5	0.40	0.40		
add 03-4	dunite	0.0098	9.723	0.0048	0.1267±0.0001	0.1267	+2.4	0.06	0.06		+7.46
add 03-4	spinel sep	4.709	110.8	0.2047	0.1268±0.0001	0.1252	+1.2	0.07	0.03		
add 04-2	pyroxenite	0.8144	3.142	1.250	0.1318±0.0001	0.1215	-1.8	0.33	f		+6.04
Newdale:											
new 03-1	harzburgite	0.0009	2.260	0.0020	0.1225±0.0003	0.1225	-1.0	0.68	0.68	+5.70	+6.36
new 03-1	spinel sep	0.0850	12.40	0.0330	0.1235±0.0001	0.1232	-0.4	0.57	0.54		
new 03-1[a]	spinel sep	0.0240	4.801	0.0241	0.1213	0.1211	-2.1	0.90	0.86		
new 04-1	harzburgite	0.1424	3.955	0.1735	0.1234±0.0002	0.1220	-1.4	0.96	0.55		+6.87
new 04-2	harzburgite	0.0152	3.372	0.0217	0.1238±0.0004	0.1236	-0.1	0.51	0.49	+7.36	+7.55
new 04-2	spinel sep	0.0172	11.54	0.0072	0.1254±0.0001	0.1253	+1.3	0.24	0.26		
new 04-3	dunite	0.1213	0.921	0.6346	0.1223±0.0002	0.1171	-5.3	f	0.71	+5.84	+6.78
new 04-3	spinel sep	0.0288	1.649	0.0841	0.1231±0.0004	0.1224	-1.0	0.71	0.59		
Daybook:											
day 03-1	dunite	0.3237	2.879	0.5414	0.1222±0.0004	0.1177	-4.8	f	0.73	+5.27	+6.70
day 03-1	spinel sep	0.4391	26.12	0.0810	0.1228±0.0001	0.1221	-1.3	0.75	0.64		
day 03-2	dunite	0.0432	7.800	0.0267	0.1218±0.0001	0.1216	-1.7	0.83	0.78	+5.13	+6.47
day 03-2	spinel sep	0.0114	52.29	0.0011	0.1224±0.0001	0.1223	-1.1	0.70	0.70		
dayb03-2[a]	spinel sep	0.0810	41.56	0.0094	0.1217	0.1216	-1.7	0.82	0.80		
Frank:											
frk 04-1	harzburgite	0.0759	0.912	0.4015	0.1330±0.0001	0.1297	+4.8	-	f	+6.62	+7.01
frk 04-2	harzburgite	0.0849	7.116	0.0574	0.1245±0.0001	0.1229	-0.7	0.65	0.56	+4.85	+5.25
frk 04-3	dunite	0.0293	1.732	0.0815	0.1200±0.0001	0.1193	-3.6	1.31	1.06	+5.10	+5.16
frk 04-3	spinel sep	0.1238	21.47	0.0278	0.1203±0.0001	0.1200	-3.0	1.09	1.01		
frk 04-4	peridotite	0.0171	2.693	0.0306	0.1225±0.0005	0.1223	-1.1	0.72	0.68		+6.23

4-5: Isotopic systematics – Oxygen

The $\delta^{18}O$ values for whole rock powders for all the bodies range from +5.16 to +7.60‰. The $\delta^{18}O$ values for individual olivine grains range from +4.85 to +7.36‰, which agree with but extend above the estimated mantle peridotite values of $5.2 \pm 0.1‰$ (Massey et al., 1994) and $5.7 \pm 0.5‰$ (Eiler et al., 1998). For samples with both whole rock and olivine analyses, a comparison of the data sets is shown in Figure 4-15.
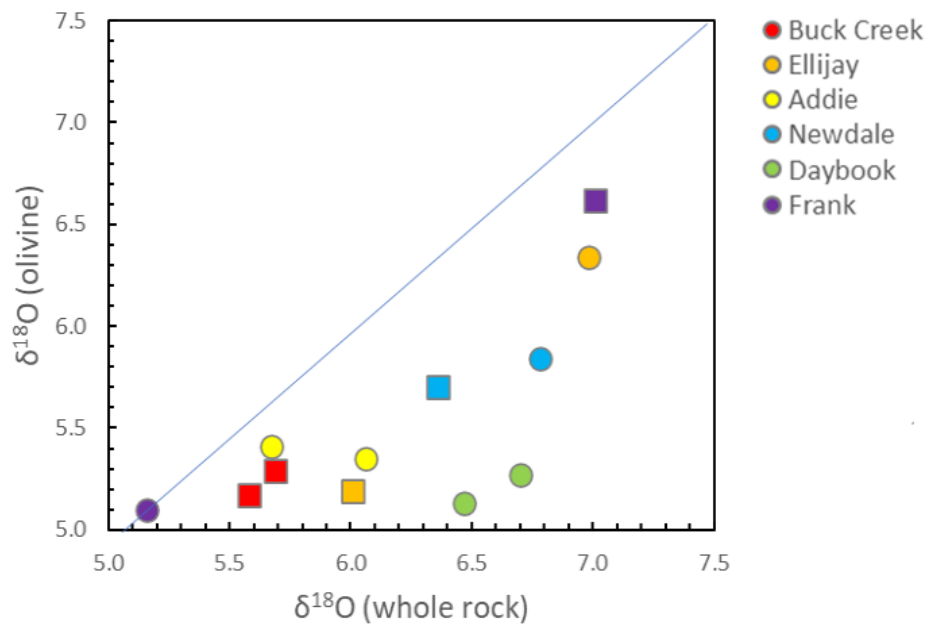

Figure 4-15. Whole rock vs. olivine separate oxygen isotopic values of dunite (circles) and harzburgite (squares) relative to SMOW.

For individual bodies, the Buck Creek whole rock $\delta^{18}O$ values (n=4) average +6.27‰, while olivine analyses (n=2) average +5.23‰. Ellijay whole rock $\delta^{18}O$ values (n=3) average +6.46‰, while olivine analyses (n=2) average +5.77‰. Addie whole rock $\delta^{18}O$ values (n=4) average +6.18‰, while olivine analyses (n=2) average +5.38‰.

Newdale whole rock $\delta^{18}O$ values (n=4) average +6.89‰, while olivine analyses (n=3) average +6.30‰. Daybook whole rock $\delta^{18}O$ values (n=2) average +6.59‰, while olivine analyses (n=2) average +5.20‰. Frank whole rock $\delta^{18}O$ values (n=4) average +5.81‰, while olivine analyses (n=3) average +5.52‰. In general, whole rock averages range slightly higher than olivine grains for the same sample although whole rock values overlap with olivine analyses for all bodies except Daybook.

Chapter 5: Discussion

5-1: Formation of the Ultramafic Bodies – Major and Trace elements

Early studies such as Pearce and Cann (1973) developed discrimination diagrams to distinguish between ophiolites created in mid-ocean ridge (MOR) settings versus those generated in supra-subduction zone (SSZ) environments. Ishiwatari et al. (1985) and Boudier and Nicolas (1985) developed the means to classify ophiolites based on the degree of partial melting in the mantle assessed through petrologic and chemical or structural considerations. The degree of partial melting assessed through chemical variations was related to spreading rate and used to divide ophiolites into types which may correspond with ultraslow-, slow- to intermediate-, and fast-spreading centers. There is also a recognition that certain isolated ultramafic bodies may have similar origins to the ultramafic portions of traditionally recognized ophiolitic assemblages and therefore assessing these bodies through the ophiolitic paradigm can potentially be useful. Further, Dilek (2003) suggested that the variety of chemical fingerprints, evolutionary paths, and tectonic environments of origin for ophiolites can reasonably be expanded to those bodies that differ from the strict definition of an ophiolite agreed to by the 1972 Penrose Conference.

To understand the origins of these bodies, it is useful to assess whether they exhibit chemical characteristics similar to a MORB cumulate, or a residue of partial melting of the DMM, equivalent to an abyssal peridotite. Although the ultramafic bodies examined here contain limited numbers of phases, it can be useful to compare the behavior of lithophile elements such as Mg, Al, Si, and Ti to that of the moderately siderophile (MSE) elements such as Ni, and the highly siderophile elements (HSE)

such as Re and Os. Under mantle partial melting conditions, a melt residue like abyssal peridotites will become depleted in SiO_2, Al_2O_3 and CaO relative to PM while a primary melt like MORB will be enriched in these elements relative to PM. Generally, a mantle melt residue will be enriched in MgO and Cr_2O_3 relative to PM while a primary melt will be depleted in these elements. With higher degrees of partial melting, the Cr# of a residue will tend to increase while Mg# tend to decrease (Niu 1997).

Enrichments and depletions resulting from partial melting of a mantle peridotite can be difficult to distinguish from those of a MORB cumulate. While a MORB melt may be enriched in incompatible elements relative to PM, when olivine crystallizes and is segregated at the bottom of a magma chamber, it will be enriched relative to the starting melts in elements compatible with crystallization and depleted in elements incompatible with crystallization. To assess these fractionations, data from the Twin Sisters dunite has been included for comparison. The Twin Sisters dunite has been interpreted to be the magma chamber cumulate of a MORB-like melt (Onyeagocha, 1974). Dunite from this location is used as a whole rock standard (DTS-1) and therefore its major and trace element content is well constrained (Jochum et al., 2005).

For all six bodies, there are depletions relative to DMM in CaO, TiO_2, and Al_2O_3 while MgO and Cr_2O_3 are enriched relative to DMM (Figure 4-1). A positive correlation between MgO and Al_2O_3 provides evidence for the variable loss of a melt component (Figure 4-3) and is comparable to the depletion trends recorded in other ophiolite peridotites (Büchl et al., 2002,; Godard et al., 2000; Schulte et al., 2009). Melt depletion trends like MgO versus CaO (Figure 4-5) are also consistent with melt

depletion. The data are broadly consistent with a mantle partial melt residue although the Twin Sisters dunite, a magma chamber cumulate, also overlaps with the data.

The trace element V can also be a sensitive indicator of mode of origin as it will be depleted relative to PM in mantle partial melt residue. However, V is sensitive to oxygen fugacity. For most samples examined here, V shows a clear positive correlation with Al_2O_3 (Figure 4-7) consistent with trends observed in abyssal peridotites. One sample each from Addie and Ellijay, however, plot off this trend. These samples are also considerably enriched in Cr, with approximately 3.5 and 2.5 wt. % Cr_2O_3 respectively suggesting that V content may be dependent, to some extent, on the availability of chromite for compatible structural sites. Overall, trace element contents and trends are broadly consistent with a mantle partial melt residue although the data again overlaps with the Twin Sisters dunite.

5-2: Formation of the Ultramafic Bodies – Chromite

When compared to whole rock chemistry and petrologic characteristics, chromite or Cr-spinel is commonly used to discriminate among different types of ultramafic bodies. All of the bodies in this study contain Cr-spinel as an accessory phase so it is useful to compare the different bodies. Since chromite is common in the ultramafic section of many ophiolites and one of the earliest minerals to form, it can serve as a sensitive indicator of the petrogenesis of its host (e.g. Barnes, 2000; Walker et al., 2002; Arai et al., 2011; Zhou et al., 2014). The degree of mantle melting, mantle composition, and pressure-temperature conditions can lead to distinct variations in the composition of chromite making it a diagnostic indicator of different tectonic settings

(e.g. Irvine, 1967; Barnes and Roeder, 2001; Arai et al., 2011). Under higher degrees of partial melting, Cr# increases and Mg# decreases yielding an inverse correlation between these parameters (Dick and Bullen, 1984).

Dunites are usually the products of melt focusing and should have higher Cr# and thus shift toward the upper right corner of Figure 5-1 (Kelemen et al., 2000; Standish et al. 2002). Fractionation of magnesium between the olivine and chromites would yield a different trend in the data than is evident in this study (Standish et al. 2002) so although these chromites have likely been either partially melted to higher degrees than most ophiolites or altered to higher Cr# and lower Mg# by alteration, their diagnostic usefulness is not entirely negated. Regardless of the modifying effects, the Cr # and Mg# data are consistent with the residue of at least one episode of partial melting.

When compared to primary ophiolite chromite described in Barnes and Roeder (1991), the chromite data for all the ultramafic bodies in this study lie outside of the fields said to encompass 90% of the ophiolite sampled in that study (Figure 5-1). This may be the result of higher degrees of partial melting, metamorphism that tends to drive Cr-spinel to more Fe-rich compositions, or the ophiolite data compiled by Barnes and Roeder are not representative of the full spectrum of ophiolite variability. Considering that only some of the data from Taitao Ophiolite fit into the 90% field, the possibility that the fields do not encompass the full range of ophiolite variability must be considered.

There is modest overlap with the forearc peridotite field from Dubois-Côté et al. (2005) for some samples, although data for most of the studied samples lie outside

these fields. Forearc peridotites are hypothesized to form in the SSZ zones that may be the tectonic settings that have generated most of the ophiolites around the world (Dilek and Furnes, 2014).
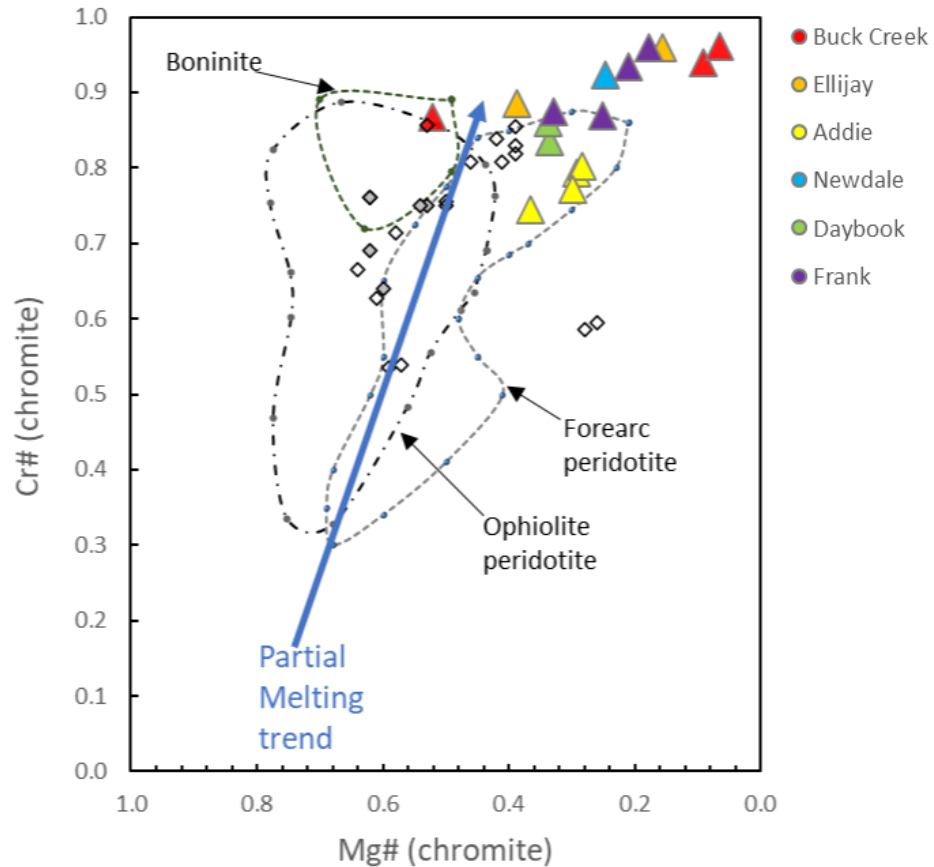

Figure 5-1: Plot of Mg# vs. Cr# for chromite grains. Data from the Taitao (Schulte et al., 2009) and Troodos (Büchl et al., 2002) Ophiolites are included for comparison. Note that values are reversed on the x-axis. The partial melting trend is from Dick and Bullen (1984) and Niu (1997), the ophiolite peridotite field is from Barnes and Roeder (1991), the forearc peridotite and boninite fields are from Dubois-Côté et al., (2005).

The Cr-spinel can also be used as a means of assessing the tectonic setting in which ultramafic bodies have been generated. Most ophiolites are hypothesized to have

been generated in either MOR- or suprasubduction zone (SSZ-) type settings although ~75% are thought to be associated with SSZ. As described by Dilek and Furness (2011), a SSZ setting is one in which oceanic crust forms above a subduction zone as the overriding plate is extended. The material generated in these zones can range from MORB-like melts to highly refractory boninite melts (Figure 5-2).
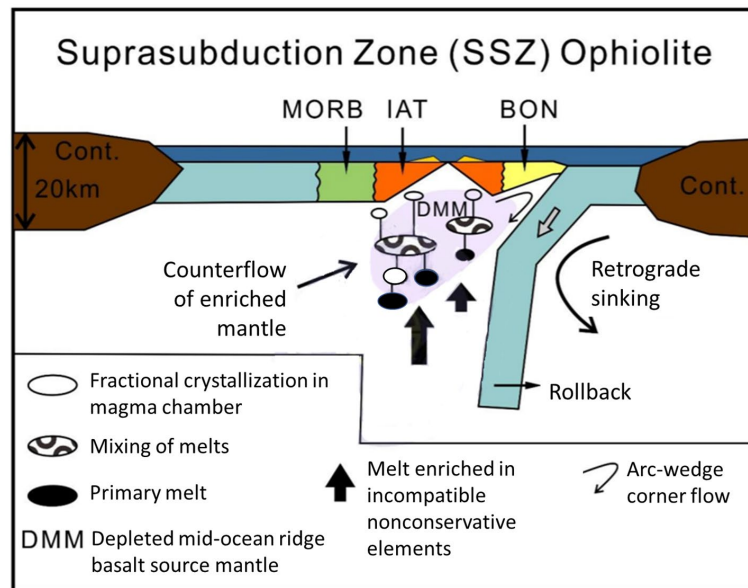

Figure 5-2: Schematic of the setting in which a SSZ ophiolite may be generated. Image is adapted from Dilek and Furnes (2014). Slab rollback is thought to extend the overriding plate and may contribute to the development of ophiolites. A tectonic regime similar to this schematic is thought to have existed prior to the Taconic orogeny in the region that is North Carolina today.

When compared to whole rock chemistry and petrologic characteristics, chromite can be used to discriminate among different types of ultramafic bodies. The

Cr#'s generally increase from lherzolites to harzburgites due to partial melting (Dick and Bullen, 1984) or melt percolation processes (Büchl et al., 2004; Kelemen et al., 1997). Ishiwatari (2003) used Cr# as an important parameter for classifying ophiolites. The LOT-type have Cr# 0.3-0.5, HOT-type 0.5-0.7 and LHOT-type 0.7-0.9. Derbyshire et al. (2013) found that Cr# greater than 0.60 correlated with ophiolites created in suprasubduction zones (SSZ) while Cr# less than 0.60 was more likely to be MOR origin. Chromite grains in this study have Cr#'s ranging from 0.75 to 0.96 consistent with peridotites generated in SSZ (Derbyshire et al., 2013) and with the depleted LHOT-type ophiolites of Ishiwatari (2003).

To form chromitite deposits, Cr must be mobilized and concentrated from the upper mantle so chromites average large domains of the DMM (Büchl et al., 2004; O'Driscoll et al., 2015). Kamenetsky et al. (2001) found that Al_2O_3 and TiO_2 concentrations in chromites largely fell into two groups or fields which could be used as a means of discriminating between spinel created in SSZ settings versus MOR settings. Samples from this study more closely match the SSZ than the MOR field (Figure 5-3). When compared to the Taitao Ophiolite which was likely generated in a MOR setting, the North Carolina spinel are distinct and do not appear to overlap with the MOR field. The Twin Sisters chromite data to not appear to overlap with either the Taitao data or North Carolina data. While the Twin Sisters data are coincident with the SSZ field, they are disparate from the North Carolina data, particularly in terms of TiO_2 concentration. Therefore, it is most likely that these bodies were generated in a SSZ setting and a cumulate origin is less favored by the data than a residual origin.
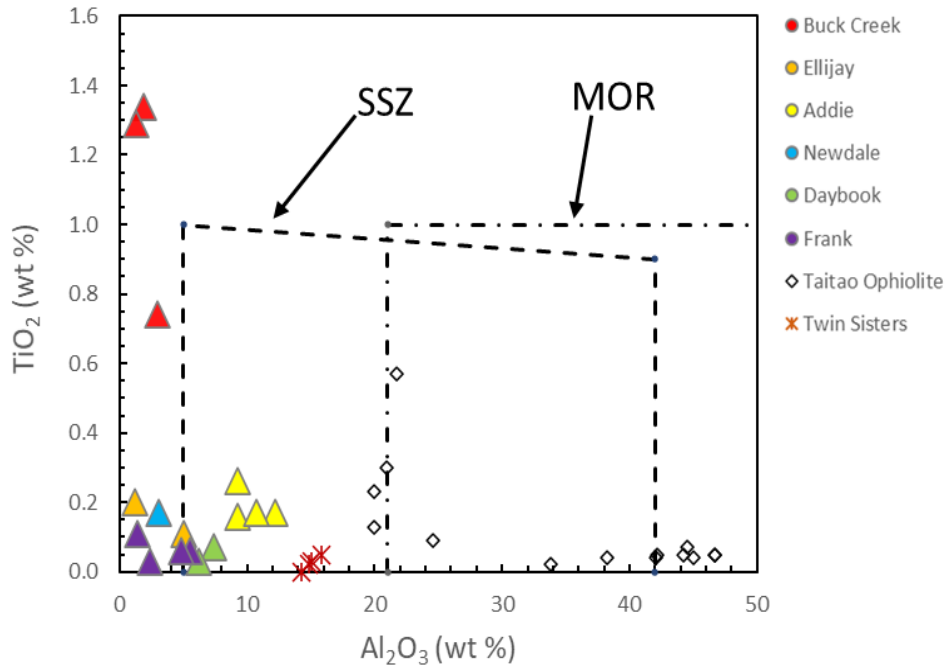
Figure 5-3: Plot of spinel Al_2O_3 vs. TiO_2 for chromite grains. Data from the Taitao Ophiolite (Schulte et al., 2009) and the Twin Sisters dunite (Onyeagocha, 1974) is included for comparison. The SSZ and MOR fields are from Kamenetsky et al. (2001).

5-3: Formation of the Ultramafic Bodies – Re-Os

The highly siderophile and chalcophile natures of Re and Os make the isotopic system particularly useful to study the origin of ultramafic bodies when compared to the evolution of DMM. The decay of ^{187}Re to the stable daughter isotope ^{187}Os through β^- emission has a half-life of $41.6 *10^9$ years (Smoliar et al., 1996). During partial melting in the mantle, Re is moderately incompatible while Os is highly compatible. Mafic oceanic crust is, therefore, enriched in Re and highly depleted in Os relative to mantle sources. With time, oceanic crust becomes highly radiogenic. Conversely, when

mafic melt is removed from the DMM, the rate of growth of the $^{187}Os/^{188}Os$ ratio in the residual upper mantle is retarded.

Abyssal peridotites are thought to be the residues of melt extraction that creates MORB. Abyssal peridotites have Os isotopic compositions that vary widely from 0.114-0.167 (e.g. Snow and Reisberg, 1995; Brandon et al., 2000; Standish et al., 2002; Alard et al., 2005; Harvey et al., 2006; Liu et al., 2008; Aldanmaz et al., 2009; Lassiter et al. 2014; Gong et al., 2019) with an average $^{187}Os/^{188}Os$ of 0.125 (Snow and Reisberg, 1995; Brandon et al., 2000; Standish et al., 2002; Alard et al., 2005; Harvey et al., 2006; Liu et al., 2008). If a relatively robust age constraint is possible, a comparison of an isotopic evolution trajectory defined by data extracted from modern abyssal peridotites can be used to assess whether the ultramafic bodies have compositions consistent with average DMM at the time of formation.

One means to assess the origin of ultramafic bodies is to consider initial isotopic ratios compared to MORB, abyssal peridotites, and ophiolite peridotites. To compare settings of different ages, it is useful to use the $\gamma_{Os(t)}$ notation which describes the percentage difference between the Os isotopic composition of a sample at time (t) compared to a chondritic reference value at that time. Samples with $\gamma_{Os(t)} > 0$ are described as enriched or suprachondritic which implies a long-term elevated $^{187}Re/^{188}Os$. Samples with $\gamma_{Os(t)} < 0$ are described as depleted or subchondritic and imply a long-term decrease in $^{187}Re/^{188}Os$ (Shirey and Walker, 1998).

Walker (2016) compiled Os data from 188 abyssal peridotites (average γ_{Os} -1.3), 125 MORB (average γ_{Os} +4.7), and over 100 samples from the Unst, Leka, and Taitao Ophiolites (average γ_{Os} -0.1) into a representative histogram. When compared

to the compiled data, the North Carolina samples appear to be slightly more radiogenic than the chondritic reference (average γ_{Os} +1.1), approximately 2.5% more radiogenic than the modern abyssal peridotite average, only 1% more radiogenic than the ophiolite average, and approximately 3.5% less radiogenic than the MORB average (Figure 5-4) and exhibit a distribution broadly similar to abyssal peridotites. The data provide support for an origin as residues from the upper mantle.
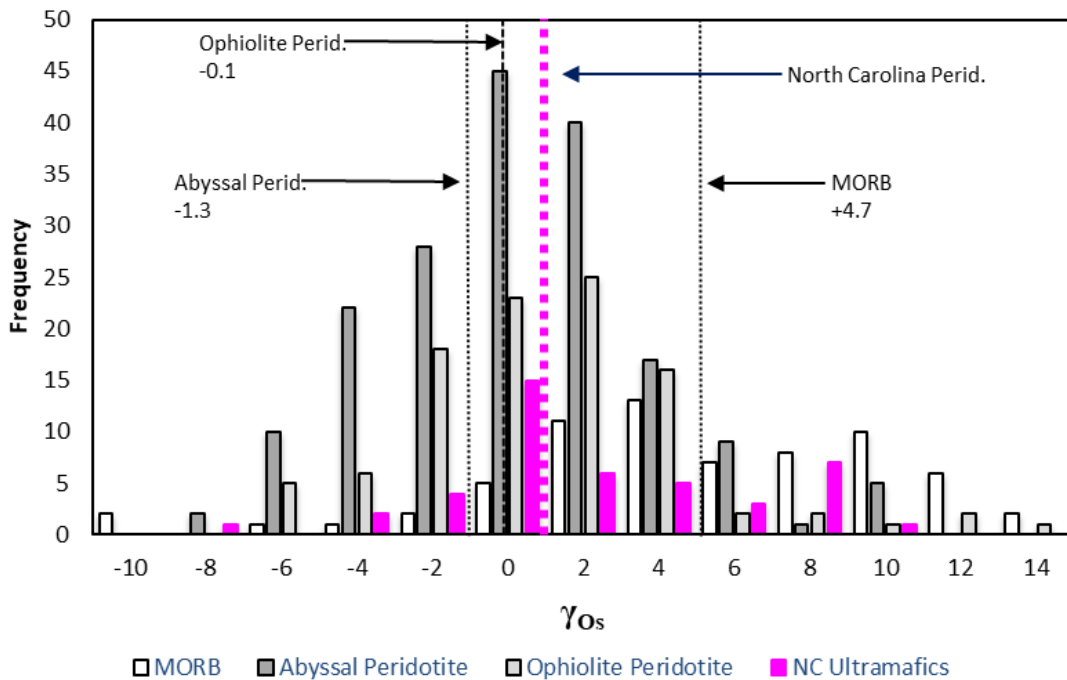

Figure 5-4. Histogram plot of γOs values of MORB, abyssal peridotite, ophiolite peridotite, and North Carolina peridotites adapted from Walker (2016). Average values are shown for comparison. Abyssal peridotite data are from Snow and Reisberg (1995), Luguet et al. (2001), Alard et al. (2005), Becker et al. (2006), Liu et al. (2009) and Lassiter et al. (2014). Ophiolite data are from Schulte et al. (2009) and O'Driscoll et al. (2012, 2015).

Nevertheless, when the bodies are assessed by host formation and geographic association rather than grouped together, a difference is noted (Figure 5-5). Values from the southern bodies hosted in the Tallulah Falls formation average +2.8. By contrast, the northern bodies hosted in the Ashe formation average -1.34, and closely match the abyssal peridotite average. This disparity between the northern and southern bodies suggests that while most major and trace element trends suggest a residual origin for these bodies, the possibility of different histories must be considered.

When compared with major and trace elements, this disparity in histories between the bodies hosted in the Tallulah Falls versus Ashe formations, the Os isotopes differences in source must be considered. Herzberg et al. (2016) found that partitioning of Ni between melt and olivine is pressure dependent. For a given MgO content, lower Ni in olivine is associated with a greater depth of melt/olivine equilibration. When the Ni contents of the two bodies are compared (Figure 4-8), there is a distinction between the bodies hosted in the different formations. If the ultramafic bodies were derived from different depths within the SSZ, they could also be derived from Os isotopic reservoirs of different compositions.
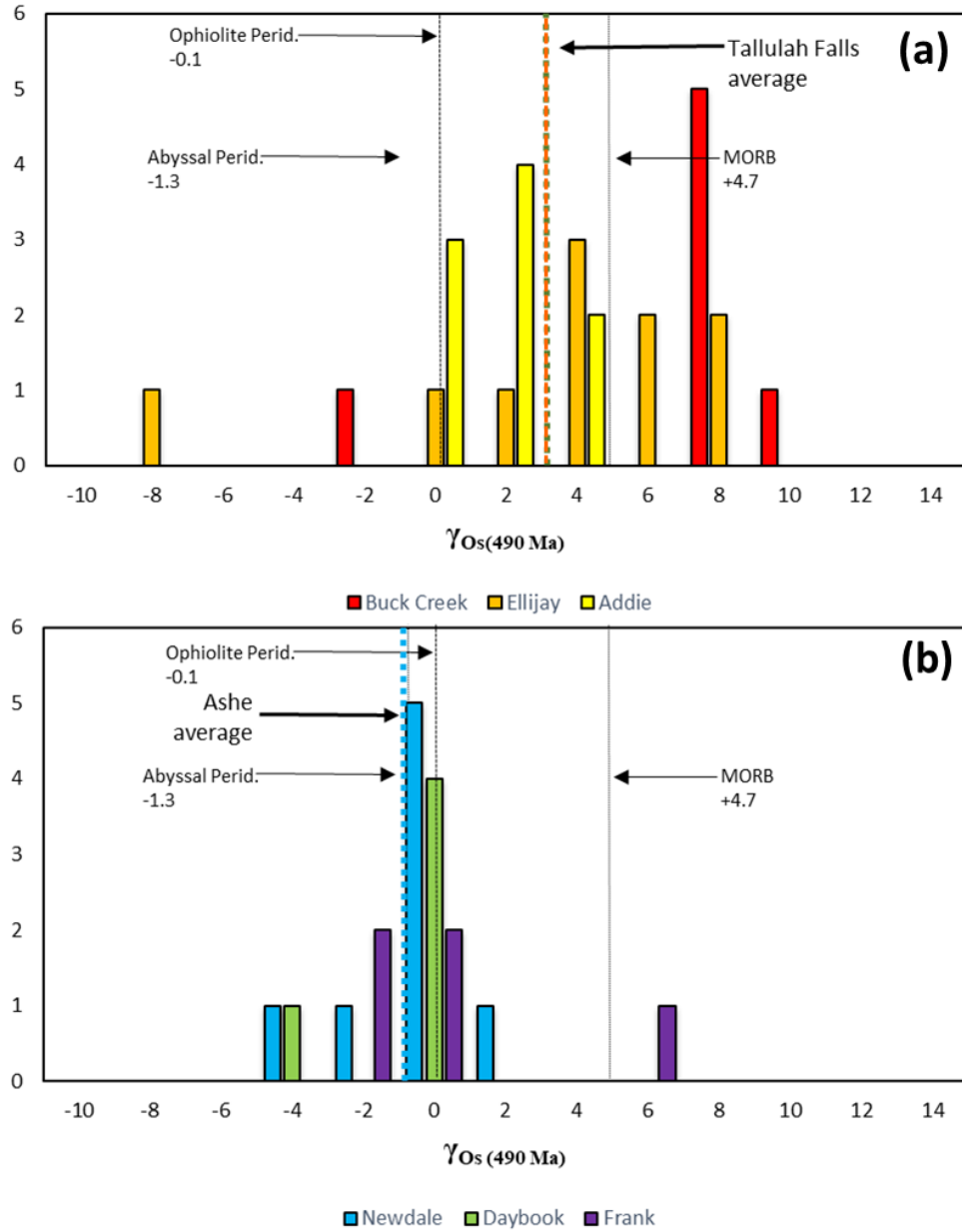
Figure 5-5. Histogram plot of γOs values of North Carolina peridotites adapted from Walker (2016). Histogram (a) shows the southern bodies hosted in the Tallulah Falls formation and a γOs average value of +2.8 while (b) shows the northern bodies hosted in the Ashe formation with a γOs average value of -1.34. Vertical lines represent the average γOs values of MORB, abyssal peridotite, and ophiolite peridotites.

5-4: Metamorphism

The application of Os isotopes in ophiolites faces some challenges. The mantle sections of almost all ophiolites are altered either through metasomatism or other metamorphic processes and constraining the effects of alteration can be difficult. In the Troodos Ophiolite Complex, Os isotopic compositions in some melt channels were significantly more radiogenic relative to PM while the surrounding harzburgites were only slightly suprachondritic suggesting that Os be modified during melt percolation (Büchl et al., 2002, 2004). This suggests that highly siderophile elements (HSE) like Os can be used as proxies for melting and enrichment processes in the mantle-derived materials but only if a careful assessment of the alteration history of the rock is possible.

A considerable amount of Os isotopic heterogeneity exists among the ultramafic units in this region. Samples with very low Re/Os, thus requiring minimal age correction, are characterized by calculated initial Os isotopic compositions that vary by 12%. Further, the Os isotopic compositions exhibit differences beyond statistical uncertainty between bodies. Isotopic heterogeneity within units is relatively minor with the exception of Buck Creek and Ellijay. Buck Creek is likely to have seen granulite facies metamorphic conditions while Ellijay is the only body to exhibit thick interlayering between Cr-spinel and dunitic layers. The isotopic heterogeneity is generally consistent with earlier studies of abyssal peridotites and individual ophiolites (0.117-0.158; Snow and Reisberg, 1995; Brandon et al., 2000; Walker et al., 2004; Harvey et al., 2006; Schulte et al., 2009; O'Driscoll et al., 2012, 2018).

One means of assessing alteration history is to evaluate the degree of serpentinization. The ultramafic bodies in this study exhibit low degrees of

serpentinization compared to abyssal peridotites and many ophiolite peridotites. Bulk rock LOI can be used as a proxy for degrees of serpentinization. When LOI is compared to γOs values, there is no obvious correlation with degree of serpentinization (Figure 5-6), and the most radiogenic samples have considerably less LOI than samples with chondritic γOs values. Based on this observation, and the agreement between whole rock and chromite separate γOs values (Figure 4-14), it is concluded that the effects of serpentinization on the relative abundances of Os isotopes were minimal and the γOs values of these samples are due to mantle source heterogeneity or processes other than serpentinization.
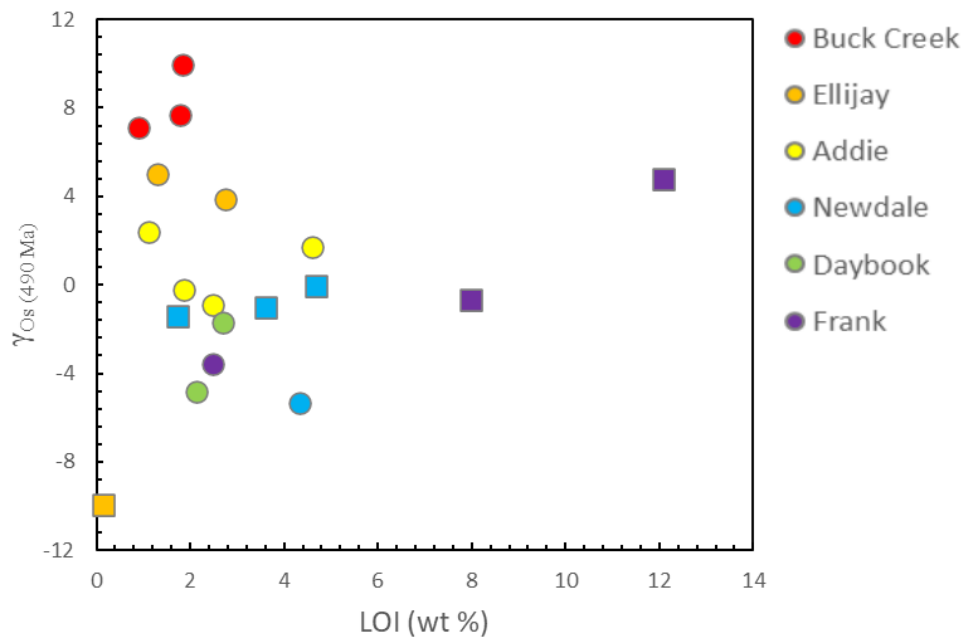

Figure 5-6. LOI vs. γOs$_{(490Ma)}$ of dunite (circles) and harzburgite (squares).

Studies of abyssal peridotites and ophiolite peridotites have found that Os systematics may be explained by recent melt extraction events modifying ancient melt depletion trends (Harvey et al., 2006; Liu et al., 2008; Schulte et al., 2009; O'Driscoll

et al., 2012). If a rock has experienced a melt depletion event, Al_2O_3 should correlate with $^{187}Os/^{188}Os$ in the residue because, like Re, it is moderately incompatible. If the initial isotopic composition of the bodies adhere to an evolution trend consistent with the DMM, this can provide a means of reference for comparison (Reisberg and Lorand, 1995; Walker et al., 1989, Rudnick et al. 2002). Samples from Buck Creek, and one each from Ellijay and Frank do not fall on the trend expected for the DMM suggesting a later process superimposed on the earlier melting event (Figure 5-7).
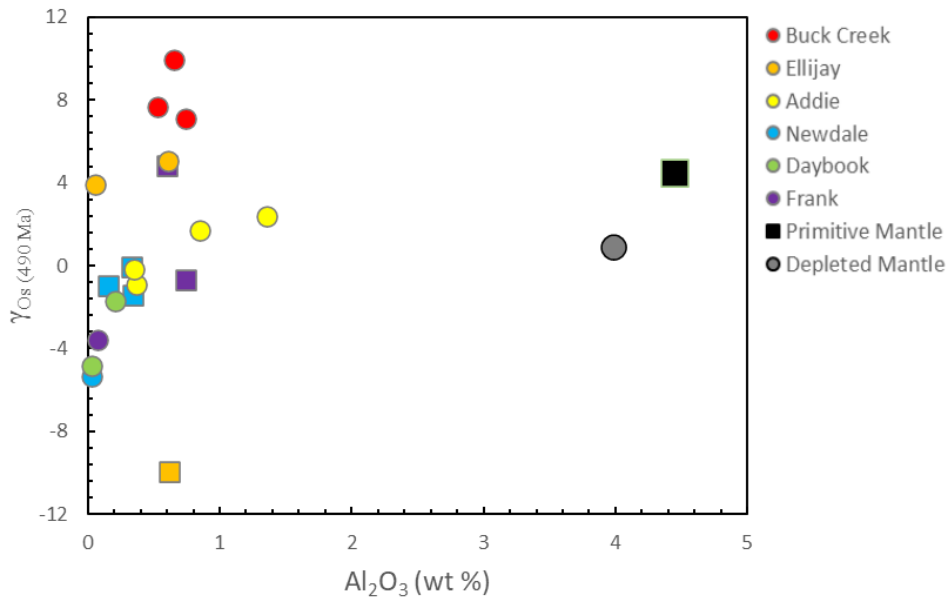

Figure 5-7. Al_2O_3 vs. $\gamma Os_{(490\ Ma)}$ of dunite (circles) and harzburgite (squares). The PM estimate is from McDonough and Sun (1995) and the DMM estimate is from Workman and Hart (2005) and Walker et al., (2002).

Comparison of $^{187}Os/^{188}Os$ with Mg #, which is a marker of fertility, has also been found to produce a linear relationship if the peridotites have undergone a melt depletion event. For most samples, there is a strong negative correlation that corresponds with the melt depletion trend (Figure 5-8). However, the same Buck Creek,

Ellijay, and Frank samples do not fall on the trend again suggesting a later process has be superimposed upon the earlier melting event.
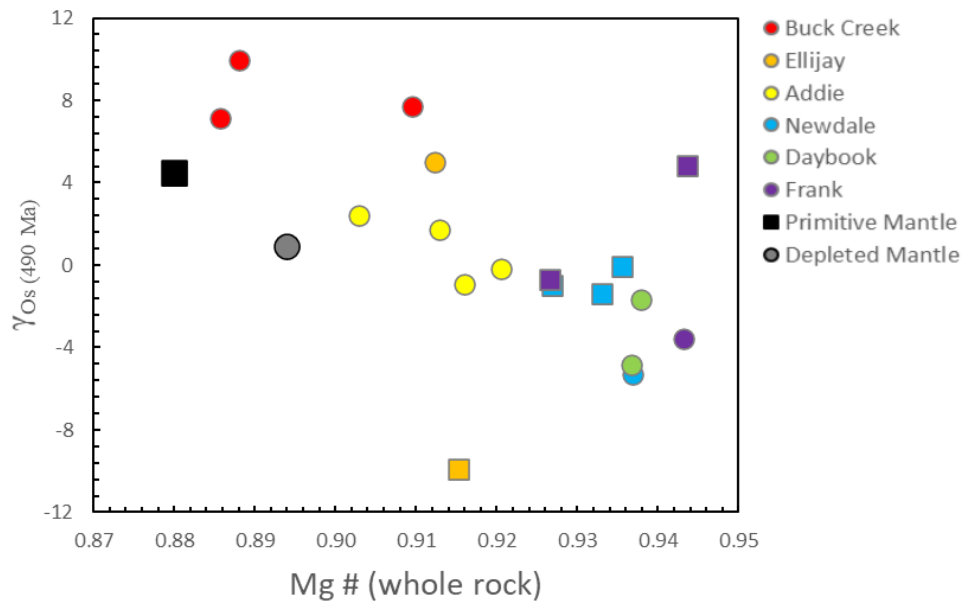

Figure 5-8. Mg # vs. $\gamma Os_{(490\ Ma)}$ of dunite (circles) and harzburgite (squares). The PM estimate is from McDonough and Sun (1995) and the DMM estimate is from Workman and Hart (2005) and Walker et al. (2002).

The source of the suprachondritic Os is difficult to assess. Chromite-whole rock pairs exhibit a general agreement in γOs composition. Chromite is more resistant to alteration which suggests that the initial isotopic values are of most samples have been retained through any later alteration process, including serpentinization (Figure 5-9). Some samples plot off the 1:1 reference line. The Ellijay sample which shows the lowest γOs value also shows an enrichment in Cr relative to other samples in the body but does not otherwise show any notable differences relative to other Ellijay samples or other bodies.

Studies of the Troodos, Shetland, and Leka ophiolites record more radiogenic Os relative to a chondritic reference (Büchl et al., 2002; O'Driscoll et al., 2012, 2015, 2018). These more radiogenic values are associated with melt channels and reflect heterogeneities at the meter scale. Melt channels were not observed in this study nor was grid sampling employed. Most of these bodies have been extensively mined so by necessity, the samples in the study were not collected from the center of the body but nearer the margins or from float so a certain level of sampling bias must be considered. Absent further sampling and observation of the bodies, the nature of this Re and radiogenic Os enrichment may not be resolvable.

5-5: Serpentinization and dehydration

The North Carolina ultramafic bodies in this study are unusual in that they exhibit relatively clean olivine and chromite with low degrees of serpentinization compared to many ophiolites. One of the hypotheses for this appearance is that the ultramafic bodies were serpentinized and subsequently dehydrated and recrystallized in an alteration event. Deschamps et al. (2013) found very minor changes in major element compositions over a broad range of serpentinization percentages therefore, major oxides are unlikely to discriminate between a peridotite that was serpentinized and subsequently dehydrated. The olivine crystals in the bodies do not have magnetite inclusions which is a textural suggestion that they have not been pervasively serpentinized, then dehydrated. Oxygen isotope ratios in potential mantle rocks can be used as a means of constraining the possibility contamination by crustal igneous rocks,

sediments, and fluids. Oxygen isotope data for both whole rock powders and olivine separates (Figure 5-10) were used to assess this possibility.

Hydrothermal alteration under lower temperature conditions and by high ^{18}O water would raise the δ^{18}O values, and at high temperature with a low ^{18}O water would reduce the δ^{18}O values. Olivine oxygen isotope compositions provide a measure of the δ^{18}O of the high temperature rock. If the whole rock values are shifted from equilibrium with the olivine, they will indicate alteration upon cooling. If the olivine is shifted from a mantle δ^{18}O value, it will indicate recrystallization of an altered rock (e.g. Chiba et al., 1989; Eiler, 2000, 2001; Miller, 2001; Widom and Farquhar, 2003; Chaumba, 2014).
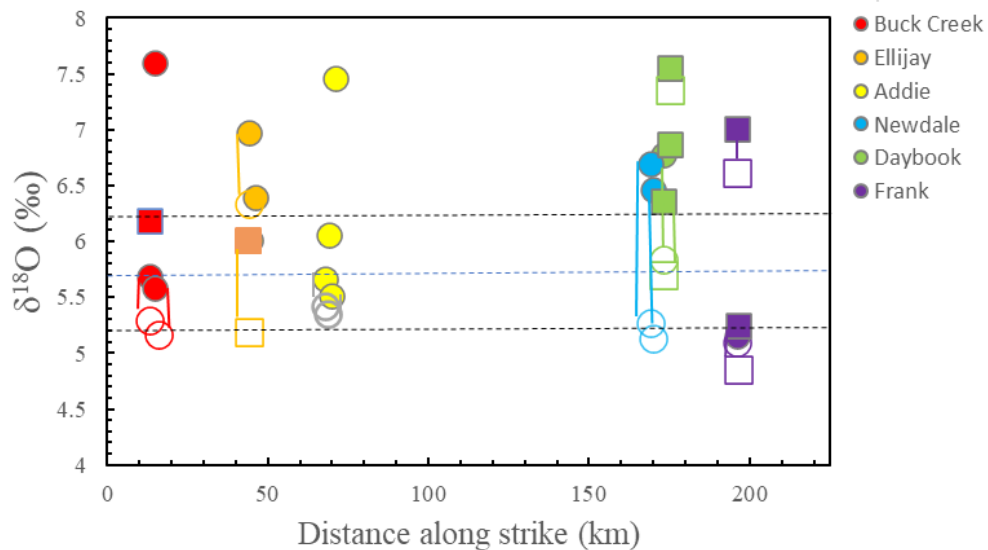

Figure 5-10: Distance along strike relative to the Georgia/South Carolina border vs. whole rock (filled symbols) and olivine separate (open symbols) oxygen isotopic values for dunite (circles) and harzburgite (squares). Tie lines link the same samples. Estimated mantle peridotite values of 5.7 ± 0.5‰ (Eiler et al., 1998) are for comparison.

Little fractionation occurs between olivine and water at either high or low temperatures. Based on calculations derived from Clayton and Keiffer (1991) and Hu and Clayton (2003), $\alpha_{olivine-water}$ at 750°C is 0.997 and 0.996 at 350°C when $\alpha_{forsterite-calcite}$ is divided by $\alpha_{calcite-water}$. Seawater and meteoric water have a $\delta^{18}O$ value of 0‰ therefore lower oceanic crust and serpentinized uppermost oceanic mantle that has interacted with seawater at high temperature will be driven to lower oxygen isotope values due to this interaction and may range in value to as low as +2‰ (Muehlenbachs and Clayton, 1976; Hart et al., 1999). The mantle-like $\delta^{18}O$ values of the olivine suggest that the grains did not alter in the presence of meteoric or seawater and therefore could not likely have been serpentinized and subsequently dehydrated.

The $\delta^{18}O$ values for individual olivine grains from these bodies range from +4.85 to +7.36‰, and the values whole rock powders range from +5.16 to +7.60‰, which broadly agrees with, but extends above the estimated mantle value of 5.2 ± 0.1‰ (Massey et al. 1994) and 5.7 ± 0.5‰ (Eiler et al. 1998). Kyser (1986) found olivine oxygen isotopes ranging from +4.5 to 7.2‰ and Lecuyer and Gruau (1996) observed olivine oxygen isotopes ranging from +4.5 to 6.5‰ in samples from the Hess Deep.

The olivine grains more closely approximate the oxygen isotopic compositions of the mantle at the time of formation while some whole rock samples reflect $\delta^{18}O$ values higher than accepted mantle values. There are a number of possible explanations for this shift to higher $\delta^{18}O$ values.

Shifts to higher $\delta^{18}O$ values might reflect incorporation of a portion of sediment or crustal material into these bodies at some point in their history. Sediments can have $\delta^{18}O$ values of +10 to 20‰. If we assume a starting $\delta^{18}O$ value of +5.7‰ and a crustal

component with a $\delta^{18}O$ value of $+12‰$, the $\delta^{18}O$ values could be shifted to $+7.0‰$ with an incorporation or mixing of 20% of the enriched material.

Contamination by this volume of crustal material would also likely be seen in other parameters such as Mg#. When comparing Mg# to oxygen isotopes, it becomes clear that there is no correlation between these parameters (Figure 5-11). Some of the highest Mg#'s have low oxygen values and the highest oxygen value has an Mg# similar to DMM. It is evident that the source of the elevated oxygen values cannot have been high temperature interaction with seawater, meteoric water, or crustal materials, therefore, the elevated oxygen values likely reflect something else, such as source heterogeneity or late stage low-temperature processes.

A late stage low temperature alteration must be considered to explain the elevated oxygen values. In the Oman ophiolite, Kelemen et al. (2011) found that when peridotite was thrust atop meta-sediments, the underlying formations produced CO_2-rich fluids that induced alteration at temperatures below 200°C. Steatization processes similar to this can produce alteration in peridotites at temperatures as low as 30°C. The alteration is concentrated along grain boundaries and fissures in the rock converting olivine to magnesite. These grain boundary alterations can be near isochemical for all elements except H_2O and CO_2 (Kelemen et al., 2011).

Magnesite has $\delta^{18}O$ values of $+25$ to $36‰$. If we assume a starting $\delta^{18}O$ whole rock value of $+5.7‰$ and magnesite with a $\delta^{18}O$ value of $+25‰$, the $\delta^{18}O$ values could be shifted to $+6.5‰$ with a grain boundary alteration of 4%, values could be shifted to $+7.6‰$ with a grain boundary alteration of 10%. This percentage of grain boundary alteration could also explain some of the elevated LOI with low apparent degrees of

serpentinization. Magnesite is 50% CO_2 therefore heating during analysis of pure mineral grains would have 51% LOI (Bishop et al., 2013). Magnesite alteration of 10% would then likely produce a LOI of at least 5%. Since this alteration is near isochemical, it would not perturb major and trace elements or Os isotopic compositions. Therefore, given the data, it is likely that the elevated $\delta^{18}O$ values are due to low temperature late-stage alteration of some of these ultramafic bodies.

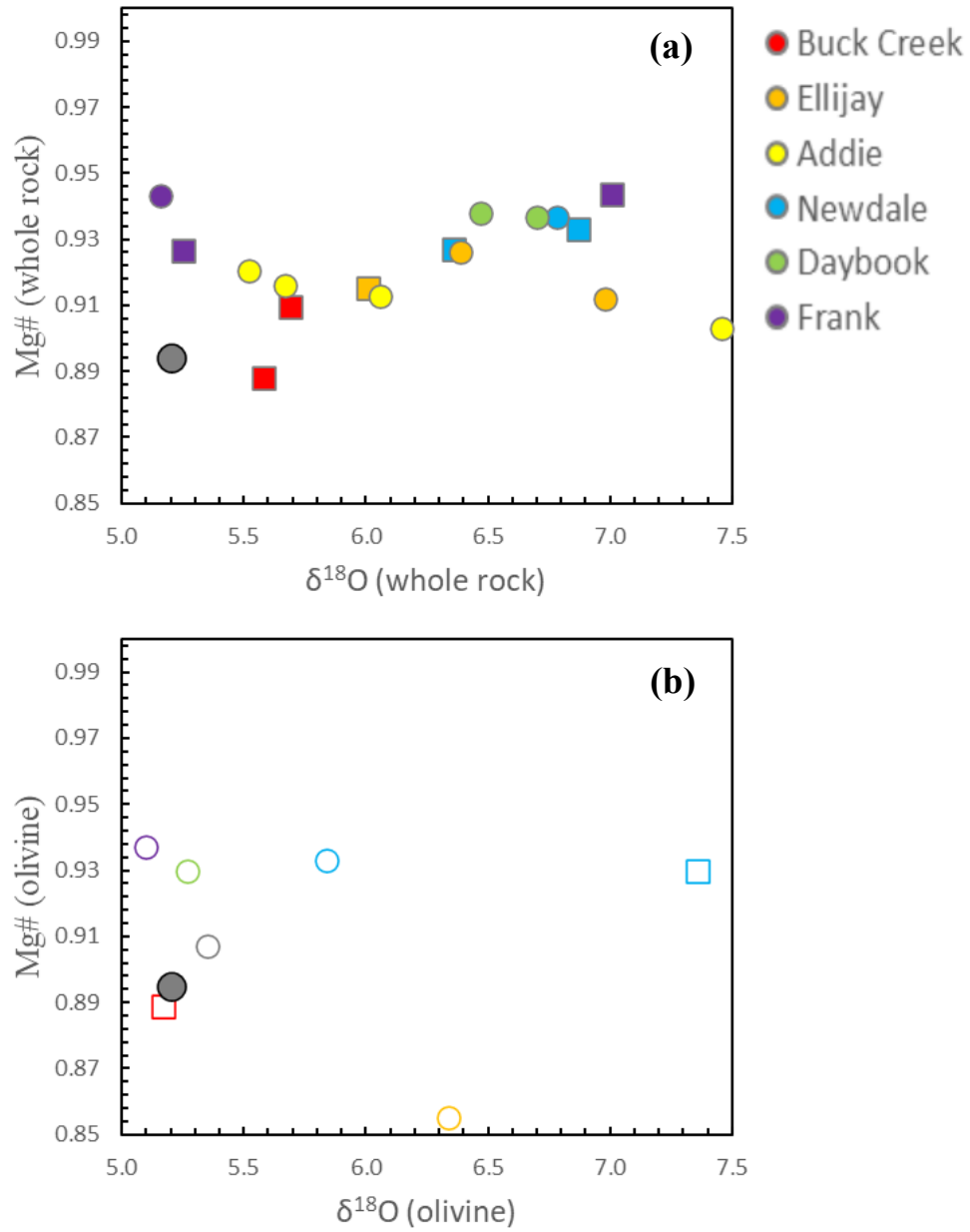Figure 5-11: Whole rock (a) and olivine (b) $\delta^{18}O$ versus Mg# of whole rock samples. Circles represent dunite, squares represent harzburgite samples. DMM Mg# is from Workman and Hart (2005), $\delta^{18}O$ value is from Eiler et al. (1998).

Chapter 6: Conclusions

This study investigates six ultramafic bodies located in the Blue Ridge Province of the Appalachian Mountains. Based on the major and trace element evidence including positive correlations between Al_2O_3 and MgO and Al_2O_3 and V, we suggest that these bodies are more similar to abyssal peridotites that MORB and therefore are likely the residue of at least one partial mantle melting event. The variable loss of a melt component is comparable to the depletion trends recorded in other ophiolite peridotites such as the Troodos, Taitao, Shetland, and Leka Ophiolites. Chromite data appear to exclude the possibility of creation of these bodies in a MOR setting but is consistent with a SSZ setting.

A typical feature of mantle peridotites from SSZ settings is considerable Os isotopic heterogeneity. In the case of the North Carolina peridotites, the γOs values share a similar distribution to abyssal peridotites and ophiolite peridotites and poor correlation with MORB γOs values. However, when the bodies are separated by host formation, Buck Creek in particular appears to suggest the addition of a radiogenic component subsequent to mantle extraction. Whether this component was melt percolation or melt/rock reaction adjacent to veins is unresolved at this time but it is unlikely to have been either recent or ancient Re addition.

The emplacement of these bodies has been the subject of debate. It has been hypothesized by other researchers that these bodies were once serpentinized and subsequently dehydrated. Oxygen isotopes in this study exhibited more variability than some ophiolite peridotites but with $\delta^{18}O$ values ranging from +4.85 to +7.60‰ serpentinization and dehydration at high temperatures can be excluded as a possibility.

The source of the higher than average values is still uncertain, but the incorporation of the volume of a crustal component necessary to shift $\delta^{18}O$ values to $>+7‰$ can be excluded due to the lack of enrichment in other parameters. It is likely that at least some of the elevated $\delta^{18}O$ values are due to low temperature late-stage steatization or alteration of some of these ultramafic bodies.

Appendix I – Analytical Standards

Table A-1 XRF Standards. Fe_2O_{3T} represents Fe_2O_3 total. Sample 98-54 is a sample repeatedly analyzed at Franklin and Marshall College. BHVO-1 is the standard.

	98-54A	98-54B	98-54C	Average	2σ	BHVO-1 Measured	BHVO-1 Accepted	% Deviation
SiO_2	51.67	52.08	51.71	51.82	0.45	49.73	49.94	0.42
TiO_2	1.22	1.23	1.22	1.22	0.01	2.72	2.71	0.37
Al_2O_3	18.10	18.15	18.03	18.09	0.12	13.67	13.8	0.94
Fe_3O_2T	8.91	8.96	9.00	8.96	0.09	11.95	12.23	2.29
MnO	0.17	0.17	0.17	0.17	0.00	0.17	0.17	0.00
MgO	5.18	5.21	5.19	5.19	0.03	7.09	7.23	1.94
CaO	7.77	7.81	7.79	7.79	0.04	11.38	11.4	0.18
Na_2O	3.98	3.97	3.97	3.97	0.02	2..41	2.26	6.64
K_2O	1.05	1.04	1.04	1.04	0.01	0.53	0.52	1.92
P_2O_5	0.59	0.59	0.59	0.59	0.00	0.28	0.27	3.70
LOI	1.24	1.19	1.23	1.22	0.07			
Total	99.88	100.40	100.10	100.1	0.6	99.93	100.53	0.60
Rb	8.5	8.5	8.7	8.6	0.23	9.5	11	13.6
Sr	792	789	789	790	.	393	403	2
Y	25.1	25.3	25	25.1	0.3	27.7	27.6	0.4
Zr	130	129	129	129	1	176	179	2
V	200	184	189	191	16	311	317	2
Ni	61	59	58	59	3	115	121	5
Cr	102	83	82	89	23	296	289	2
Nb	8.9	8.7	8.7	8.8	0.2	19.8	19	4.2
Ga	20.7	20.3	20.7	20.6	0.5	21.1	21	0
Cu	76	74	78	76	4	123	136	10
Zn	85	83	83	84	2	101	105	4
Ba	560	576	563	566	17	132	139	5
U	0.5	0.7	0.9	0.7	0.4	0.8	0.4	100
Th	0.6	1.2	0.8	0.9	0.6	1.3	1.1	18.2
Co	31	30	31	31	1	41	45	9
La	19	22	21	21	3	14	16	13
Ce	42	43	42	42	1	36	39	8
Pb	7	8	7	7	1	4	3	33
Sc	22	21	21	21	1	31	32	3

Table A-2 Forsterite Fo90 olivine standard over a three-day period. Standard deviation (STD) is reported at the 1σ level.

Fo (90) Standard	MgO	CoO	Al$_2$O$_3$	CaO	SiO$_2$	MnO	Cr$_2$O$_3$	FeO	NiO	Total
OL-080204	48.99	0.053	n.d.	0.10	40.45	0.08	0.02	9.69	0.44	99.83
OL-080204	49.18	0.033	0.01	0.10	40.63	0.09	0.01	9.26	0.37	99.68
OL-080204	49.63	0.044	0.05	0.15	40.71	0.09	n.d.	9.51	0.38	100.56
OL-080204	49.40	0.035	0.02	0.12	40.80	0.08	0.02	9.63	0.30	100.39
OL-080204	49.27	0.038	0.00	0.08	40.79	0.09	0.02	9.59	0.41	100.30
OL-080204	49.47	0.028	0.01	0.13	40.97	0.07	0.02	9.57	0.29	100.56
OL-080304	49.60	0.046	n.d.	0.10	40.71	0.08	n.d.	9.40	0.38	100.33
OL-080304	48.93	0.036	0.01	0.11	41.00	0.11	0.01	9.59	0.34	100.14
OL-080304	49.64	0.012	n.d.	0.10	40.89	0.08	n.d.	9.30	0.30	100.32
OL-080304	49.47	0.061	n.d.	0.17	40.94	0.09	0.03	9.57	0.38	100.71
OL-080304	49.62	0.044	0.01	0.12	40.91	0.12	n.d.	9.44	0.41	100.66
Average	**49.38**	**0.039**	**0.01**	**0.12**	**40.80**	**0.09**	**0.01**	**9.51**	**0.37**	**100.32**
STD	0.26	0.013	0.01	0.03	0.16	0.01	0.01	0.14	0.05	0.33
Accepted Composition	49.42				40.81	0.14		9.55	0.37	100.29
% Deviation	0.01 %				0.15 %	-36%		0.73 %	1.40 %	0.01%

Table A-3 Typical Bushveld chromite standard analysis. Standard deviation (STD) is reported at the 1σ level.

Standard	MgO	CoO	Al$_2$O$_3$	MnO	SiO$_2$	Cr$_2$O$_3$	ZnO	NiO	FeO	TiO2	Total
Bush	10.71	0.05	15.0	0.40	0.00	45.9	0.06	0.09	25.49	0.56	98.2
Bush	10.70	0.07	15.1	0.45	0.00	46.3	0.08	0.11	25.55	0.56	99.0
Bush	10.55	0.07	14.9	0.41	0.00	46.1	0.06	0.07	25.59	0.53	98.2
Bush	10.63	0.08	15.0	0.45	0.00	46.5	0.05	0.10	25.62	0.49	99.0
Bush	10.67	0.06	14.8	0.43	0.00	46.6	0.09	0.10	25.55	0.5	98.9
Average	**10.65**	**0.07**	**15.0**	**0.43**	**0.00**	**46.3**	**0.07**	**0.09**	**25.56**	**0.53**	**98.7**
STD	0.06	0.01	0.1	0.02	0.00	0.3	0.02	0.02	0.05	0.03	0.4

Table A-4 Total Analytical Blank (TAB) Data.

TAB	Re (pg)	Os (pg)	$^{187}Os/^{188}Os$
6/7/2004	2.0	2.0	0.174
7/7/2004	1.6	2.3	0.192
11/24/2004	2.5	4.2	0.143
3/11/2005	7.4	3.0	0.151
5/10/2005	12.4	3.6	0.156
6/6/2005	3.9	4.5	0.143
7/5/2005	4.4	3.3	0.155

Table A-5 Osmium standard analyses for VG Sector 54 TIMS. 2SDM represents the percent

of standard deviation of the mean at the 2σ level.

VG Sector 54	$^{187}Os/^{188}Os$	2SDM	$^{186}Os/^{188}Os$	2SDM	$^{190}Os/^{188}Os$	2SDM	$^{189}Os/^{188}Os$	2SDM
6/9/2004	0.1138	0.0100	0.1199	0.0046	1.9837	0.0008	1.2198	0.0009
6/9/2004	0.1138	0.0427	0.1198	0.0174	1.9837	0.0022	1.2198	0.0025
7/15/2004	0.1138	0.0233	0.1198	0.0137	1.9837	0.0017	1.2197	0.0027
7/16/2004	0.1139	0.0365	0.1199	0.0183	1.9838	0.0021	1.2198	0.0022
10/26/2004	0.1138	0.0314	0.1199	0.0165	1.9836	0.0019	1.2197	0.0019
10/27/2004	0.1137	0.0524	0.1199	0.0242	1.9837	0.0026	1.2198	0.0041
2/17/2005	0.1137	0.0641	0.1198	0.0221	1.9838	0.0022	1.2198	0.0038
2/18/2005	0.1139	0.1080	0.1199	0.0476	1.9844	0.0041	1.2199	0.0072
2/19/2005	0.1139	0.0606	0.1198	0.0216	1.9839	0.0025	1.2198	0.0037
5/5/2005	0.1138	0.0630	0.1199	0.0195	1.9837	0.0027	1.2197	0.0031
5/6/2005	0.1139	0.0370	0.1199	0.0118	1.9837	0.0016	1.2197	0.0020
5/6/2005	0.1138	0.0338	0.1199	0.0148	1.9837	0.002	1.2197	0.0026
7/7/2005	0.1138	0.0357	0.1199	0.0146	1.9837	0.0018	1.2198	0.0026
7/9/2005	0.1137	0.0473	0.1199	0.0208	1.9837	0.0021	1.2198	0.0032
7/9/2005	0.1139	0.0364	0.1199	0.0111	1.9837	0.0014	1.2198	0.0025
average	0.1138	0.0455	0.1199	0.0186	1.9838	0.0021	1.2198	0.0030

Table A-6 Osmium standard analyses for NBS Bobcat TIMS. 2SDM represents the percent of

standard deviation of the mean at the 2σ level.

NBS Bobcat	$^{187}Os/^{188}Os$	2SDM	$^{190}Os/^{188}Os$	2SDM	$^{192}Os/^{188}Os$	2SDM
4/5/2004	0.1140	0.0001	1.9836	0.0097	3.0758	0.0029
1/1/2005	0.1140	0.0001	1.9836	0.0010	3.0758	0.0029
2/19/2005	0.1144	0.0002	1.9843	0.0018	3.0641	0.0039
5/6/2005	0.1148	0.0004	1.9811	0.0059	3.0772	0.0109
6/22/2005	0.1140	0.0003	1.9835	0.0019	3.0621	0.0053
7/6/2005	0.1143	0.0026	1.9866	0.0046	3.0643	0.0091
average	0.1142	0.0006	1.9838	0.0041	3.0699	0.0058

Table A-7 The University of Wisconsin (UWG-2) garnet standard. Standard deviation (STD)

is reported at the 1σ level.

Standard	$\delta^{17}O$	$\delta^{18}O$	$\delta^{17}O$
UWG-2	3.00	5.70	0.02
UWG-2	3.05	5.86	-0.02
UWG-2	3.03	5.78	0.01
UWG-2	3.07	5.86	0.00
average	**3.04**	**5.80**	
stdev	0.03	0.08	0.02

Appendix II – Sample Descriptions

Chromite textures have been divided into common types by Lipin (1984). Clean chromite (Figure. A-1a), is the most common and occurs in all localities. Clean chromites do not contain inclusions and are fairly homogenous. Lattice chromite (Figure. A-1b) are characterized by the replacement of chromite by chlorite along the three crystallographic axes. Lattice-type chromite is present in the Buck Creek and Daybook bodies. Poikiloblastic chromite (Figure. A-1c) has a vuggy appearance and is found in the Frank, Addie, and Ellijay bodies. Most localities contain clean chromite and may contain one or more of the other types.
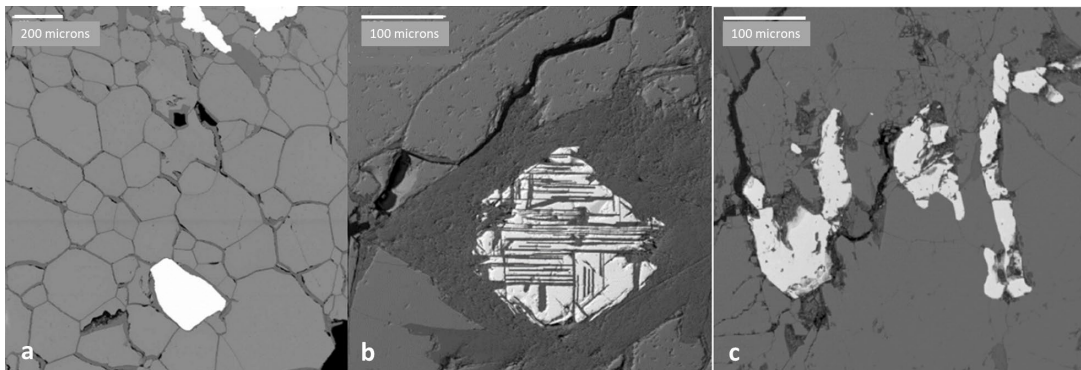
Figure A-1: Back-scattered electron images with representative textures and structures of chromium spinel. Clean chromite (a) does not contain visible inclusions and has sharp grain boundaries. Lattice chromite (b) exhibits replacement of chromite by chlorite along three crystallographic boundaries. Poikiloblastic chromite (c) has a vuggy appearance and is commonly parted along the grain.

Buck Creek:

The Buck Creek complex contains both mafic and ultramafic rocks in five distinct units: dunite, metatroctolite, edenite-margarite schist, actinolite-chlorite schist, and amphibolite (Berger et al. 2001). Rocks from geographically distinct regions of this display different metamorphic textures ranging from slightly altered olivine with sharp 120º grain boundaries and relatively little chromite, to highly altered olivine with moderate amounts of lattice-type chromite. The Buck Creek ultramafic formation samples are from two distinct locations- Corundum Knob at the south-central edge of the body and a power line/stream cut on the eastern side of the body. Peridotites are found adjacent to sapphirine-bearing metatroctolites and apatite-containing pyroxenite. Samples from Corundum Knob (Buck 04-1, 04-4) contain extremely fractured and altered olivine with chromite found generally as inclusions. Chromites, which make up 1-2% of the bulk rocks, exhibit lattice-type exsolution lamellae and have significant alteration to magnetite and kammererite. Bulk rocks are ~5% Orthopyroxene (Opx) and up to 50% serpentine minerals. Images of thin sections in both plane-polarized (PPL) and cross-polarized light (XPL) are provided for each sample.

Buck 04-1

1mm

Buck 04-4

1mm
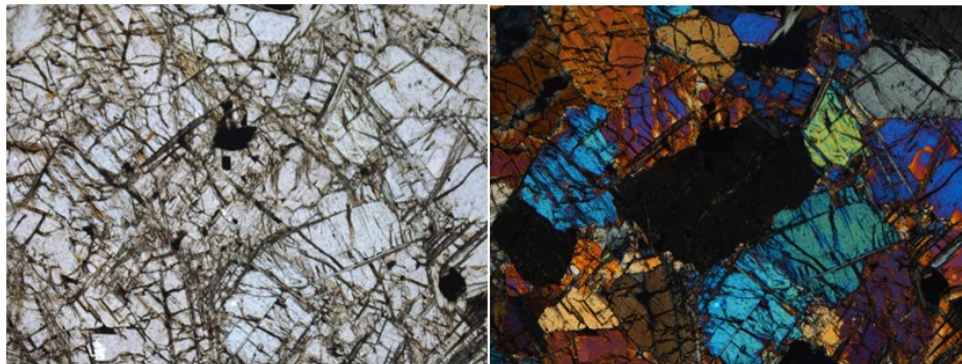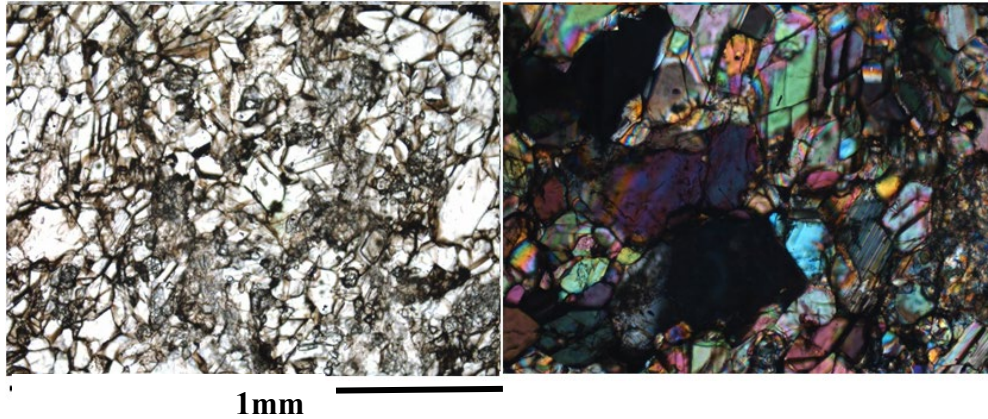
Samples from the power line and stream cuts (Pow04-1, Buck-str) have iron staining in hand sample. They contain 3-5% lattice-type chromite, altered to magnetite, contained mostly as inclusions within highly altered and fractured olivine. The bulk rock contains ~20% serpentine minerals, 1-2% Opx, and <1% Clinopyroxene (Cpx). These samples can be considered float as they were not collected from an intact outcrop.

Pow 04-1

1mm
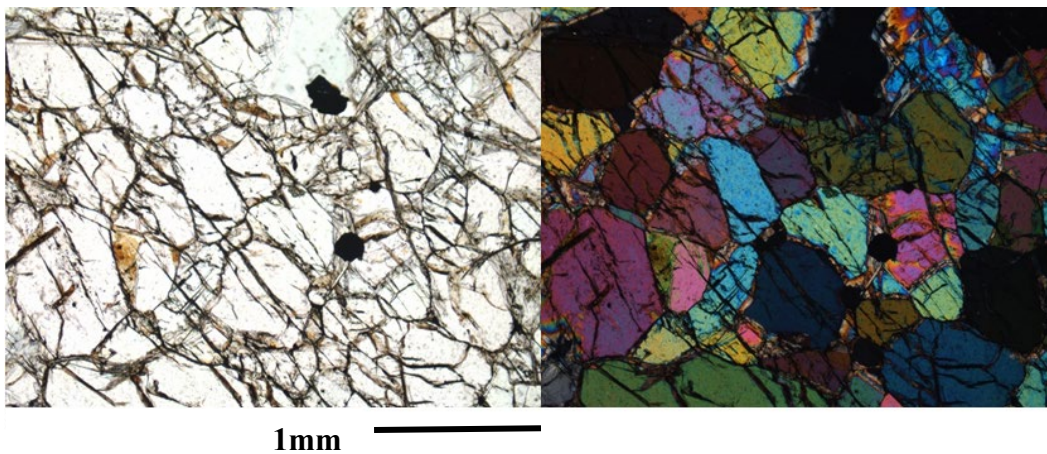
Buck-str
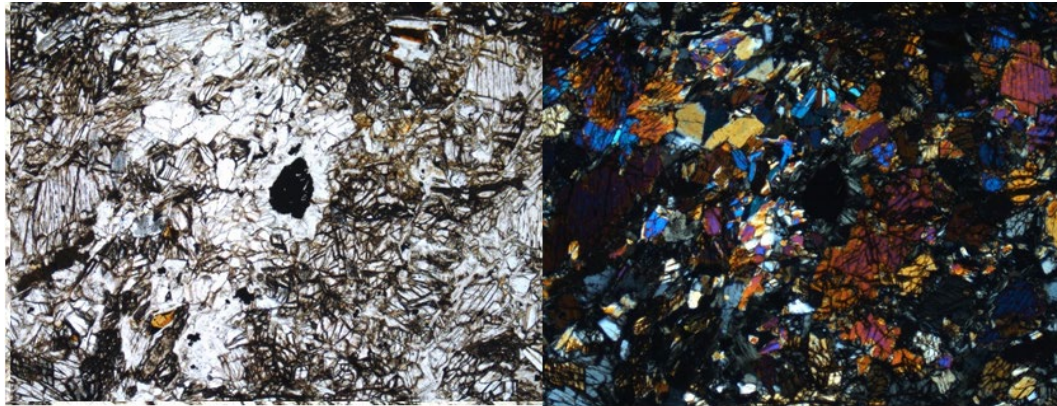
1mm

Ellijay (Olivine #9):

The Ellijay body consists of dunite and harzburgite containing chromite layers up to several centimeters thick that display some post-metamorphic brittle deformation. Some dunitic portions of the body also contain disseminated chromite. Ellijay has been quarried in the past and is now a pit with ultramafic rocks exposed along the sides as well as a great number of detached blocks in the excavated portion of the pit. Samples are physically distinct from each other in that some have strongly defined chromite layers, some have weakly defined diffuse layering, and others have no layering but abundant disseminated chromite. Thin sections show clean olivine interlayered with chromite in some portions of the body while other portions are strongly serpentinized. The strongly layered sample (Ell03-1) has two 2-3 cm wide bands of >95% euhedral interlocking chromite containing euhedral olivine and some serpentine minerals between the chromite layers with very sharp delineations in composition at the edges of the bands. Between the bands are areas of >90% fractured olivine with minor alteration along the grain boundaries. Minor amounts of small chromite and Opx are

disseminated throughout the dunitic layers. Images of thin sections in both plane-polarized (PPL) and cross-polarized light (XPL) are provided for each sample.

Ell 03-1
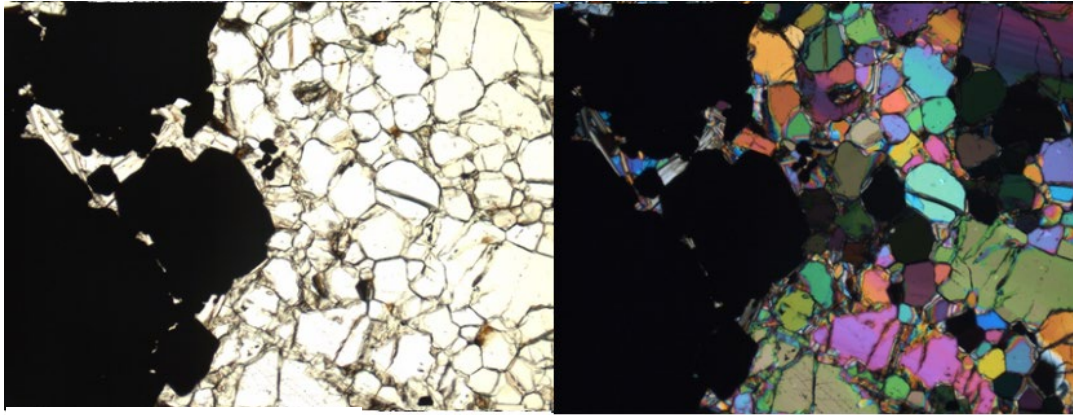
1mm

The weakly layered sample (Ell 04-1) had smaller chromite grains that grade into the dunitic domains of the rock. Dunitic portions contain minor disseminated chromite and Opx. Samples containing only disseminated euhedral chromite (Ell 03-2, 04-1) contain >90% large olivine grains with 120° grain boundaries. Serpentine (2-3%) minerals occur along some grain boundaries. Chromite occurs as large euhedral grains comprising 2-3% of the bulk rock.

Ell 04-1
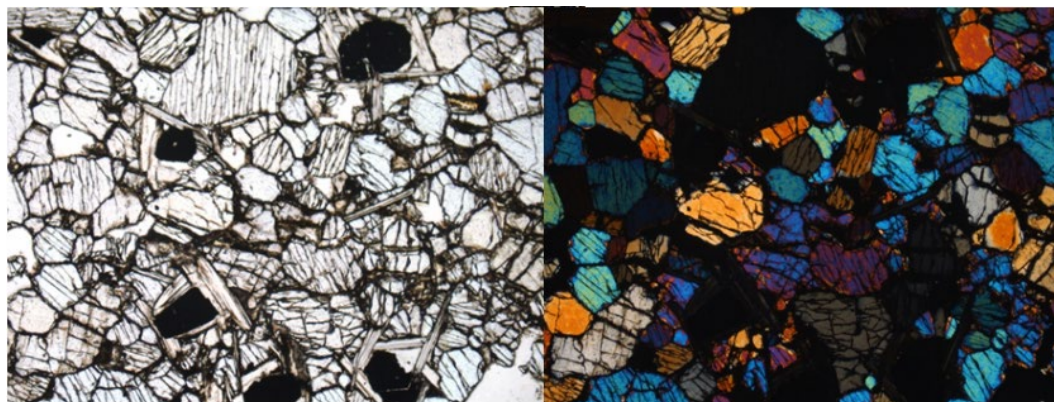
1mm

Webster-Addie:

The Webster-Addie complex consists of dunite, websterite, and enstatite pyroxenite in a 9.5 by 4.8 km ring structure. This location is unusual in that Cpx is uncommon in the myriad of ultramafic bodies in the southern Blue Ridge region, but this body is the type locality for Websterite. Contacts with the country rock are faulted and Miller (1953) concluded that the complex intruded as a sheet-like mass and was deformed and domed after emplacement. The deposit is cut by pegmatite veins. Thin sections exhibit a range of metamorphic textures from clean olivine and subhedral chromites with sharp grain boundaries to moderately altered olivine adjacent to chromites surrounded by thick chlorite (kammererite) rims.

Addie dunitic and harzburgitic samples are from the southern portion of a ring structure also containing websterite and enstatite pyroxenite. The dunitic samples (Add 03-2, 03-3, 03-4) contain 2-3% large euhedral chromites with poikiloblastic texture. Olivine is euhedral and transected by uneven fractures. Alteration of 5-7% begins along the fractures and grain boundaries. Addie peridotites contain large fractured euhedral olivine with alteration along the boundaries and in localized channels. Serpentinization comprises 10-15% of the bulk rock. Large euhedral chromites occur in weak layers and some contain olivine inclusions. One pyroxenite sample (add 04-2) is composed of bright green, coarsely crystalline interlocking grains of enstatite, no olivine, and small magnesian spinel. Images of thin sections in both plane-polarized (PPL) and cross-polarized light (XPL) are provided for each sample.
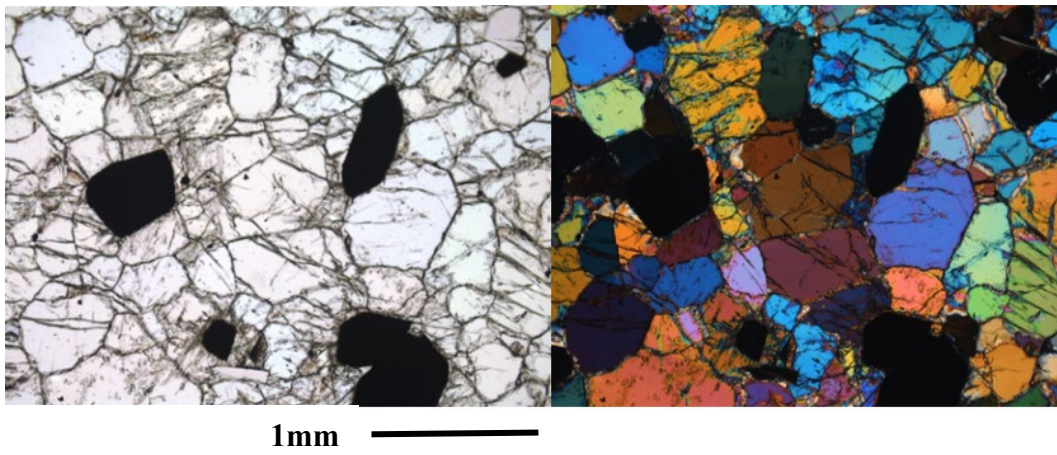
Add 03-2

1mm

Add 03-3


1mm

Add 03-4

1mm
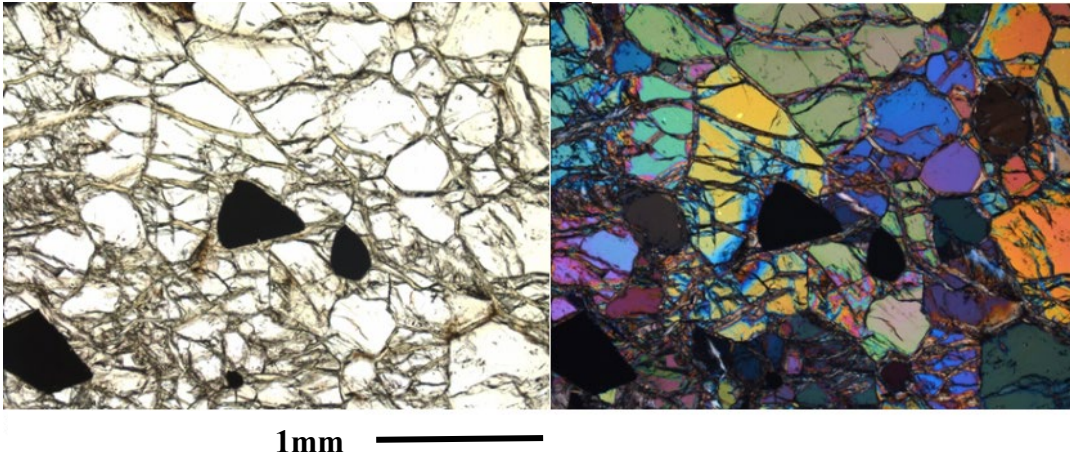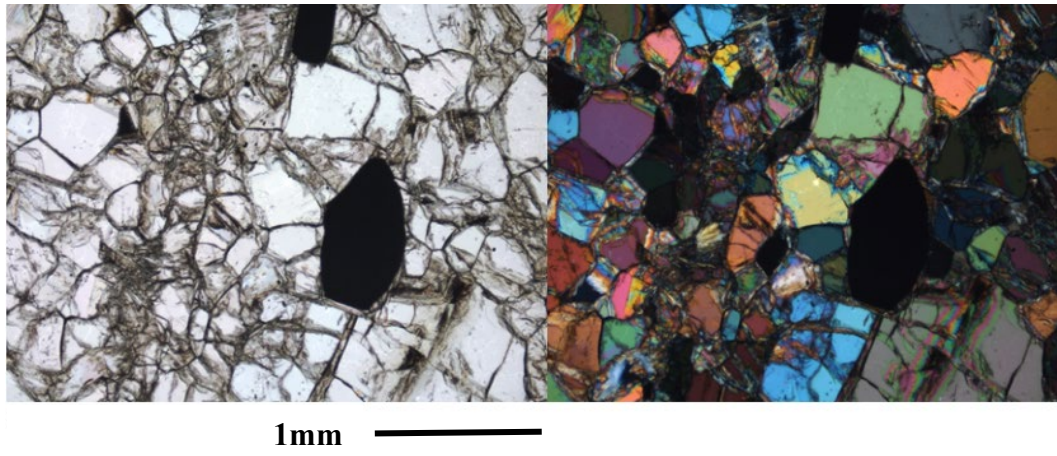
Newdale:

Newdale is described as a folded body exhibiting three distinct phases of deformation including one that predates the surrounding rock (Raymond and Abbott 1997). The body is fault bounded. The dunite that dominates the site is crosscut by veins of talc, anthophyllite, tremolite, chlorite, magnetite, magnesite, and serpentine. In thin section, two populations of chromites dominate. Either large, fractured, but unzoned chromites are found with highly serpentinized olivine or small chromites are found predominately in areas of relatively unaltered olivine.

All samples were collected from a small portion of the periphery of the body. Newdale samples (New 03-1, 04-1, and 04-2) exhibit regions of large, interlocking, fractured and grain boundary altered olivine distinct from concentrated channels of almost complete serpentinization that make up approximately 10% of the bulk rock. Chromites (3-5%) were euhedral but fractured and parted, Opx was 2-5%, and minor amounts of Cpx were contained in the bulk rock. Anthophyllite is observed in the hand samples but not in thin section. Images of thin sections in both plane-polarized (PPL) and cross-polarized light (XPL) are provided for each sample.
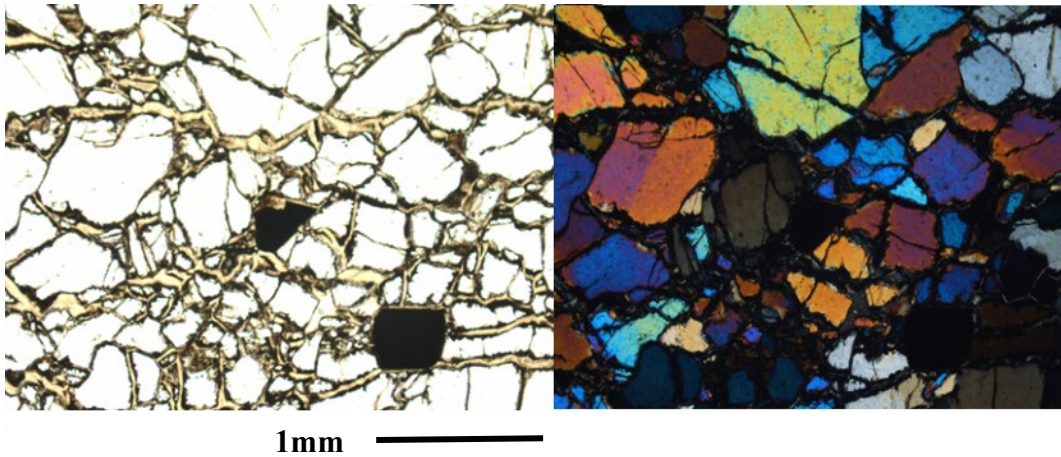
New 04-1

1mm

New 04-2

1mm ────────
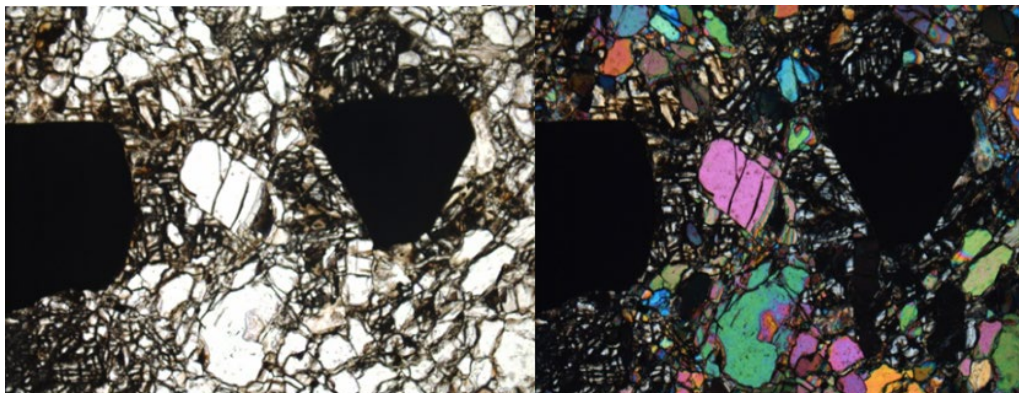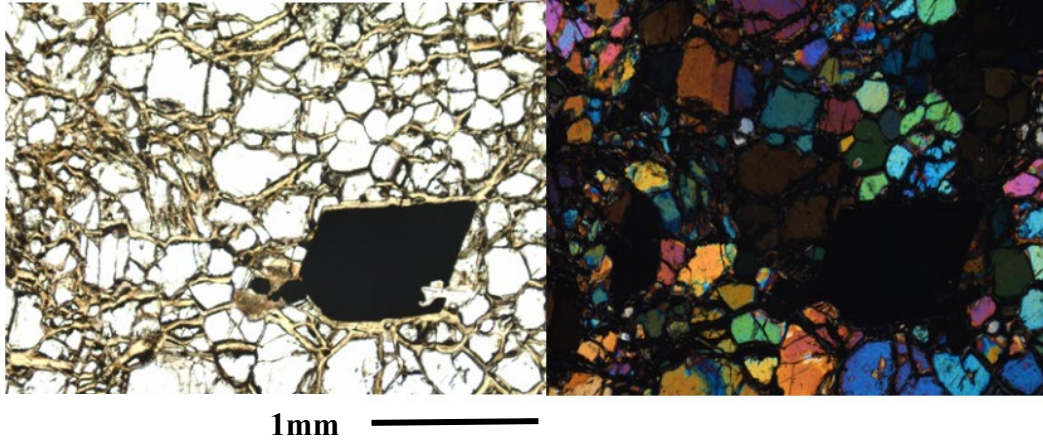
One sample (New 04-3) is iron stained in hand sample. It also has zones of clear and unfractured olivine with concentrated channels of fractured and extensively altered olivine in approximately 8% of the rock. Euhedral variably sized chromite composes 1-2% of the rock, zoned Opx 10-15% and up to 1-2% is Cpx.

New 04-3

1mm ────────

Daybook:

The Daybook body has been extensively mined and consists of dunite with minor Opx and chromium-rich spinel, chromitite, and harzburgite (Raymond and Abbott 1997). Swanson (1981) describes the original body as being surrounded by gneiss and amphibolites of the Blue Ridge Thrust sheet as well as intruded by quartz monzonite-granodiorite pegmatites which were not observed during this study. Dikes extend into the ultramafic body from an adjacent tabular granitoid pluton. Along the margins of these dikes veins extend which contain vermiculite, phlogopite, talc, magnesite, anthophyllite, tremolite, chlorite, antigorite, and lizardite. Swanson (1981) describes the contact with country rock as a metasomatic reaction zone consisting of anthophyllite with rocks ranging from relatively clean olivine with minor amounts of pyroxene and large fractured but unzoned chromites, to moderately serpentinized, zoned pyroxenes and chromites exhibiting lattice exsolution lamellae.

The Daybook deposit has been extensively mined so all samples were obtained from mine waste piles. Chromite pods of up to 3m within the dunite have been reported but were not observed during this study. Daybook dunites (Day 03-1, 03-2) are mostly composed of olivine of equant polygonal grains that meet at 120° triple junctions with minor alteration along grain boundaries. Serpentine minerals (5%) are primarily confined to localized channels along with minor anthophyllite. Large fractured Cpx (1-3%) and Opx (2-3%) can also be found. Chromite that occurs outside of the serpentinized channels is large, euhedral, with poikiloblastic textures. Chromite within the serpentinized channels is extensively altered with lattice-type exsolution lamellae.

Images of thin sections in both plane-polarized (PPL) and cross-polarized light (XPL) are provided for the sample.

Day 03-1
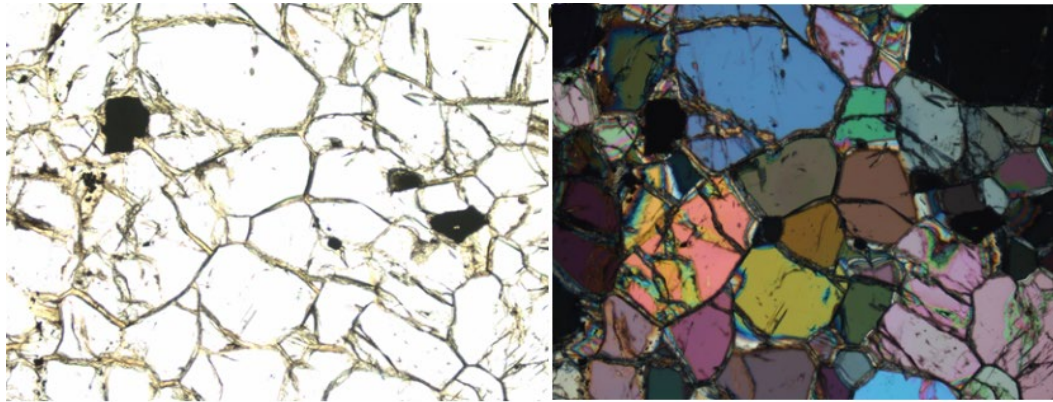
1mm

Frank:

The contacts of the Frank body have been mapped as thrust faults (Raymond and Abbott 1997). The body consists of dunite, lherzolite, and metamorphic assemblages of anthophyllite, tremolite, talc chlorite, and serpentine. This study also noted lizardite. Some rocks contain olivine with sharp boundaries and virtually no chromite, while other rocks exhibit serpentinized olivine with abundant anthophyllite and large (1-2mm) chromite with poikiloblastic texture. Much of the deposit also contains secondary Opx.

The Frank mine has been excavated to a depth of 30 meters, so all samples collected are from discrete blocks within the pit or piles along the edges. Frank harzburgites (Frk 04-1, 04-2, 04-4) have some textural and compositional variations. Both contain relatively unaltered olivine interspersed with highly serpentinized regions that comprise up to 30% of the bulk rock. Opx and Cpx are concentrated in these

portions of the rock making up to 20% of the total rock. Frk 04-4 contains highly fractured and altered chromite (2-3%) as well as chromite blebs within veins. Frank 04-2 has no chromite but minor pentlandite. Anthophyllite and lizardite were observed in hand sample but not in thin section. Images of thin sections in both plane-polarized (PPL) and cross-polarized light (XPL) are provided for each sample.

Frk 04-1
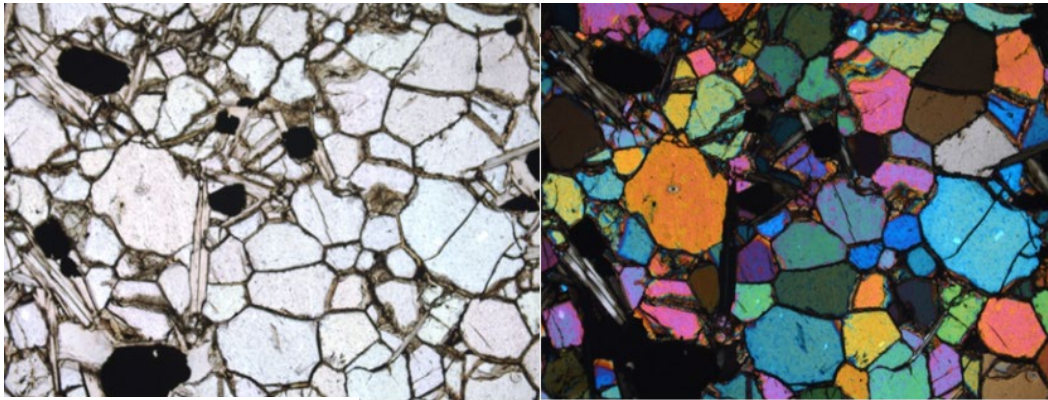
1mm
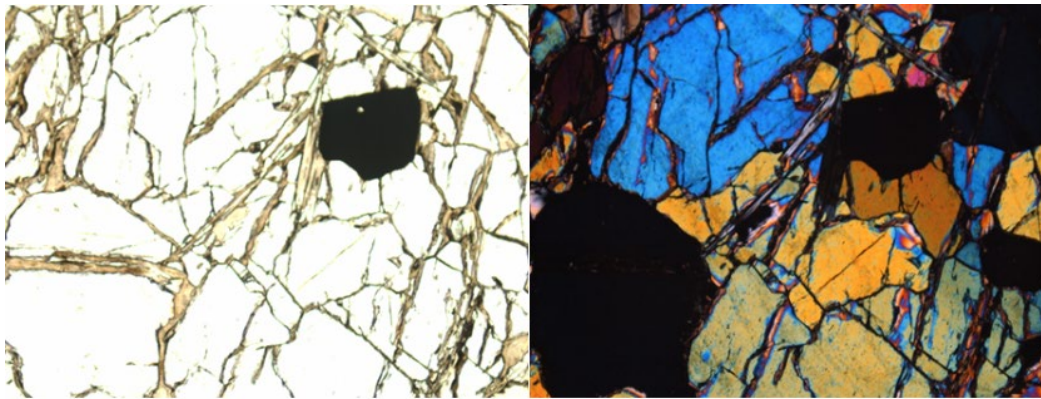
Frk 04-2
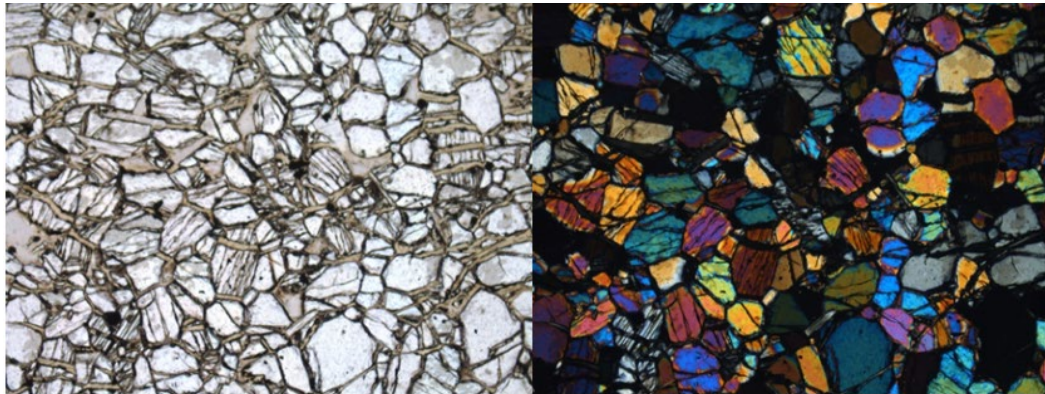
1mm

Frank dunites (Frk 04-3) contain >90% equant polygonal olivine grains with 120° borders and minor alteration along boundaries. Serpentine minerals (3-5%) are concentrated in highly serpentinized channels. Chromite (1-4%) is either large and

euhedral or very small with some alteration to magnetite. Minor zoned Opx and Cpx compose 1% of the bulk rock.

Frk 04-3

1mm

Glossary of Terms

Partial melting – the process that occurs when a portion of the mantle melts; incompatible elements partition into the melt while compatible elements remain in the residue; the melt and residue have different bulk compositions

Melt residue – the mantle material remaining after a partial melt has been extracted

Melt depletion – incompatible elements partition into melt and are preferentially removed during a partial melting event

MORB – mid-ocean ridge basalt created by the partial melting of the upper mantle

DMM – the depleted MORB mantle, or the upper mantle that is the source of mid-ocean ridge volcanism

PM – a hypothetical undepleted reservoir that represents the composition of the mantle before mafic crust was extracted by partial melting

Dunite – an ultramafic rock composed of >90% olivine and may contain minor amounts of pyroxene and chromite; a variety of peridotite

Harzburgite – an ultramafic rock composed of 40 to 90% olivine with variable amounts of orthopyroxene and spinel; a variety of peridotite

Lherzolite – an ultramafic rock composed of 40 to 90% olivine with orthopyroxene, clinopyroxene, and spinel; a variety of peridotite

Peridotite – an ultramafic rock composed of mostly olivine and pyroxene with variable proportions of pyroxenes, spinel, plagioclase, and amphibole

Websterite – an ultramafic rock composed of orthopyroxene and clinopyroxene; a variety of pyroxenite

Boninite – a mafic rock high in magnesium and silica but extremely depleted in incompatible trace elements; typical of suprasubduction zones

Ophiolite peridotite – ultramafic rock layers at the stratigraphic base of an ophiolite sequence

Abyssal peridotite – the residues of mantle melting beneath ocean ridges

MORB cumulate – a collection of olivine, chromite, and other early crystallizing minerals that settle and accumulate from MORB melts, often in large magma chambers

Refertilization – interaction between depleted peridotites and a melt formed deeper in the mantle

References

Abily, B., & Ceuleneer, G. (2013). The dunitic mantle-crust transition zone in the Oman ophiolite: Residue of melt-rock interaction, cumulates from high-MgO melts, or both? *Geology*, *41*(1), 67–70.

Alard, O., Luguet, A., Pearson, N. J., Griffin, W. L., Lorand, J.-P., Gannoun, A., Burton, K. W., & O'Reilly, S. Y. (2005). In situ Os isotopes in abyssal peridotites bridge the isotopic gap between MORBs and their source mantle. *Nature*, *436*(7053), 1005–1008.

Aldanmaz, E., Schmidt, M. W., Gourgaud, A., & Meisel, T. (2009). Mid-ocean ridge and supra-subduction geochemical signatures in spinel–peridotites from the Neotethyan ophiolites in SW Turkey: Implications for upper mantle melting processes. *Lithos*, *113*(3–4), 691–708.

Arai, S. (1994). Characterization of spinel peridotites by olivine-spinel compositional relationships: Review and interpret. *Chemical Geology*, *113*(3–4), 191–204.

Arai, S., Okamura, H., Kadoshima, K., Tanaka, C., Suzuki, K., & Ishimaru, S. (2011). Chemical characteristics of chromian spinel in plutonic rocks: Implications for deep magma processes and discrimination of tectonic setting. *Island Arc*, *20*(1), 125–137. Arai, S., & Miura, M. (2016). Formation and modification of chromitites in the mantle. *Lithos*, *264*, 277–295.

Batanova, V. G., Brügmann, G. E., Bazylev, B. A., Sobolev, A. V., Kamenetsky, V. S., & Hofmann, A. W. (2008). Platinum-group element abundances and Os isotope composition of mantle peridotites from the Mamonia complex, Cyprus. *Chemical Geology*, *248*(3–4), 195–212.

Becker, H., Horan, M. F., Walker, R. J., Gao, S., Lorand, J.-P., & Rudnick, R. L. (2006). Highly siderophile element composition of the Earth's primitive upper mantle: Constraints from new data on peridotite massifs and xenoliths. *Geochimica et Cosmochimica Acta*, *70*(17), 4528–4550.

Berger, S., Cochrane, D., Simons, K., Savov, I., Ryan, J., & Peterson, V. (2001). Insights from Rare Earth Elements into the Genesis of the Buck Creek Complex, Clay County, MC. *Southeastern Geology*, *40*(3), 201–212.

Bézos, A., Lorand, J.-P., Humler, E., & Gros, M. (2005). Platinum-group element systematics in Mid-Oceanic Ridge basaltic glasses from the Pacific, Atlantic, and Indian Oceans. *Geochimica et Cosmochimica Acta*, *69*(10), 2613–2627.

Bindeman, I. (2008). Oxygen Isotopes in Mantle and Crustal Magmas as Revealed by Single Crystal Analysis. *Reviews in Mineralogy and Geochemistry*, *69*(1), 445–478.

Bishop, J. L., Perry, K. A., Darby Dyar, M., Bristow, T. F., Blake, D. F., Brown, A. J., & Peel, S. E. (2013). Coordinated spectral and XRD analyses of magnesite-nontronite-forsterite mixtures and implications for carbonates on Mars. *Journal of Geophysical Research: Planets*, *118*(4), 635–650.

Böhlke, J. K., Alt, J. C., & Muehlenbachs, K. (1984). Oxygen isotope–water relations in altered deep-sea basalts: Low-temperature mineralogical controls. *Canadian Journal of Earth Sciences*, *21*(1), 67–77.

Boudier, F., & Nicolas, A. (1985). Harzburgite and lherzolite subtypes in ophiolitic oceanic environments. *Earth and Planetary Science Letters*, *76*(1–2), 84–92.

Brandon, A. D., Creaser, R. A., Shirey, S. B., & Carlson, R. W. (1996). Osmium

Recycling in Subduction Zones. *Science*, *272*(5263), 861–863.

Brookins, D.G., (1989). Aqueous geochemistry of rare earth elements, in Lipin, B.R. and McKay, G.A., eds., Geochemistry and mineralogy of rare earth elements: Washington, D.C., Mineralogical Society of America, 201-225.

Büchl, A., Brügmann, G., Batanova, V. G., Münker, C., & Hofmann, A. W. (2002). Melt percolation monitored by Os isotopes and HSE abundances: A case study from the mantle section of the Troodos Ophiolite. *Earth and Planetary Science Letters*, *204*(3–4), 385–402.

Büchl, A., Brügmann, G., & Batanova, V. G. (2004). Formation of podiform chromitite deposits: Implications from PGE abundances and Os isotopic compositions of chromites from the Troodos complex, Cyprus. *Chemical Geology*, *208*(1–4), 217–232.

Büchl, A., Brügmann, G. E., Batanova, V. G., & Hofmann, A. W. (2004). Os mobilization during melt percolation: The evolution of Os isotope heterogeneities in the mantle sequence of the Troodos ophiolite, Cyprus. *Geochimica et Cosmochimica Acta*, *68*(16), 3397–3408.

Carlson, R. W. (2005). Application of the Pt–Re–Os isotopic systems to mantle geochemistry and geochronology. *Lithos*, *82*(3–4), 249–272.

Carpenter, J., & Chen, H. (1978). Petrology and Bulk Rock Geochemistry of the Frank Ultramafic Body, Avery County, NC and Associated Ultramafic Rock Bodies of the Southern Appalachians. *Southeastern Geology*, *20*(1), 21–26.

Chacko, T., Hu, X., Mayeda, T. K., Clayton, R. N., & Goldsmith, J. R. (1996). Oxygen isotope fractionations in muscovite, phlogopite, and rutile.

Geochimica et Cosmochimica Acta, *60*(14), 2595–2608.

Chaumba, J. B. (2013). The Soapstone Ridge Complex, Southern Appalachians: Petrographic, mineral compositional, and oxygen isotope investigation. *Canadian Journal of Earth Sciences*, *50*(4), 423–438.

Chaumba, J. (2014). Relict and re-set oxygen isotope ratios from the Russell Lake Allochthon, Southern Appalachians. *The Canadian Mineralogist*, *52*, 473–486.

Chiba, H., Chacko, T., Clayton, R. N., & Goldsmith, J. R. (1989). Oxygen isotope fractionations involving diopside, forsterite, magnetite, and calcite: Application to geothermometry. *Geochimica et Cosmochimica Acta*, *53*(11), 2985–2995.

Clayton, R. N., Goldsmith, J. R., & Mayeda, T. K. (1989). Oxygen isotope fractionation in quartz, albite, anorthite and calcite. *Geochimica et Cosmochimica Acta*, *53*(3), 725–733.

Cottrell, E., & Kelley, K. A. (2011). The oxidation state of Fe in MORB glasses and the oxygen fugacity of the upper mantle. *Earth and Planetary Science Letters*, *305*(3–4), 270–282.

Day, J. M. D., O'Driscoll, B., Strachan, R. A., Daly, J. S., & Walker, R. J. (2017). Identification of mantle peridotite as a possible Iapetan ophiolite sliver in south Shetland, Scottish Caledonides. *Journal of the Geological Society*, *174*(1), 88–92.

Day, J. M. D., Walker, R. J., & Warren, J. M. (2017). 186Os–187Os and highly siderophile element abundance systematics of the mantle revealed by abyssal

peridotites and Os-rich alloys. *Geochimica et Cosmochimica Acta*, *200*, 232–254.

Derbyshire, E. J., O'Driscoll, B., Lenaz, D., Gertisser, R., & Kronz, A. (2013). Compositionally heterogeneous podiform chromitite in the Shetland Ophiolite Complex (Scotland): Implications for chromitite petrogenesis and late-stage alteration in the upper mantle portion of a supra-subduction zone ophiolite. *Lithos*, *162–163*, 279–300.

Deschamps, F., Godard, M., Guillot, S., & Hattori, K. (2013). Geochemistry of subduction zone serpentinites: A review. *Lithos*, *178*, 96–127.

Dick, H. J. B., & Bullen, T. (1984). Chromian spinel as a petrogenetic indicator in abyssal and alpine-type peridotites and spatially associated lavas. *Contributions to Mineralogy and Petrology*, *86*(1), 54–76.

Dilek, Y., & Robinson, P. T. (Eds.). (2003). Magmatic, metamorphic, and tectonic processes in ophiolite genesis. In *Ophiolites in Earth History* (Vol. 218, p. 0). Geological Society of London.

Dilek, Y. (2003). Ophiolite concept and its evolution. In Yildirim Dilek & S. Newcomb, *Ophiolite concept and the evolution of geological thought*. Geological Society of America.

Dilek, Y., & Furnes, H. (2009). Structure and geochemistry of Tethyan ophiolites and their petrogenesis in subduction rollback systems. *Lithos*, *113*(1–2), 1–20.

Dilek, Y., & Furnes H (2014). Ophiolites and Their Origins. *Elements*, *10*(2), 93-100.

Droop, G. T. R. (1987). A general equation for estimating Fe^{3+} concentrations in ferromagnesian silicates and oxides from microprobe analyses, using

stoichiometric criteria. *Mineralogical Magazine*, *51*(361), 431–435.

Dubois-Côté, V., Hébert, R., Dupuis, C., Wang, C. S., Li, Y. L., & Dostal, J. (2005).
Petrological and geochemical evidence for the origin of the Yarlung Zangbo
ophiolites, southern Tibet. *Chemical Geology*, *214*(3–4), 265–286.

Eiler, J. M. (2000). Oxygen Isotope Geochemistry of Oceanic-Arc Lavas. *Journal of
Petrology*, *41*(2), 229–256.

Eiler, J. M. (2001). Oxygen Isotope Variations of Basaltic Lavas and Upper Mantle
Rocks. *Reviews in Mineralogy and Geochemistry*, *43*(1), 319–364.

Elthon, D. (1991). Geochemical evidence for formation of the Bay of Islands
ophiolite above a subduction zone. *Nature*, *354*(6349), 140–143.

Farquhar, J., & Rumble, D. (1998). Comparison of oxygen isotope data obtained by
laser fluorination of olivine with KrF excimer laser and CO2 laser.
Geochimica et Cosmochimica Acta, *62*(18), 3141–3149.

Furnes, H., Pedersen, R. B., & Stillman, C. J. (1988). The Leka Ophiolite Complex,
central Norwegian Caledonides: Field characteristics and geotectonic
significance. *Journal of the Geological Society*, *145*(3), 401–412.

Furnes, H., & Dilek, Y. (2017). Geochemical characterization and petrogenesis of
intermediate to silicic rocks in ophiolites: A global synthesis. *Earth-Science
Reviews*, *166*, 1–37.

Gannoun, A., Burton, K. W., Parkinson, I. J., Alard, O., Schiano, P., & Thomas, L. E.
(2007). The scale and origin of the osmium isotope variations in mid-ocean
ridge basalts. *Earth and Planetary Science Letters*, *259*(3–4), 541–556.

Gong, X.-H., Xu, J.-F., Liu, X.-J., Huang, X.-X., Zhang, Z.-G., Zhou, H.-L., Yang, Z.-Y., & Zhao, W.-X. (2019). Widespread Os-isotopically ultradepleted mantle domains in the Paleo-Asian oceanic upper mantle: Evidence from the Tianshan ophiolites (NW China). *International Journal of Earth Sciences*.

Gregory, R. T., & Taylor, H. P. (1981). An oxygen isotope profile in a section of Cretaceous oceanic crust, Samail Ophiolite, Oman: Evidence for $\delta\,^{18}$ O buffering of the oceans by deep (>5 km) seawater-hydrothermal circulation at mid-ocean ridges. *Journal of Geophysical Research: Solid Earth*, *86*(B4), 2737–2755.

Guentert, J. (1984). *Petrology and Origin of the Day Book Dunite, Yancey County, North Carolina*.

Harvey, J., Gannoun, A., Burton, K. W., Rogers, N. W., Alard, O., & Parkinson, I. J. (2006). Ancient melt extraction from the oceanic upper mantle revealed by Re–Os isotopes in abyssal peridotites from the Mid-Atlantic ridge. *Earth and Planetary Science Letters*, *244*(3–4), 606–621.

Hatcher, R. D. H., Thomas, W. A., & Viele, G. W. (1989). *The Appalachian-Ouachita Orogen in the United States*. Geological Society of America.

Hatcher, R. D., & Goldberg, S. A. (1991). The Blue Ridge geologic province. In *The geology of the Carolinas; Carolina Geological Society fiftieth anniversary volume (ed. J. W. Horton, Jr. And V. A. Zullo)* (pp. 11–35).

Herzberg, C., Vidito, C., & Starkey, N. A. (2016). Nickel–cobalt contents of olivine record origins of mantle peridotite and related rocks. *American Mineralogist*, *101*(9), 1952–1966.

Hu, G., & Clayton, R. N. (2003). Oxygen isotope salt effects at high pressure and high temperature and the calibration of oxygen isotope geothermometers. *Geochimica et Cosmochimica Acta*, *67*(17), 3227–3246.

Hunter, C. E. (1941). *Forsterite olivine deposits of North Carolina and Georgia*. N. C. Division of Mineral Resources Bulletin.

Irvine, T.N., 1967. Chromian spinel as a petrogenetic indicator Part 2. Petrologic applications. Canadian Journal of Earth Sciences 4, 71 -103.

Ishiwatari, A., Sokolov, S. D., & Vysotskiy, S. V. (2003). Petrological diversity and origin of ophiolites in Japan and Far East Russia with emphasis on depleted harzburgite. *Geological Society, London, Special Publications*, *218*(1), 597–617.

Jochum, K. P., Nohl, U., Herwig, K., Lammel, E., Stoll, B., & Hofmann, A. W. (2005). GeoReM: A New Geochemical Database for Reference Materials and Isotopic Standards. *Geostandards and Geoanalytical Research*, *29*(3), 333–338.

Kamenetsky, V. S. (2001). Factors Controlling Chemistry of Magmatic Spinel: An Empirical Study of Associated Olivine, Cr-spinel and Melt Inclusions from Primitive Rocks. *Journal of Petrology*, *42*(4), 655–671.

Kelemen, P. B., Matter, J., Streit, E. E., Rudge, J. F., Curry, W. B., & Blusztajn, J. (2011). Rates and Mechanisms of Mineral Carbonation in Peridotite: Natural Processes and Recipes for Enhanced, in situ CO_2 Capture and Storage. *Annual Review of Earth and Planetary Sciences*, *39*(1), 545–576.

Kuntz, M. A., & Hedge, C. E. (1981). Petrology and major-element, minor-element, and Rb-Sr geochemistry of the Ophiolite complex at Buck Creek, North Carolina. *EOS- American Geophysical Union Transactions*, *62*(1088).

Lang, H. M., Wachter, A. J., Peterson, V. L., & Ryan, J. G. (2004). Coexisting clinopyroxene/spinel and amphibole/spinel symplectites in metatroctolites from the Buck Creek ultramafic body, North Carolina Blue Ridge. *American Mineralogist*, *89*(1), 20–30.

Lassiter, J.C., Byerly, B.L., Snow, J.E., Hellebrand, E. (2014) Constraints from Os-isotope variations on the origin of Lena Trough abyssal peridotites and implications for the composition and evolution of the depleted upper mantle. Earth and Planetary Science Letters 403, 178-187.

Lecuyer, G. and Gruau, (1996). G. Mevel, C., Gillis, K. M., Allan, J. F., & Meyer, P. S. (Eds.). *Proceedings of the Ocean Drilling Program, 147 Scientific Results* (Vol. 147). Ocean Drilling Program.

Lipin, B. R. (1984). Chromite from the Blue Ridge Province of North Carolina. *American Journal of Science*, *284*(4–5), 507–529.

Luck, J.-M., & Alle`gre, C. J. (1991). Osmium isotopes in ophiolites. *Earth and Planetary Science Letters*, *107*(2), 406–415.

Luguet, A., Alard, O., Lorand, J. P., Pearson, N. J., Ryan, C., & O'Reilly, S. Y. (2001). Laser-ablation microprobe (LAM)-ICPMS unravels the highly siderophile element geochemistry of the oceanic mantle. *Earth and Planetary Science Letters*, *189*(3–4), 285–294.

Massey, M. A., & Moecher, D. P. (2005). Deformation and metamorphic history of the Western Blue Ridge-Eastern Blue Ridge terrane boundary, southern Appalachian Orogen. *Tectonics*, *24*(5), 1643-1673.

Mattey, D., Lowry, D., & Macpherson, C. (1994). Oxygen isotope composition of mantle peridotite. *Earth and Planetary Science Letters*, *128*(3–4), 231–241.

McDonough, W., & Frey, F. (1989). Rare earth elements of upper mantle rocks. *Rev. Mineral.*, *21*.

McElhaney, M. S., & McSween, H. Y. (1983). Petrology of the Chunky Gal Mountain mafic-ultramafic complex, North Carolina. *GSA Bulletin*, *94*(7), 855–874.

McSween, H. Y., Abbott, R. N., & Raymond, L. A. (1989). Metamorphic conditions in the Ashe Metamorphic Suite, North Carolina Blue Ridge. *Geology*, *17*(12), 1140–1143.

Meisel, T., Walker, R. J., & Morgan, J. W. (1996). The osmium isotopic composition of the Earth's primitive upper mantle. *Nature*, *383*(6600), 517.

Meisel, Thomas, Walker, R. J., Irving, A. J., & Lorand, J.-P. (2001). Osmium isotopic compositions of mantle xenoliths: A global perspective. *Geochimica et Cosmochimica Acta*, *65*(8), 1311–1323.

Metcalf, R. V., & Shervais, J. W. (2008). Suprasubduction-zone ophiolites: Is there really an ophiolite conundrum? In *Special Paper 438: Ophiolites, Arcs, and Batholiths: A Tribute to Cliff Hopson* (Vol. 438, pp. 191–222). Geological Society of America.

Mével, C. (2003). Serpentinization of abyssal peridotites at mid-ocean ridges. *Comptes Rendus Geoscience*, *335*(10–11), 825–852.

Miller, B. V., Fetter, A. H., & Stewart, K. G. (2006). Plutonism in three orogenic pulses, Eastern Blue Ridge Province, southern Appalachians. *Geological Society of America Bulletin*, *118*(1–2), 171–184.

Misra, K. C., & Keller, F. (1978). Ultramafic Bodies in the Southern Appalachians: A Review. *American Journal of Science*, *v.278*, 389–418.

Moecher, D., Hietpas, J., Samson, S., & Chakraborty, S. (2011). Insights into southern Appalachian tectonics from ages of detrital monazite and zircon in modern alluvium. *Geosphere*, *7*(2), 494–512.

Muehlenbachs, K., & Clayton, R. N. (1976). Oxygen isotope composition of the oceanic crust and its bearing on seawater. *Journal of Geophysical Research*, *81*(23), 4365–4369.

Nicolas, A., & Boudier, F. (2003). Where ophiolites come from and what they tell us. In Yildirim Dilek & S. Newcomb, *Ophiolite concept and the evolution of geological thought*. Geological Society of America.

Niu, Y. (1997). Mantle Melting and Melt Extraction Processes beneath Ocean Ridges: Evidence from Abyssal Peridotites. *Journal of Petrology*, *38*(8), 1047–1074.

O'Driscoll, B., Walker, R. J., Clay, P. L., Day, J. M. D., Ash, R. D., & Daly, J. S. (2018). Length-scales of chemical and isotopic heterogeneity in the mantle section of the Shetland Ophiolite Complex, Scotland. *Earth and Planetary Science Letters*, *488*, 144–154.

O'Driscoll, B., Walker, R. J., Day, J. M. D., Ash, R. D., & Daly, J. S. (2015). Generations of Melt Extraction, Melt–Rock Interaction and High-Temperature Metasomatism Preserved in Peridotites of the ~497 Ma Leka Ophiolite Complex, Norway. *Journal of Petrology*, *56*(9), 1797–1828.

O'Driscoll, Brian, Day, J. M. D., Walker, R. J., Daly, J. S., McDonough, W. F., & Piccoli, P. M. (2012). Chemical heterogeneity in the upper mantle recorded by peridotites and chromitites from the Shetland Ophiolite Complex, Scotland. *Earth and Planetary Science Letters*, *333–334*, 226–237.

Onyeagocha, A. C. (1974). Alteration of Chromite from the Twin Sisters Dunite, Washington. *American Mineralogist*, *59*, 608–612.

Osozawa, S., Shinjo, R., Lo, C.-H., Jahn, B., Hoang, N., Sasaki, M., Ishikawa, K., Kano, H., Hoshi, H., Xenophontos, C., & Wakabayashi, J. (2012). Geochemistry and geochronology of the Troodos ophiolite: An SSZ ophiolite generated by subduction initiation and an extended episode of ridge subduction? *Lithosphere*, *4*(6), 497–510.

Owens, B., & Uschner, N. E. (2001). Mineralogy and geochemistry of metamorphosed ultramafic rocks in the Central Piedmont Province of Virginia. *Southeastern Geology*, *40*(3), 213–229.

Page, P., & Barnes, S.-J. (2009). Using Trace Elements in Chromites to Constrain the Origin of Podiform Chromitites in the Thetford Mines Ophiolite, Quebec, Canada. *Economic Geology*, *104*(7), 997–1018.

Pearce, J. A., Lippard, S. J., & Cann, Roberts, S. (1984). Characteristics and tectonic significance of supra-subduction zone ophiolites. *Geological Society, London, Special Publications*, *16*(1), 77–94.

Pearce, Julian A., & Parkinson, I. J. (1993). Trace element models for mantle melting: Application to volcanic arc petrogenesis. *Geological Society, London, Special Publications*, *76*(1), 373–403.

Peterson, V., Ryan, J. G., & 1997–1998 REU Participants (2009). Petrogenesis and structure of the Buck Creek mafic-ultramafic suite, southern Appalachians: Constraints on ophiolite evolution and emplacement in collisional orogens. *Geological Society of America Bulletin*, *121*(3–4), 615–629.

Ragan, D. M. (1963). Emplacement of the Twin Sisters dunite, Washington. *American Journal of Science*, *261*(6), 549–565.

Rankin, D.W., (1970). The Blue Ridge and the Reading Prong: stratigraphy and structure of Precambrian rocks in northwestern North Carolina: in Fisher, G.W., Pettijohn, F.J., Reed, J.C. and Weaver, K.N., (ed.), Studies of Appalachian Geology, Central and Southern: New York, Wiley, 227-245.

Raymond, R. A., & Abbott, R. N. (1997). Petrology and tectonic significance of ultramafic rocks near the Grandfather Mountain window in the Blue Ridge belt, Toe Terrane, Western Piedmont Zone, North Carolina. In *Paleozoic structure, metamorphism, and tectonics of the Blue Ridge of western North Carolina. (Ed. K. G. Stewart, M. G. Adams, and C. H. Trupe)* (pp. 67–85).

Raymond, L., Love, A., & McCarter, R. (2001). Petrology of the Hoots ultramafic body, blue ridge belt, northwestern North Carolina. *Southeastern Geology*, *40*, 149–162.

Raymond, L. A., Swanson, S. E., Love, A. B., & Allan, J. F. (2003). Cr-spinel compositions, metadunite petrology, and the petrotectonic history of Blue Ridge ophiolites, Southern Appalachian Orogen, USA. *Geological Society, London, Special Publications*, *218*(1), 253–278.

Raymond, L. A., Merschat, A., & Vance, R. K. (2016). Metaultramafic schists and dismembered ophiolites of the Ashe Metamorphic Suite of northwestern North Carolina, USA. *International Geology Review*, *58*(7), 874–912.

Roy-Barman, M., & Allègre, C. J. (1994). Ratios of mid-ocean ridge basalts and abyssal peridotites. *Geochimica et Cosmochimica Acta*, *58*(22), 5043–5054.

Rudnick, R. L., & Lee, C.-T. (2002). Osmium Isotope Constraints on Tectonic Evolution of the Lithosphere in the Southwestern United States. *International Geology Review*, *44*(6), 501–511.

Schulte, R. F., Schilling, M., Anma, R., Farquhar, J., Horan, M. F., Komiya, T., Piccoli, P. M., Pitcher, L., & Walker, R. J. (2009). Chemical and chronologic complexity in the convecting upper mantle: Evidence from the Taitao ophiolite, southern Chile. *Geochimica et Cosmochimica Acta*, *73*(19), 5793–5819.

Scotford, D., & Williams, J. (1983). Petrology and geochemistry of metamorphosed ultramafic bodies in a portion of the Blue Ridge of North Carolina and Virginia. *American Mineralogist*, *68*, 78–94.

Sharma, M., & Wasserburg, G. J. (1996). The neodymium isotopic compositions and rare earth patterns in highly depleted ultramafic rocks. *Geochimica et Cosmochimica Acta*, *60*(22), 4537–4550.

Shi, R., Griffin, W. L., O'Reilly, S. Y., Huang, Q., Zhang, X., Liu, D., Zhi, X., Xia, Q., & Ding, L. (2012). Melt/mantle mixing produces podiform chromite deposits in ophiolites: Implications of Re–Os systematics in the Dongqiao Neo-Tethyan ophiolite, northern Tibet. *Gondwana Research*, *21*(1), 194–206.

Shirey, S. B., & Walker, R. J. (1995). Carius tube digestion for low-blank rhenium-osmium analysis. *Analytical Chemistry*, *67*, 2136–2141.

Shirey, S. B., & Walker, R. J. (1998). The Re-Os Isotope System in Cosmochemistry and High-Temperature Geochemistry. *Annual Review of Earth and Planetary Sciences*, *26*(1), 423–500.

Smoliar, M. I., Walker, R. J., & Morgan, J. W. (1996). Re-Os Ages of Group IIA, IIIA, IVA, and IVB Iron Meteorites. *Science*, *271*(5252), 1099–1102.

Snow, J. E., & Reisberg, L. (1995). Os isotopic systematics of the MORB mantle: Results from altered abyssal peridotites. *Earth and Planetary Science Letters*, *133*(3), 411–421.

Standish, J. J., Hart, S. R., Blusztajn, J., Dick, H. J. B., & Lee, K. L. (2002). Abyssal peridotite osmium isotopic compositions from cr-spinel. *Geochemistry, Geophysics, Geosystems*, *3*(1), 1–24.

Sturm, M. E., Klein, E. M., Karsten, J. L., & Karson, J. A. (2000). Evidence for subduction-related contamination of the mantle beneath the southern Chile Ridge: Implications for ambiguous ophiolite compositions. In *Special Paper*

349: Ophiolites and oceanic crust: New insights from field studies and the Ocean Drilling Program (Vol. 349, pp. 13–20). Geological Society of America.

Swanson, S. E. (2001). Ultramafic rocks of the spruce pine area, western North Carolina: A sensitive guide to fluid migration and metamorphism. *Southeastern Geology*, *40*, 163–182.

Swanson, S. E., & Raymond, L. (2010). Petrogenesis of chromite in metaultramafic rocks of the spruce pine area. *Southeastern Geology*, *47*, 147–172.

Tenthorey, E. A., Ryan, J. G., & Snow, E. A. (1996). Petrogenesis of sapphirine-bearing metatroctolites from the Buck Creek ultramafic body, southern Appalachians. *Journal of Metamorphic Geology*, *14*(2), 103–114.

Tessalina, S. G., Bourdon, B., Gannoun, A., Capmas, F., Birck, J.-L., & Allègre, C. J. (2007). Complex Proterozoic to Paleozoic history of the upper mantle recorded in the Urals lherzolite massifs by Re–Os and Sm–Nd systematics. *Chemical Geology*, *240*(1–2), 61–84.

Trupe, C., Stewart, K. G., & Adams, M. (2003). The Burnsville fault: Evidence for the timing and kinematics of southern Appalachian Acadian dextral transform tectonics. *GSA Bulletin*, *115*(11), 1365–1376.

Tsuru, A., Walker, R. J., Kontinen, A., Peltonen, P., & Hanski, E. (2000). Re–Os isotopic systematics of the 1.95 Ga Jormua Ophiolite Complex, northeastern Finland. *Chemical Geology*, *164*(1–2), 123–141.

Valley, J. W., Kitchen, N., Kohn, M. J., Niendorf, C. R., & Spicuzza, M. J. (1995). UWG-2, a garnet standard for oxygen isotope ratios: Strategies for high

precision and accuracy with laser heating. *Geochimica et Cosmochimica Acta*, *59*(24), 5223–5231.

Walker, R. J., Hanski, E., Vuollo, J., & Liipo, J. (1996). The Os isotopic composition of Proterozoic upper mantle: Evidence for chondritic upper mantle from the Outokumpu ophiolite, Finland. *Earth and Planetary Science Letters*, *141*(1–4), 161–173.

Walker, R. J., Prichard, H. M., Ishiwatari, A., & Pimentel, M. (2002). The osmium isotopic composition of convecting upper mantle deduced from ophiolite chromites. *Geochimica et Cosmochimica Acta*, *66*(2), 329–345.

Walker, R.J., (2016). Siderophile elements in tracing planetary formation and evolution. *Geochemical Perspectives*, *5*(1), 1–143.

Warner, R, & Swanson, S. E. (2010). Metamorphism of cpx-rich rocks from webster-addie ultramafic complex. *Southeastern Geology*, *47*, 123–145.

Warner, Richard. (2001). Mineralogy and Petrology of Metaultramafic Rocks at Buck Creek, North Carolina. *Southeastern Geology*, *40*(3), 183–200.

Warren, J. M. (2016). Global variations in abyssal peridotite compositions. *Lithos*, *248–251*, 193–219.

Widom, E., & Farquhar, J. (2003). Oxygen isotope signatures in olivines from São Miguel (Azores) basalts: Implications for crustal and mantle processes. *Chemical Geology*, *193*(3–4), 237–255.

Workman, R. K., & Hart, S. R. (2005). Major and trace element composition of the depleted MORB mantle (DMM). *Earth and Planetary Science Letters*, *231*(1–2), 53–72.

Yumul, G. P. (2004). Zambales Ophiolite Complex (Philippines) Transition-Zone

Dunites: Restite, Cumulate, or Replacive Products? *International Geology

Review*, *46*(3), 259–272.

Zhao, Z.-F., Zheng, Y.-F., Chen, R.-X., Xia, Q.-X., & Wu, Y.-B. (2007). Element

mobility in mafic and felsic ultrahigh-pressure metamorphic rocks during

continental collision. *Geochimica et Cosmochimica Acta*, *71*(21), 5244–5266.